Étude théorique d'ondes de volume, localisées et de surface dans les cristaux phononiques granulaires

Hélène Pichard

Thèse de Doctorat

Hélène PICHARD

Mémoire présenté en vue de l'obtention du
grade de Docteur de l'Université du Maine
sous le label de L'Université Nantes Angers Le Mans

École doctorale : SPIGA

Discipline : 60
Spécialité : Acoustique
Unité de recherche : Laboratoire d'Acoustique de l'Université du Maine — UMR CNRS 6613

Soutenue le 28 novembre 2014

Étude théorique d'ondes de volume, localisées et de surface dans les cristaux phononiques granulaires

JURY

Rapporteurs :	**N. Declercq**, Professeur, GATECH (Metz,Atlanta) **B. Djafari-Rouhani**, Professeur, IEMN (Lille)
Examinateurs :	**F. Coulouvrat**, Directeur de recherche CNRS, IJLRDA (Paris) **M. Deschamps**, Directeur de recherche CNRS, I2M (Bordeaux)
Invité :	**V. Tournat**, Directeur de recherche CNRS, LAUM (Le Mans)
Directeur de thèse :	**V. Gusev**, Professeur, LAUM (Le Mans)
Co-directeur de Thèse :	**A. Duclos**, Maître de Conférence, LAUM (Le Mans) **J-P. Groby**, Chargé de recherche CNRS, LAUM (Le Mans)

Remerciements

Ces trois années de thèse ont été une riche expérience, c'est avec plaisir que je tiens à remercier les personnes, qui, de près ou de loin, ont contribué à la réalisation de ce projet.

Je tiens tout d'abord à remercier mes directeurs de thèse de m'avoir proposé ce sujet. Merci à Vitalyi Gusev pour son soutien, son aide, sa disponibilité et pour m'avoir transmis sa passion. Ce fut un réel plaisir et un honneur de travailler avec lui pendant ces trois années.
Merci à Aroune Duclos et Jean-Philippe Groby, pour leurs conseils et leur accompagnement qui m'ont permis de mener à bien ce travail. Je remercie aussi Vincent Tournat pour ses conseils avisés et son soutien lors des congrès.

Je remercie Bahram Djafari-Rouhani et Nico Declercq d'avoir accepté d'être rapporteur, ainsi que François Coulouvrat, Marc Deschamps et Vincent Tournat d'avoir accepté de faire partie du jury.

Merci à Andreev Valeryi pour son aide et ses conseils durant la réalisation de différentes expérimentations.

Je remercie Yves Aurégan et Joël Gilbert, ancien et actuel directeur du laboratoire, de m'avoir acceuilli au sein du LAUM. Merci à tout le personnel du LAUM, grâce à qui l'ambiance de travail a été très agréable. Merci aux membres de l'équipe granulaire, et en particulier à Aurélien Merkel et Georgios Theocharis pour leurs discussions enrichissantes et à Thibaut pour ses cookies.
L'enseignement effectué en parallèle du travail de recherche a été très enrichissant. Merci à tous les enseignants qui, après m'avoir transmis leur savoir durant ma formation, m'ont formé au métier d'enseignant. Merci à Anne-Marie Brulé, Valérie Hermann et Julie Béhu pour leur aide dans l'organisation des congrès et l'achat de matériel.

Un merci tout particulier à "mon tuteur", Olivier Richoux, pour sa sympathie, son aide et pour avoir accepté sa défaite durant nos battles fois gras... Merci aux deux papas poules, Simon Felix et Bertrand Lihoreau, qui m'ont acceuilli dans leur bureau, où, à ma grande surprise, les discussions ont davantage porté sur les couches que sur le foot ! Je leur souhaite plein de bonheur avec leurs filles.

Merci à tous les anciens et actuels doctorants ainsi qu'à "mes joueurs" du foot du vendredi, Vivien, Margaux, Alexey, Matthieu, JB, Miguel, Baptiste, Navid, Sylvain, Vicent, Clément, Jérémy, Damien, Julien, Thibault W., Thibaut D., Antonin, Côme, Alberto, Sergey, Florian, Cédric, Lei, Frédéric, Chris-

tophe, Tomas, Roberto, Jens, Jamal, Ali, Omar, André, Antonin, Charly... Leur coach est fière de leurs progrès techniques !

Je souhaite remercier tout particulièrement Laurianne et Balbine pour leur amitié, leur soutien, pour les très bons moments passés avec elles, et pour avoir accepté de nous voir débarquer avec le barbeuc' dans leur cour à toute heure.

Un grand merci à ma famille. Merci à mes parents, grâce à qui j'ai pu en arriver jusque là. Merci pour leur soutien et leur confiance. Une grande pensée pour mes frères et soeurs, Benoît, Quentin, Claire et Elsa, merci pour les welshs, les côtes de boeuf, les tartes aux citrons, les soirées pizza maison...qui m'ont permis de tenir le coup durant ces 3 ans !

Finalmente, me gustaria dar gracias a mi novio, Ely, para su apoyo, sus bromas, su cocina, por enseñarme el serrucho... y sobre todo para hacerme feliz.

Table des matières

Introduction générale **1**

1 Propagation des ondes acoustiques dans les cristaux phononiques granulaires **7**

1.1 Introduction . . . 7
1.2 Propagation des ondes dans les milieux périodiques . . . 7
1.3 États de l'art des études sur les cristaux phononiques granulaires . . . 9
1.3.1 Chaînes granulaires . . . 9
1.3.2 Cristaux phononiques granulaires bi- et tridimensionnels . . . 10
1.4 Importance des degrés de liberté en rotation des particules . . . 11
1.5 Description mécanique du contact entre deux particules . . . 13
1.5.1 Théorie du contact de Hertz-Mindlin . . . 13
1.5.2 Cas particulier des particules cylindriques . . . 14
1.6 Modélisation théorique de la propagation dans les chaînes granulaires . . . 16
1.6.1 Modes normaux de propagation dans une chaîne masses-ressorts monoatomique 17
1.6.2 Modes normaux de propagation dans une chaîne masses-ressorts diatomique . . 18
1.7 Conclusions . . . 20
Bibliographie . . . 21

2 Localized transversal-rotational modes in linear chains of equal masses **29**

2.1 Introduction . . . 30
2.2 Infinite linear granular chain . . . 32
2.2.1 Theory . . . 32
2.2.2 Dispersion curves of the propagating modes . . . 34
2.3 Localized modes . . . 36
2.3.1 General description of the dispersion curves . . . 36
2.3.2 Determination of the frequency of the modes induced by the boundary condition 38
2.3.3 Determination of the transversal and rotational displacements of the localized modes . . . 39
2.3.4 Results for different boundary conditions . . . 40
2.4 Conclusions . . . 44
Bibliography . . . 46

3 Two-dimensional discrete granular phononic crystal for shear wave control 49
3.1 Introduction . . . 50
3.2 Theory . . . 52
3.2.1 Longitudinal and shear rigidities at the contacts . . . 52
3.2.2 Bending rigidity at the contacts . . . 54
3.2.3 Dispersion curves . . . 54
3.3 Influence of the parameters on the dispersion curves . . . 56
3.3.1 Without bending rigidity . . . 56
3.3.2 Dirac-like point . . . 57
3.3.3 With bending rigidity . . . 59
3.4 Description of the nonmonotonous modes along the ΓM direction . . . 60
3.4.1 Birefraction phenomenon . . . 60
3.4.2 Hybridization of the modes . . . 62
3.4.3 Influence of the parameters η, p and p_B on the zero-group velocity point . . . 63
3.4.4 Physical explanation . . . 65
3.5 Conclusions . . . 67
Bibliography . . . 69

4 Surface waves in granular phononic crystals 73
4.1 Introduction . . . 74
4.2 Rayleigh-type surface waves . . . 76
4.2.1 Dispersion curves of the propagating modes . . . 76
4.2.2 Boundary conditions for Rayleigh-type SAWs propagating at the (010) free surface along [100] direction . . . 78
4.2.3 Pure longitudinal mode . . . 81
4.2.4 Surface modes description . . . 82
4.2.5 Rayleigh-type SAWs propagating at the (110) surface along $[1\bar{1}0]$ direction . . . 83
4.3 Shear-Horizontal (SH) type surface waves . . . 85
4.3.1 Dispersion curves of the propagating modes . . . 85
4.3.2 Boundary conditions for SH-type SAWs propagating at the (010) surface along [100] direction . . . 87
4.3.3 Surface mode description . . . 90
4.3.4 SH-type SAWs propagating at the (110) surface along $[1\bar{1}0]$ direction . . . 90
4.4 Comparison with the Cosserat theory . . . 93
4.4.1 Brief introduction to the Cosserat theory . . . 93
4.4.2 Comparison of SAWs in granular crystals and in reduced Cosserat medium . . . 93
4.5 Conclusions . . . 95
Bibliography . . . 97

Conclusion générale 99

A Description of the band structure of the chain of cylinders 103
A.1 General description of the dispersion curves . . . 103

A.1.1 Analysis of $\sin^2 q_\pm$ as a function of the parameters 103
A.1.2 Summary of the description when the two evanescent waves lies in a band gap . 106
A.2 Form of the wave number 107

B Supplementary material on chapter 4 **109**
B.1 Dispersion relation in the granular phononic crystal with particles possessing two translational and one rotational *dofs* 109
B.2 Pure longitudinal mode 110
B.3 Dispersion relation in the granular phononic crystal with particles possessing one translational and two rotational *dofs* 110
B.4 Inexistence of SH surface waves in the absence of bending rigidity 111
B.5 Cosserat and reduced Cosserat models 111
Bibliography 114

Introduction générale

L'étude des propriétés des cristaux phononiques ainsi que le contrôle des ondes élastiques/acoustiques par les métamatériaux, sont devenus des domaines de recherche très actifs, conduisant par exemple, parmi leurs nombreuses applications, au filtrage hautes fréquences d'ondes acoustiques de surface [1, 2]. Les cristaux phononiques sont des structures dont les propriétés varient périodiquement dans l'espace. La structure de bandes complexes de ces matériaux révèle des bandes de fréquences interdites à la propagation des ondes, où seuls des modes évanescents peuvent être excités. Des modes localisés, associés à une perturbation locale dans la périodicité de structures phononiques, peuvent également exister dans les bandes interdites de la structure non perturbée. La capacité à contrôler l'évanescence des ondes dans ces structures périodiques a ouvert des possibilités indéniables pour de nouvelles applications, telle que l'imagerie *super-résolution* [3, 4]. L'existence de vibrations localisées ou d'ondes de surface présente un intérêt considérable en mécanique et acoustique en raison du rôle important de ces modes dans de nombreux processus physiques [5–7]. Ainsi, la description théorique des mécanismes liés aux ondes de surface dans des cristaux phononiques est un enjeu majeur. Afin de caractériser la propagation d'ondes de surface dans les structures cristallines, des modèles discrets ont été appliqués à des structures mono, bi et tridimensionnelles possédant différents types d'interaction inter-atomiques [8]. Ces dernières années, un renouveau d'intérêt concernant les modèles discrets a largement été stimulé par les récents progrès de fabrication de nouveaux matériaux constitués d'un arrangement périodique de micro- et nano-grains, sous forme de super-réseaux ou de membranes [9–13], ou bien de cristaux colloïdaux [14–16]. Ces structures, composées de particules organisées de manière périodique, disposent de propriétés physiques remarquables (optique, thermique, acoustique, etc.) qui leur assurent un large domaine d'application : micro et nano-électroniques, photonique et interaction photon/phonon.

Les cristaux phononiques granulaires, étudiés dans ce travail de thèse, sont des matériaux singuliers car ils allient à la fois les propriétés des milieux granulaires et les propriétés des milieux périodiques. Les milieux granulaires présentent des comportements physiques spécifiques ; ils peuvent avoir un comportement de gaz (chocs de billes en mouvement dans une boîte), de fluide (grains du sablier) ou bien de solide (sable mouillé). En conséquence, ces milieux sont étudiés dans de nombreuses branches de l'industrie (agro-alimentaire, pharmaceutique, génie civil des matériaux etc.). En vue de décrire le comportement acoustique/vibratoire des cristaux phononiques granulaires, il est nécessaire de décrire le contact entre les particules caractérisant leur interaction. Ce contact s'effectue à l'échelle microscopique et contribue au comportement macroscopique de l'assemblage. Selon l'importance relative des différents couplages, l'interaction entre les différents mouvements des particules peut produire une variété de courbes de dispersion. Les particules forment une structure cristalline qui possède des symé-

tries. Elles confèrent un caractère discret au matériau, induisant notamment une forte dispersion dans la propagation des différents modes acoustiques. Dans le cadre d'une étude acoustique, l'arrangement périodique des cristaux granulaires autorise, sous certaines hypothèses, l'utilisation des mêmes outils que ceux développés pour les cristaux. Des analogies importantes peuvent être faites avec les cristaux photoniques en optique, ainsi qu'avec la théorie harmonique du cristal en physique du solide [17].

Pour décrire le comportement hautes fréquences (petites longueurs d'onde) de ce type de structure, l'approximation continue de la théorie de l'élasticité devient inexacte car la nature discrète du milieu doit explicitement être prise en compte. Pour la plupart des structures discrètes, les particules peuvent être considérées comme des masses discrètes interagissant entre elles. Pour modéliser le comportement élastique d'un milieu granulaire composé de particules de tailles finies, il devient nécessaire de prendre en compte les dimensions des particules ainsi que leurs degrés de liberté en rotation. Dans l'élasticité classique, les rotations des éléments infinitésimaux ne sont pas considérées. Une généralisation de la théorie classique de l'élasticité prenant en compte ces degrés de liberté additionnels, appelée théorie de Cosserat ou théorie micropolaire, a été proposée pour la première fois par les frères Cosserat en 1909 [18]. Elle a été adaptée à la description des milieux granulaires à partir des années 1980. Des modèles de milieux granulaires composés de particules disposées de manière périodique ont été développés pour extraire, dans la limite grandes longueurs d'onde, l'origine physique des constantes élastiques utilisées dans la théorie de Cosserat d'un continuum élastique. Cependant, lorsque la longueur d'onde devient du même ordre de grandeur que la taille des particules, ces théories ne décrivent plus correctement le caractère dispersif associé aux structures phononiques. Des modes de rotation et des modes couplés rotation/translation ont été mis en évidence théoriquement et expérimentalement dans un cristal phononique granulaire tridimensionnel [19]. La comparaison théorique de la propagation des ondes dans ce cristal granulaire avec celle dans un milieu de Cosserat a démontré que pour décrire correctement le comportement du milieu pour de petites et grandes longueurs d'onde, la théorie de Cosserat doit être combinée avec des modèles micropolaires d'ordres supérieurs [20].

Ce travail de thèse porte sur l'étude de la propagation d'ondes de volume, localisées et de surface dans des cristaux phononiques granulaires dans un régime linéaire. Différents aspects sont développés dans ce manuscrit. Les conséquences de la prise en compte des degrés de liberté en rotation des particules sur la structure de bandes de différents cristaux phononiques granulaires sont étudiées. En effet, l'introduction de ces degrés de liberté additionnels rend possible l'existence de modes de rotation qui interagissent fortement avec les modes transverses. Cela produit une variété de structure de bandes. L'influence de ces degrés de liberté supplémentaires est étudiée dans des cristaux phononiques granulaires qui diffèrent dans leur structure, dans la forme et l'arrangement des particules les constituant, ainsi que dans les mécanismes d'interaction entre les particules. Ce travail s'intéresse aussi à l'effet de conditions aux limites appliquées aux frontières de ces cristaux dans le but d'étudier l'existence de modes localisés ou de modes de surface dans ces structures, ainsi que dans le but de comparer les théories développées avec les prédictions de la théorie de Cosserat.

Cette thèse est composée de quatre chapitres. Une revue non exhaustive des recherches sur les milieux périodiques ainsi que sur les cristaux phononiques granulaires est présentée dans le premier chapitre. Quelques notions utiles à la compréhension des outils utilisés pour décrire la propagation dans

un cristal phononique granulaire ainsi que l'importance de la prise en compte des degrés de liberté en rotation des particules sont aussi exposées.

Le deuxième chapitre est consacré à l'étude d'une chaîne phononique granulaire monoatomique composée de particules possédant un degré de liberté en rotation et un degré de liberté en translation. Deux modes propagatifs et dispersifs sont prédits dans cette chaîne. En considérant la chaîne semi-infinie avec une condition aux limites appliquées à son extrémité, le modèle analytique démontre l'existence de modes localisés, chaque mode étant composé de deux modes évanescents. Les caractéristiques de ces modes (condition d'existence, fréquence, décroissance spatiale...) sont analysées en fonction du type de conditions aux limites appliquées ainsi qu'en fonction des différentes interactions entre les particules. Cette étude, portant sur une structure simple, est un premier pas vers l'étude de modes de surface dans des structures plus complexes.

Une description théorique des modes se propageant dans un cristal phononique granulaire bidimensionnel est ensuite présentée au troisième chapitre. Les particules possèdent trois degrés de liberté, deux en translation et un en rotation. L'analyse des interactions entre ondes de translation et ondes de rotation permet de mettre en évidence une grande richesse de structure de bandes ainsi que des phénomènes particuliers : bandes interdites complètes, cône de Dirac, modes non-monotones et phénomène de double réfraction.

Dans le dernier chapitre, une analyse de l'existence d'ondes à la surface mécaniquement libre de deux cristaux phononiques granulaires est présentée. Selon le type de degré de liberté des particules, des ondes de type Rayleigh ou des ondes de type cisaillement horizontal sont analysées. Une comparaison des résultats de la théorie développée avec les prédictions d'ondes acoustiques à la surface libre des milieux de Cosserat, ouvre la possibilité d'établir les limites de la théorie de Cosserat dans la description des ondes de surface dans les milieux micro- et nano-inhomogènes.

Bibliographie

[1] P. Sheng. Metamaterials : Acoustic lenses to shout about. *Nature Materials*, 8 :928–929, 2009.

[2] Y. Pennec, J.O. Vasseur, B. Djafari-Rouhani, L. Dobrzynski, and P.A. Deymier. Two-dimensional phononic crystals : Examples and applications. *Surface science reports*, 65 :229–291, 2010.

[3] J.B. Pendry. Negative refraction makes a perfect lens. *Phys. Rev. Lett.*, 85 :3966–3969, October 2000.

[4] N. Fang, H. Lee, C. Sun, and X. Zhang. Sub-diffraction-limited optical imaging with a silver superlens. *Science*, 308 :534, 2005.

[5] J. Mahanty, A.A. Maradudin, and G.H. Weiss. Vibrational thermodynamic properties of lattices with defects. *Progress of theoretical physics*, 20 :1–26, September 1958.

[6] V. Keppens, D. Mandrus, B.C. Sales, B.C. Chakoumakos, P. Dai, R. Coldea, M.B. Maple, D.A. Gajewski, E.J. Freeman, and S. Bennington. Localized vibrational modes in metallic solids. *Nature*, 395 :876–878, 1998.

[7] J. Mock, T. Hill, Y.-J. Tsai, A. Chilkoti, and D.R. Smith. Probing dynamically tunable localized surface plasmon resonances of film-coupled nanoparticles by evanescent wave excitation. *Nano Letters*, 12(4) :1757–1764, April 2012.

[8] R.F. Wallis. Theory of surface modes of vibration in two- and three- dimensional crystal lattices. *Phys. Rev.*, 116 :302–308, 1959.

[9] E.V. Shevchenko, D.V. Talapin, C.B. Murray, and S.O'Brien. Structural characterisation of self-assembled multifunctional binary nanoparticles. *Journal of the American Chemical Society*, 128 :3620–3637, 2006.

[10] K.E. Mueggenburg, X.-M Lin, R.H. Goldslith, and H.M. Jaeger. Elastic membranes of close-packed nanoparticle arrays. *Nature Materials*, 6 :656–660, 2007.

[11] W. Cheng, M.J. Campolongo, J.J. Cha, S.J. Tan, C.C. Umbach, D.A. Miller, and D. Luo. Free standing nanoparticle superlattice sheets controlled by DNA. *Nature Materials*, 8 :519–525, 2009.

[12] A. Dong, J. Chen, P.M. Vora, J.M. Kikkawa, and C.B. Murray. Binary nanocrystal superlattice membranes self-assembled at the liquid-air interface. *Nature (London)*, 466 :474–477, 2010.

[13] E. Auyeun, J.I. Cutler, R.J. Macfarlane, M.R. Jones, J. Wu, G. Liu, K. Zhang, D. Osberg, and C.A. Mirkin. Synthetically programmable nanoparticle superlattices using a hollow three-dimensional spacer approach. *Nature Nanotechnologies*, 7 :24–28, 2012.

[14] A. Van Blaaderena, R. Ruel, and P. Wiltzius. Template-directed colloidal crystallisation. *Nature (London)*, 385 :321323, 1997.

[15] Z. Cheng, W.B. Russel, and P.M. Chaikin. Controlled growth of hard-sphere colloidal crystals. *Nature (London)*, 401 :893–895, 1999.

[16] J.D. Joannopoulos. Self-assembly lights up. *Nature*, 414 :257–258, 2001.

[17] N.W. Ashcroft and N.D. Mermin. *Solid States Physics*. Saunders College Publishing, Philadelphia, 1976.

[18] E. Cosserat and F. Cosserat. *Théorie des corps déformables*. Herman et Fils, Paris, 1909.

[19] A. Merkel, V. Tournat, and V.E. Gusev. Experimental evidence of rotational elastic waves in granular phononic crystals. *Phys. Rev. Lett.*, 107(22) :225502, 2011.

[20] A.A. Vasiliev, A.E. Miroshnichenko, and M. Ruzzene. Multifield model for Cosserat media. *Journal of mechanics of materials and structures*, 3 :1365, 2008.

Chapitre 1

Propagation des ondes acoustiques dans les cristaux phononiques granulaires

1.1 Introduction

Les cristaux phononiques granulaires sont des arrangements périodiques de particules pouvant être de différentes formes. Ce sont des matériaux biphasiques avec une phase solide composée par les grains et une phase fluide représentant le fluide saturant les pores entre les grains. L'intérêt considérable pour la propagation des ondes dans les milieux périodiques allié aux propriétés des milieux granulaires, a grandement motivé les recherches sur les cristaux phononiques granulaires ces dernières années.

Ce premier chapitre, à caractère introductif, présente tout d'abord un état de l'art non exhaustif des recherches menées sur les milieux périodiques et les cristaux phononiques granulaires permettant de situer le contexte de cette étude. En particulier, l'importance de la prise en compte des degrés de liberté de rotation des particules est présentée. Le comportement macroscopique d'un arrangement granulaire dépend de l'interaction mécanique au niveau microscopique entre les grains. La modélisation de cette interaction est présentée dans les cas de particules sphériques et cylindriques en contact. Enfin, les propriétés de la propagation acoustique linéaire dans une chaîne périodique monoatomique et diatomique de sphères sont décrites. Ces cas simplifiés sont présentés dans le but de se familiariser avec les outils permettant de modéliser la propagation des ondes dans les cristaux phononiques granulaires.

1.2 Propagation des ondes dans les milieux périodiques

L'idée du caractère discret de la propagation des ondes est due à Newton qui faisait l'hypothèse que le son se propage dans l'air de la même façon que les ondes élastiques se propagent dans un réseau de masses ponctuelles [1]. Dès lors, de multiples recherches se sont attelées à la compréhension de la propagation de nombreux types d'ondes dans des structures périodiques. Les plus anciens travaux concernent la propagation des ondes dans les solides cristallins, telle que l'étude de la propagation d'électrons dans des semi-conducteurs. Ce concept intervient aussi par exemple lors de l'étude de la diffraction des rayons X ou des ondes optiques en milieu solide ou liquide, des systèmes multicouches ou super-réseaux, très prisés dans les domaines optiques et acoustiques. Le phénomène le plus commun existant dans ces structures est la présence de bandes de fréquences interdites. Ces bandes interdites proviennent de la diffraction des ondes par la structure périodique et des phénomènes d'interférences destructives qui en résultent. Les ondes dont la fréquence est située dans une bande interdite ne peuvent

pas se propager dans le cristal, leur énergie est alors principalement réfléchie par celui-ci.

Dans le domaine de l'optique, l'attention s'est notamment portée sur la recherche de larges bandes interdites dans la structure de bande de matériaux périodiques diélectriques. Ces matériaux sont appelés cristaux photoniques et ont été proposés sous différentes géométries : des systèmes de la forme de matrice de Bragg unidimensionnels [2, 3], des systèmes bidimensionnels (2D) composés de cylindres intégrés dans une matrice ou des cristaux tridimensionnels (3D) avec une distribution périodique de sphères [4–6].

L'analogie mathématique entre les équations de Maxwell et les équations de l'élasticité linéaire a mené les chercheurs à étudier ce type de structure, appelée alors cristaux phononiques dans le domaine de l'acoustique. Dans les cristaux phononiques, la densité ainsi que les constantes élastiques sont des fonctions périodiques de l'espace. Ces dernières années, la recherche de bandes interdites acoustiques dans les milieux hétérogènes a suscité un grand nombre d'investigations théoriques, numériques et expérimentales allant des échelles macroscopique à nanoscopique. Le concept de cristaux phononiques a été introduit de façon quasiment simultanée par Kushwaha et al. [7] d'une part, et Economou et Sigalas [8, 9] d'autre part en 1993. Ces auteurs mirent en évidence les propriétés liées à la périodicité du matériau ainsi que les possibilités d'applications prometteuses des cristaux phononiques : structures anti-vibratoires, système d'isolation phonique, structures anti-sismiques ou encore filtrage, etc. La première démonstration expérimentale de l'effet d'une structure phononique sur la propagation du son a été réalisée sur une sculpture minimaliste de l'espagnol Eusebio Sempere exposée à la Juan March Fundation à Madrid [10]. Une diminution du niveau du signal transmis, correspondant à une bande interdite directionnelle a été constatée autour de 2 kHz à la sortie de la sculpture. Suite à cette première observation encourageante, des composites périodiques présentant des bandes interdites complètes ont été conçus et étudiés expérimentalement [11, 12]. Divers cristaux phononiques ont par la suite été étudiés. Parmi eux, on peut trouver des systèmes composites inclusions-matrice fluides-fluide, solides-fluide ou solides-solide. Dans tous les cas, l'apparition des bandes interdites est liée à l'arrangement, à la géométrie des inclusions, à la périodicité, mais aussi au contraste entre les matériaux constituant les inclusions et la matrice. Les ondes dont la fréquence est située dans une bande interdite seront réfléchies par le cristal.

L'un des avantages de l'acoustique par rapport aux domaines optiques et électroniques, réside dans la possibilité d'observer ces effets de bandes interdites élastiques sur de vastes gammes de fréquences, autorisant la fabrication de dispositifs macroscopiques et élargissant leur champ d'application. Celui-ci s'étend de l'atténuation des ondes sismiques, au filtrage radio-fréquence, en passant par l'isolation phonique ou les interactions acousto-optiques. Outre la présence de bandes de fréquence interdites, d'autres phénomènes sont rencontrés dans ces structures. Parmi eux, les phénomènes de guidage des ondes tels que la réfraction négative [13], l'effet de superprisme [14], d'auto-collimation [15] et de focalisation [16] peuvent être cités. L'idée est d'étudier l'effet de courbure des courbes équifréquences [17] pour contrôler la dispersion spatiale des ondes à l'intérieur de la structure périodique. D'un autre côté, la linéarité des courbes de dispersion à grandes longueurs d'onde a motivé l'application des théories d'homogénéisation [18] dans le but de définir des paramètres effectifs caractérisant le système. La présence de bandes interdites a aussi motivé l'analyse de modes localisés ou modes de défaut [19–21]. L'existence

de ces modes est liée à la possibilité de contrôler les propriétés évanescentes des ondes dans les composites périodiques. Une imagerie *super-résolution* [22, 23] peut alors être obtenue en couplant les modes évanescents avec d'autres mécanismes permettant leur amplification afin de transporter l'information des ondes évanescentes dans le système.

1.3 États de l'art des études sur les cristaux phononiques granulaires

Les phénomènes se produisant dans les cristaux granulaires, non seulement dans les régimes fortement non linéaires, mais aussi dans les régimes faiblement non linéaires et linéaires, ont reçu un intérêt considérable et font aujourd'hui l'objet de recherches très actives. La capacité d'utiliser une large gamme de matériaux, de tailles et de types de particules, ainsi que la réponse optimisable entre régime linéaire et fortement non linéaire, est un paradigme pour l'exploration physique de la propagation des ondes dans ces structures. Les premiers travaux sur des milieux granulaires ordonnés ont porté sur des chaînes granulaires.

1.3.1 Chaînes granulaires

L'étude des cristaux granulaires a émergé dans les années 1983 avec les travaux de V.F. Nesterenko et A.N. Lazaridi sur des chaînes granulaires monodimensionnelles [24, 25]. Dès lors, l'intérêt s'est grandement porté sur les comportements physiques de ces structures. Nesterenko étendit ses travaux portant sur l'existence d'ondes solitaires et d'ondes de choc (phénomène de vide sonique) aux chaînes granulaires fortement non linéaires [26]. L'étude de ces milieux fortement non linéaires a notamment abouti à l'observation d'absorbeur de choc [27] et d'effet de diode acoustique [28]. Les non linéarités existant dans ces milieux résultent du contact Hertzien entre deux particules. La réponse dynamique de ce type de système peut être contrôlée afin de passer d'un régime linéaire à un régime faiblement ou fortement non linéaire. Des chaînes contraintes [29, 30] et non contraintes [24, 29] ont été étudiées dans le but d'élucider les importantes différences entre les réponses linéaires et non linéaires observées dans les systèmes granulaires.

Différents aspects de la propagation dans des chaînes fortement non linéaires ont été étudiés. Le fait de pouvoir contrôler la réponse dynamique des cristaux granulaires a été utile pour étudier les phénomènes non linéaires comme la génération d'harmoniques ou d'auto-démodulation [31–33]. Des analyses expérimentales, numériques et des méthodes analytiques ont été développées afin de décrire l'interaction d'ondes solitaires avec une interface [34], avec un défaut [35], et à l'interface entre deux cristaux granulaires [36]. Dans la continuité de ces travaux, une combinaison d'approches théoriques, numériques et expérimentales a été menée sur la propagation d'ondes solitaires dans des chaînes composées de particules en acier recouvertes d'une couche de polymère [37] et de particules en Téflon [38], ainsi que dans des chaînes désordonnées [39]. L'effet de la dissipation [40] dans des chaînes de sphères composées d'une variété de matériaux (acier, Téflon, cuivre), a été étudié à partir de résultats expérimentaux et de simulations, afin d'améliorer la prise en compte de cet effet dans le modèle dynamique de Hertz.

Dans le domaine de la physique du solide, il est bien connu qu'une vibration localisée dans une matrice de particules peut exister en raison de la présence d'un désordre qui va briser la symétrie

parfaite du cristal. Suivant la même idée, des modes localisés dus à la présence de défauts ont été révélés dans des chaînes granulaires faiblement non linéaires [35, 41–43]. L'association des effets non linéaires au phénomène de localisation de l'énergie rend ces études particulièrement pertinentes [44] pour la conception de nouveaux dispositifs de filtrage [45]. L'existence de modes localisés a aussi été étudiée théoriquement et expérimentalement dans des chaînes linéaires de sphères diatomiques collées [46], soudées [47] ou bien comprimées [30]. Les chaînes granulaires linéaires ont fait l'objet de nombreux travaux analytiques, expérimentaux et numériques. Ces systèmes présentent en particulier des propriétés de bandes interdites accordables. L'existence de sub-résonances dans une chaîne de sphères identiques liées aux modes résonants d'une sphère individuelle a aussi été démontrée [48].

1.3.2 Cristaux phononiques granulaires bi- et tridimensionnels

L'étude de cristaux phononiques granulaires bidimensionnels et tridimensionnels est un peu moins développée. Ceci est en particulier dû aux difficultés expérimentales rencontrées lorsqu'il s'agit d'assembler un cristal "parfait". Néanmoins, un renouveau d'intérêt concernant les modèles discrets appliqués à des structures de plus grande dimensionalité a largement été stimulé par les récents progrès de fabrication de nouveaux matériaux constitués d'un arrangement périodique de micro- et nano-grains sous forme de super-réseaux ou de membranes [49–53], ou bien de cristaux colloïdaux [54–56].

Les analyses de cristaux granulaires 2D utilisant des techniques photoélastiques font partie des premiers travaux expérimentaux [57, 58]. Différents aspects influençant la propagation des ondes dans un assemblage de disques et de particules elliptiques ont été étudiés tels que l'effet de la disposition géométrique des particules [59], le rôle de la forme des particules [60] et la présence de défauts dans les particules [61]. Une autre géométrie alternative de chaînes constituées de sphères magnétiques a été mise en oeuvre dans des structures 1D et 2D [62]. L'effet de modulation de la magnétisation permettant de maintenir la cohésion entre les particules a notamment été mis en évidence. Des études ont été conduites sur des cristaux granulaires hexagonaux fortement comprimés, où l'effet de la force de précontrainte statique sur le comportement (Hertzien ou non Hertzien) du système a été présenté [63, 64]. La réponse dynamique d'un cristal granulaire 2D soumis à un impact a aussi été révélée expérimentalement et numériquement via des méthodes par éléments discrets (DEM) [65, 66]. La propagation d'ondes élastiques dans un cristal granulaire 2D, non linéaire et soumis à différentes contraintes a été étudiée expérimentalement et numériquement [67, 68]. La possibilité de contrôler les propriétés du front d'onde dans le cristal granulaire a été démontrée. L'effet de la déformation d'un cristal granulaire sous une compression uniaxiale sur la bande interdite a été reporté expérimentalement et numériquement [69]. Les résultats permettent d'envisager de nouvelles directions d'étude pour la création de matériaux mous avec des propriétés acoustiques et optiques optimisées. Un cristal phononique formé d'une colonne de particules cylindriques disposées orthogonalement sous la forme d'un tas de bois (*woodpile phononic crystals*) a récemment été étudié [70]. Les modes propres de flexion des particules cylindriques permettent d'obtenir des résonances locales, la structure présentant alors des propriétés de bandes interdites optimisables.

Bien que l'approche théorique de l'analyse des ondes acoustiques dans les milieux discrets et périodiques ait été traitée auparavant [71], les analyses de structures 2D et 3D composées de particules de taille finie ont été limitées pour la plupart à l'étude des propriétés des modes acoustiques de type

longitudinal et de cisaillement [72–75] ainsi qu'aux modes guidés de cisaillement dans les cristaux granulaires inhomogènes [76–78]. Depuis seulement quelques années, les modes rotationnels et couplés translation/rotation ont été inclus dans les analyses [79–82]. La description de la propagation des ondes de volume dans un cristal hexagonal compact de billes a été réalisée [79–81]. L'analyse théorique permet de démontrer la nécessaire prise en compte des degrés de liberté de rotation dès que la friction est mise en jeu. Ce travail a en particulier mis en évidence la propagation de modes rotationnels et couplés rotation/translation expérimentalement. Lors de simulations numériques, les relations de dispersion des modes rotationnels ont été mises en évidence dans un cristal cubique à faces centrées [83]. Un modèle discret 2D avec des particules possédant un degré de liberté en translation et deux degrés de liberté en rotation a permis d'analyser le comportement d'une membrane granulaire formée d'une couche de particules [82]. En particulier, le mouvement hors plan prenant en compte la rotation des particules a été étudié pour la première fois.

1.4 Importance des degrés de liberté en rotation des particules

Plusieurs travaux ont démontré que la prise en compte de la rotation des inclusions pouvait modifier la propagation des modes volumiques dans une structure phononique [84–89]. La résonance des modes de rotation peut interagir fortement avec les bandes de Bragg, ce qui mène à de larges bandes interdites d'hybridation [87]. L'idée de prendre en compte ces degrés de liberté additionnels revient aux travaux des frères Cosserat [90]. En 1909, ils développent une généralisation de la théorie de l'élasticité, appelée théorie de Cosserat ou théorie micropolaire, dans le but de prendre en compte l'effet de la microstructure des matériaux sur la propagation des ondes. Le modèle classique s'applique à un milieu où non seulement les déplacements, mais aussi les rotations d'éléments structuraux doivent être pris en compte. On compte parmi ces applications les milieux granulaires [91–93], les matrices sous forme de poutres (*beam lattices*) [94], les matériaux auxétiques [95], les matériaux de structures chirales [96], les cristaux liquides ou bien les cristaux diélectriques [97, 98].

Dans cette théorie, chaque particule possède six degrés de liberté, trois en translation et trois en rotation. Le mouvement libre du continuum élastique est décrit par les équations, pour le vecteur déplacement $\mathbf{u}$ et le vecteur rotation $\boldsymbol{\phi}$ [99, 100]

$$\rho\frac{\partial^2 u_i}{\partial t^2} = \frac{\partial \sigma_{ij}}{\partial x_j}, \quad I\frac{\partial^2 \phi_i}{\partial t^2} = \frac{\partial M_{ij}}{\partial x_j} + E_{ijk}\sigma_{jk} \ , \tag{1.1}$$

où ρ est la masse volumique du matériau, I le moment d'inertie et E_{ijk} le tenseur de Levi-Civita d'ordre trois. Dans le cas d'un matériau isotrope et centrosymétrique, le tenseur des contraintes σ_{ij} et le tenseur des moments M_{ij} sont reliés aux gradients des composantes des vecteurs $\mathbf{u}$ et $\boldsymbol{\phi}$ par

$$\begin{aligned} \sigma_{ij} &= 2\mu\epsilon_{(ij)} + 2\alpha\epsilon_{<ij>} + \lambda\epsilon_{kk}\delta_{ij} \ , \\ M_{ij} &= 2\gamma\Phi_{(ij)} + 2\varepsilon\Phi_{<ij>} + \beta\Phi_{kk}\delta_{ij} \ , \end{aligned} \tag{1.2}$$

où $\epsilon_{ij} = \partial u_i/\partial x_j + \epsilon_{ijk}\phi_k$, et $\Phi_{ij} = \partial\phi_i/\partial x_j$. Les parenthèses () et <> définissent les parties symétrique et antisymétrique des tenseurs, respectivement.

En plus des constantes μ et λ similaires aux constantes de Lamé et de la masse volumique du matériau ρ, la microstructure est caractérisée par quatre constantes élastiques γ, β, ε et α ainsi que par

le moment d'inertie I. Lorsque le tenseur des moments est absent, c'est-à-dire lorsque les constantes élastiques γ, β et ε sont négligeables par rapport à la constante α, la différence fondamentale entre la théorie de Cosserat et la théorie classique de l'élasticité réside seulement dans les valeurs non nulles du moment d'inertie et de la constante élastique α, ce qui induit une asymétrie du tenseur des contraintes. C'est le cas par exemple d'un matériau où les rigidités de flexion et de torsion entre les particules sont négligées. La théorie de Cosserat est alors appelée théorie de Cosserat réduite [101–103]. La prise en compte de la rotation a deux effets majeurs sur la propagation des ondes : la présence de modes rotationnels et l'interaction avec les modes transverses. En revanche, la rotation n'a aucune influence sur les ondes longitudinales ou de compression. Si une contrainte isotrope est appliquée sur l'assemblage, les rotations des billes ne sont pas sollicitées [92].

Le formalisme de Cosserat a été adapté à la description des milieux granulaires à partir des années 1980 [104–106]. Cependant, il n'y a jamais eu de preuves expérimentales indiscutables de sa validité dans ces milieux. Ceci est en partie lié au manque d'informations concernant les valeurs des constantes élastiques γ, β, ε et α pour des matériaux réels. La prise en compte des degrés de liberté en rotation est importante dans un milieu granulaire. Négliger la rotation dans un assemblage granulaire revient à rigidifier artificiellement la structure et peut conduire à des résultats erronés. En effet, contrairement à un matériau classique où la taille des particules est négligeable par rapport aux distances entre les atomes, dans un milieu granulaire, cette taille est comparable à la distance entre deux grains. Les forces s'appliquent aux niveaux des contacts et le contact entre deux billes fait apparaître une rigidité perpendiculaire à l'axe reliant leur centres. Les degrés de liberté en rotation doivent alors être traités au même niveau que les degrés de liberté en translation. L'existence de modes de rotation et couplés rotation/translation a été prouvée dans un cristal phononique granulaire 3D, Fig. 1.1. La comparaison théorique de la propagation des ondes dans un cristal granulaire avec celle dans un milieu de Cosserat a démontré que la théorie de Cosserat ne permet pas de prendre correctement en compte les inhomogénéités du matériau [81]. Pour autant, ces travaux ont montré que cette théorie généralisée pouvait décrire le comportement des milieux granulaires aux grandes longueurs d'onde. En revanche, l'échelle spatiale des inhomogénéités devrait intervenir afin de prendre en compte les effets dus à la diffusion multiple dans le milieu [80, 81]. Afin de décrire correctement le comportement du milieu pour de petites et grandes longueurs d'onde, la théorie de Cosserat ou théorie micropolaire doit être combinée avec des modèles micropolaires d'ordres supérieurs [107]. Ces aspects seront développés dans le chapitre 4.

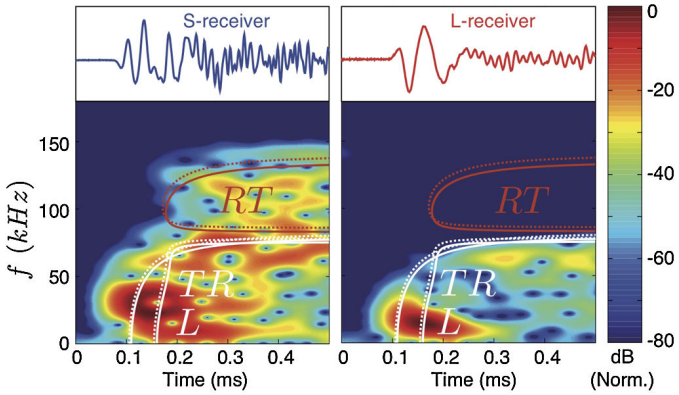

Figure 1.1 – Mise en évidence expérimentale des modes couplés de rotation/translation (TR/RT) et des modes longitudinaux (L) dans un cristal phononique granulaire hexagonal. Signaux mesurés avec un transducteur en cisaillement (à gauche) et avec un transducteur longitudinal (à droite) après transmission à travers le cristal [81].

1.5 Description mécanique du contact entre deux particules

Le comportement du contact entre deux sphères identiques de rayon R peut être décrit par la théorie de Hertz-Mindlin. La première description du contact entre deux sphères a été réalisée par Hertz [108] en 1881. Il étudiait les franges d'interférences optiques de Newton entre deux lentilles de verre en contact, dont la surface subissait une déformation élastique due à leur contact mutuel sous pression. Il a en particulier résolu le problème du contact entre deux sphères élastiques soumises à une contrainte axiale, c'est-à-dire une contrainte dirigée selon l'axe formé par les deux centres des billes [109]. Cette théorie a ensuite été étendue par Mindlin qui a formulé une théorie éponyme en prenant en compte les forces tangentielles en plus des forces normales entre les deux sphères [72, 109–111].

1.5.1 Théorie du contact de Hertz-Mindlin

Les hypothèses de la théorie de Hertz-Mindlin sont les suivantes. La surface de contact est plane, ce qui permet de découpler les relations force-déplacement normales des relations tangentielles. Cette surface est de forme elliptique dans le cas général. Pour le calcul des déformations locales, chaque sphère est vue comme un demi-espace élastique linéaire, chargée sur une petite région elliptique de sa surface plane. Sous cette hypothèse, les contraintes, qui sont concentrées au niveau des contacts, sont traitées indépendamment de la distribution générale de contraintes entre les deux sphères. Pour que cette simplification soit justifiée, les régions de contact doivent être petites devant les rayons des sphères.

La figure 1.2 présente un schéma du contact entre deux billes. La composante normale du champ de contraintes est maximum au centre du contact et s'annule à la périphérie. Le rayon r de la surface de contact entre deux sphères identiques s'écrit

$$r = \left(\frac{3(1-\nu^2)aN}{8E} \right)^{1/3} , \tag{1.3}$$

où a est le diamètre des billes, N la force normale appliquée sur les contacts, ν et E sont respectivement le coefficient de Poisson et le module d'Young du matériau constituant les billes. La relation entre le

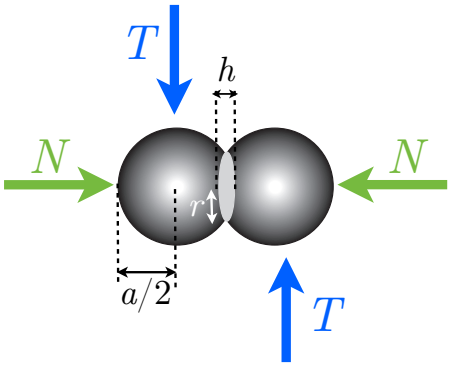

Figure 1.2 – Schéma du contact entre deux sphères.

déplacement relatif des billes h et la composante normale de la force appliquée N s'écrit alors

$$h = 2\left[\frac{3}{4}\frac{(1-\nu^2)N}{E\sqrt{a/2}}\right]^{2/3} . \tag{1.4}$$

Cette relation force-déplacement est fortement non linéaire puisque le déplacement est proportionnel à la puissance 2/3 de la force normale appliquée. Dans ce cas, les non linéarités proviennent de la géométrie du contact et augmentent avec la force de compression appliquée.

Si une force tangentielle T est appliquée en plus de la force normale, elle cause une déformation élastique à l'interface. Dans le cas où il n'y a pas de glissement au niveau du contact, les déplacements tangentiels de tous les points de la zone de contact sont identiques. Lorsque le glissement est pris en compte, la relation entre le déplacement relatif tangentiel des billes δ, la force T et la force normale N s'écrit

$$\delta = \mu_f(2-\nu)(1+\nu)\left(\frac{9}{8}\frac{N^2}{a(1-\nu^2)E^2}\right)^{1/3}\left[1-\left(1-\frac{T}{\mu_f N}\right)^{2/3}\right] , \tag{1.5}$$

où μ_f est le coefficient de friction du matériau constituant les billes. D'après la loi de Coulomb, si $T < \mu_f N$, les deux billes restent en contact. La relation (1.5) est aussi non linéaire et les possibilités de glissement peuvent faire apparaître un comportement hystérétique du contact selon le chargement axial ou tangentiel et le chemin de variation de ces contraintes [109, 111].

Dans le cas d'un système en équilibre, chaque contact peut être considéré comme deux ressorts, un premier ressort décrivant les interactions normales, de raideur

$$\xi^N = \left(\frac{3a}{8}N\right)^{1/3} E^{2/3}(1-\nu^2)^{-2/3} , \tag{1.6}$$

et un second ressort décrivant les interactions transverses, de raideur

$$\xi^S = (3aN)^{1/3}E^{2/3}\frac{(1-\nu^2)^{1/3}}{(1+\nu)(2-\nu)} . \tag{1.7}$$

1.5.2 Cas particulier des particules cylindriques

La zone de contact créée par la compression de deux cylindres dépend de l'angle d'orientation α entre les axes des deux cylindres. Pour de petites déformations, la zone de contact peut être circulaire

($\alpha = 90°$), elliptique ($0° < \alpha < 90°$) ou rectangulaire ($\alpha = 0°$). Dans les deux premiers cas, le contact entre deux particules peut être décrit par la loi de Hertz. La relation entre la force de contact F et le déplacement normal δ_c relatif entre deux cylindres identiques en compression est donnée par [109]

$$F = \frac{4}{3}\frac{\sqrt{R_e}E^*}{F_2^{3/2}}\delta_c^{3/2} = \xi_{cyl}^N\,\delta_c^{3/2}\ , \tag{1.8}$$

où $R_e = R_c/\sin\alpha$ est un rayon équivalent avec R_c le rayon des cylindres, E^* est le module effectif défini par $E^* = \dfrac{E}{2(1-\nu^2)}$. Le facteur de correction F_2 dépendant de l'excentricité de la zone elliptique $\epsilon = \sqrt{1-(b/a)^2}$ est défini par

$$F_2 = \frac{2}{\pi}K(\epsilon)\left[\frac{4}{\pi\epsilon^2}\sqrt{\left[\left(\frac{a}{b}\right)^2 E(\epsilon) - K(\epsilon)\right][K(\epsilon) - E(\epsilon)]}\right]^{-1/3}\ , \tag{1.9}$$

où $K(\epsilon)$ et $E(\epsilon)$ sont respectivement des intégrales elliptiques complètes de première et deuxième espèces, a et b sont la demi-longueur et demi-largeur de la zone elliptique de contact avec $\dfrac{b}{a} \approx \left(\dfrac{1+\cos\alpha}{1-\cos\alpha}\right)^{-2/3}$. Par exemple, dans le cas $\alpha = 90°$, $F_2 = 1$. Ces modèles sont valides lorsque l'aire de contact entre les cylindres est très petite par rapport à leur rayon, ce qui assure que chaque cylindre peut être considéré comme un demi-espace élastique.

Lorsque $0° < \alpha < 90°$, le comportement du contact en compression peut être généralisé sous la forme d'une loi de puissance du type

$$F = \xi_{cyl}^N(\alpha)\,\delta_c^{n(\alpha)}\ , \tag{1.10}$$

avec l'exposant n dépendant de l'angle α, Fig. 1.3(c). Lorsque $\alpha \to 90°$, la valeur de n est proche de $3/2$, et l'équation (1.10) se rapproche de la loi de comportement Hertzienne non linéaire du cas de deux sphères en contact.

Lorsque $\alpha = 0°$, les deux cylindres sont parallèles. L'aire de contact se réduit à un rectangle de très petite largeur. Dans ce cas, pour deux cylindres parallèles de même rayon soumis à une force de compression F^* (où F^* est une force par unité de longueur), le déplacement δ_c est donné par [109]

$$\delta_c = 2F^*\frac{1-\nu^2}{\pi E}\left[2\ln\left(\frac{4R_c}{b}\right) - 1\right]\ , \tag{1.11}$$

où $b = \sqrt{\dfrac{4F^*R_c(1-\nu^2)}{\pi E}}$ est la demi-largeur de l'aire de contact. La force de contact est

$$F^* = \frac{\pi E}{1-\nu^2}\left[\frac{\delta_c}{2}\frac{1}{W\left(-\dfrac{e\delta_c}{8R_c}\right)}\right]\ , \tag{1.12}$$

où W est la fonction de Lambert et e est la constante de Neper.

Pour une chaîne de cylindres parallèles ($\alpha = 0°$) faiblement comprimée, le comportement du contact ne suit pas strictement une loi de puissance mais peut être approché par la formulation en loi de puissance donnée par l'équation (1.10) avec $n \simeq 1.15$ [112, 113]. Les différents comportements du

contact entre deux cylindres en compression sont illustrés en Fig. 1.3. Khatri et al. [113] ont comparé les résultats obtenus suivant la loi de Hertz avec les résultats de simulations par éléments finis pour différents angles d'orientation entre les axes des deux cylindres. Lorsque $\alpha \to 0°$, le comportement du contact devient linéaire.

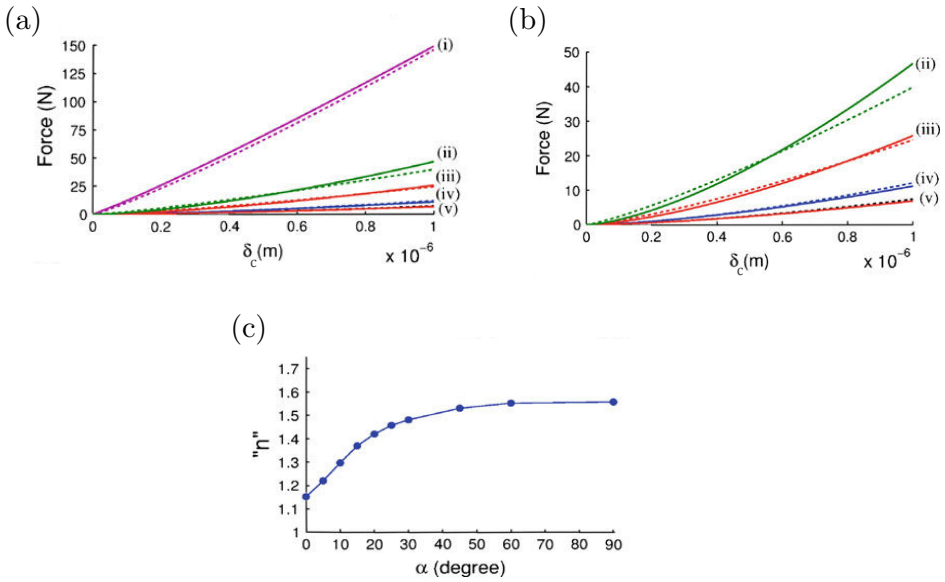

Figure 1.3 – (a) Comparaison des relations force/déplacement du contact entre deux cylindres obtenus avec la loi de Hertz (courbes solides) et par méthode éléments finis (courbes pointillées). Les résultats sont obtenus pour un contact entre les particules orientées avec $\alpha = 0°$ (groupe (i)), $\alpha = 5°$ (groupe (ii)), $\alpha = 10°$ (groupe (iii)), $\alpha = 30°$ (groupe (iv)) et $\alpha = 90°$ (groupe (v)), (b) Vue détaillée des cas $\alpha = 5°, 10°, 30°$ et $90°$, (c) Dépendance de l'exposant n de la loi de puissance Eq. (1.10) sur l'orientation α entre les cylindres. Ces figures sont extraites de [113].

Dans le cas d'une force tangentielle entre deux cylindres identiques parallèles, la rigidité transversale est donnée par [109]

$$\xi^s_{cyl} = \frac{GL}{(1-\nu/2)}\frac{1}{F_2}\ , \tag{1.13}$$

avec G le module de cisaillement, L la longueur des cylindres et F_2 le facteur de correction donné par l'équation (1.9).

1.6 Modélisation théorique de la propagation dans les chaînes granulaires

Une chaîne monodimensionnelle de sphères, étudiée en premier lieu par Nesterenko [24], représente le cas le plus simple de cristal granulaire que l'on peut rencontrer. La propagation d'ondes longitudinales dans une chaîne monoatomique et diatomique est brièvement décrite dans cette partie afin de rappeler les outils utilisés pour modéliser théoriquement la propagation des ondes dans un cristal granulaire.

1.6.1 Modes normaux de propagation dans une chaîne masses-ressorts monoatomique

Sous les hypothèses de la théorie de Hertz, c'est-à-dire de contraintes localisées au niveau du contact et de petites déformations, une chaîne de sphères identiques sous précontrainte est modélisée par une chaîne de masses ponctuelles reliées par des ressorts. Les fréquences considérées doivent être très inférieures à la fréquence de résonance d'une sphère. Une représentation schématique de ce problème est présentée sur la figure 1.4. Considérons une chaîne de masses identiques m_s, espacées d'une distance a égale au diamètre des sphères et reliées par des ressorts longitudinaux identiques de raideur ξ^n. Chaque sphère possède un degré de liberté en translation suivant l'axe de la chaîne. L'élongation des ressorts induit un déplacement longitudinal de chaque sphère i, notée u_i. Dans l'approximation linéaire, l'équation du mouvement de la particule centrale, notée n, du réseau périodique est donnée par [114]

$$m_s \frac{\partial^2 u_n}{\partial t^2} = \xi^n [u_{n+1} + u_{n-1} - 2u_n] \ , \tag{1.14}$$

où t est le temps. La relation de dispersion entre le nombre d'onde k et la pulsation ω s'obtient

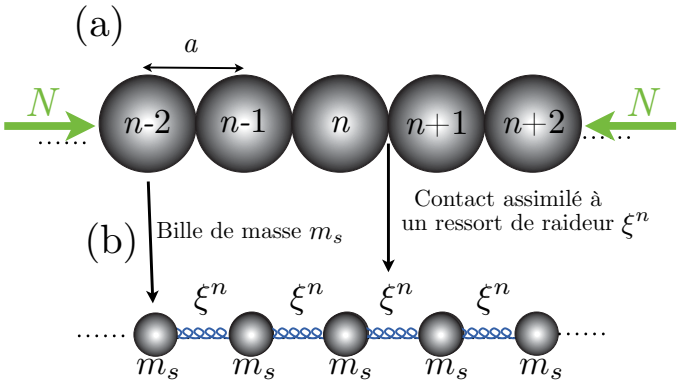

Figure 1.4 – (a) Représentation d'une chaîne monoatomique de sphères soumise à une force de compression N et (b) son réseau équivalent masses-ressorts.

en substituant un déplacement sous la forme $u_n = Ae^{i(\omega t - kna)}$, avec A l'amplitude de l'onde, dans l'équation du mouvement (1.14). Il vient

$$\omega^2 = \frac{4\xi^n}{m_s} \sin^2\left(\frac{ka}{2}\right) \ . \tag{1.15}$$

La solution de la relation de dispersion (1.15) est représentée sur la figure 1.5 pour des valeurs du nombre d'onde limitées à la première zone de Brillouin du réseau réciproque [1]. La pulsation de coupure de la chaîne, c'est à dire la pulsation au-delà de laquelle les modes acoustiques longitudinaux considérés deviennent évanescents, vaut alors

$$\omega_c = 2\sqrt{\frac{\xi^n}{m_s}} \ . \tag{1.16}$$

En dessous de cette pulsation de coupure $\omega \leq \omega_c$, le nombre d'onde est réel et s'écrit

$$k = \pm \frac{2}{a} \arcsin\left(\frac{\omega}{\omega_c}\right) \ , \tag{1.17}$$

où le signe "+" correspond aux ondes se propageant vers la droite (direction positive) et le signe "−" correspond aux ondes se propageant vers la gauche (direction négative). Dans la zone au-dessus de la

pulsation de coupure $\omega > \omega_c$, zone appelée bande interdite, le nombre d'onde est complexe et s'écrit

$$k = \frac{\pi}{a} - i\frac{2}{a}\text{arccosh}\left(\frac{\omega}{\omega_c}\right) \quad . \tag{1.18}$$

Cette dernière équation décrit la dispersion des modes évanescents qui sont atténués dans la direction positive, c'est-à-dire lorsque n augmente. La description complète de la relation de dispersion de la chaîne est donnée par la combinaison des équations (1.17) et (1.18).

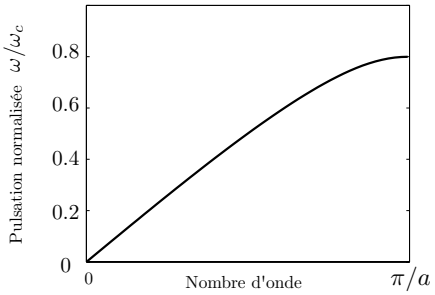

Figure 1.5 – Relation de dispersion du mode longitudinal d'une chaîne monoatomique.

1.6.2 Modes normaux de propagation dans une chaîne masses-ressorts diatomique

La chaîne diatomique représente le cas le plus simple d'un réseau de Bravais à motif. Le problème d'une chaîne, illustrée sur la figure 1.6, dont la cellule élémentaire comporte deux atomes de masses différentes m_s et M_s, reliés par un ressort longitudinal ξ^n permet de comprendre l'impact d'une cellule élémentaire comportant plusieurs atomes sur le spectre des modes normaux de vibrations. La taille de la cellule élémentaire est dans ce cas la distance séparant deux masses identiques. Il est alors nécessaire de décrire le déplacement d'une masse m_s, noté u_n, ainsi que le déplacement d'une masse M_s, noté U_n.

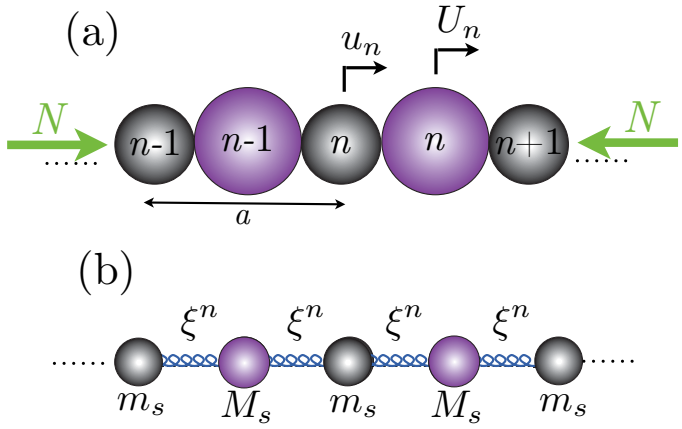

Figure 1.6 – (a) Représentation d'une chaîne unidimensionnelle diatomique de sphères soumise à une force de compression N et (b) son réseau équivalent masses-ressorts.

Les équations du mouvement pour chacune des masses constituant la cellule élémentaire s'écrivent [114]

$$m_s \frac{\partial^2 u_n}{\partial t^2} = \xi^n (U_{n-1} + U_n - 2u_n) \ , \tag{1.19a}$$

$$M_s \frac{\partial^2 U_n}{\partial t^2} = \xi^n (u_{n+1} + u_n - 2U_n) \ . \tag{1.19b}$$

Similairement au cas de la chaîne monoatomique, les solutions de la relation de dispersion, tracées en figure 1.7, sont obtenues en substituant les formes de solutions $u_n = Ae^{i(\omega t - kna)}$ et $U_n = Be^{i(\omega t - kna)}$ dans les équations du mouvement (1.19)

$$\omega_{\pm}^2 = \left(\frac{1}{m_s} + \frac{1}{M_s}\right) \xi^n \pm \xi^n \sqrt{\left(\frac{1}{m_s} + \frac{1}{M_s}\right)^2 - \frac{4}{m_s M_s} \sin^2\left(\frac{ka}{2}\right)} \ . \tag{1.20}$$

En raison du recouvrement de la zone de Brillouin, le passage de la chaîne monoatomique à la chaîne diatomique ouvre une bande interdite et deux branches apparaissent. La branche supérieure (signe "+" de l'équation (1.20)) est appelée branche ou mode optique, la pulsation est différente de zéro lorsque le nombre d'onde est nul. La branche inférieure (signe "−" de l'équation (1.20)) est appelée branche ou mode acoustique, la pulsation est égale à zéro lorsque le nombre d'onde est nul. Il est important de noter ici, que dans une chaîne monodimensionnelle monoatomique et diatomique, il existe un seul mode pour chaque fréquence, soit propagatif si la fréquence est située dans une branche propagative, soit évanescent si la fréquence est située dans une bande interdite, car les particules possèdent un seul degré de liberté. Deux branches existent dans la relation de dispersion de la chaîne diatomique car la zone de Brillouin considérée est deux fois plus petite que la zone de Brillouin de la chaîne monoatomique, le mode est alors "replié". En effet, lorsque $m_s = M_s$ les deux branches se rejoignent au maximum de la zone de Brillouin, Fig. 1.7(b). Le nombre de modes est directement relié au nombre de degrés de liberté autorisés ainsi qu'au nombre d'atomes de la cellule unitaire. Si N degrés de libertés sont pris en compte pour un cristal avec Z atomes par cellule unitaire, le nombre de mode prédits est égal à $N \times Z$.

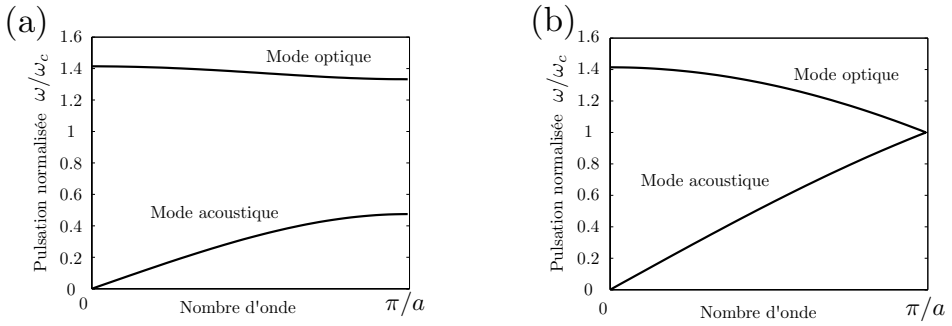

Figure 1.7 – Relation de dispersion des modes longitudinaux d'une chaîne diatomique, (a) $m_s \neq M_s$, (b) $m_s = M_s$.

Également, ici les modes de vibration d'une sphère individuelle se situent à très haute fréquence par rapport aux modes normaux de la structure [115]. Les bandes de fréquences de propagation des modes normaux sont donc clairement distinctes des bandes de fréquences de propagation des modes supérieurs.

1.7 Conclusions

Les cristaux phononiques granulaires présentent donc des comportements spécifiques menant à des phénomènes particuliers sur la propagation acoustique dans ces milieux : bandes interdites optimisables, localisation de l'énergie, guidage des ondes etc. La propagation des ondes dans ces structures dépend de divers facteurs : la diffusion due à la périodicité de la structure, sa dimensionalité (1D, 2D ou 3D), l'interaction entre les particules (degrés de liberté, non linéarités) ou bien la présence de défaut. Par conséquent, des phénomènes nouveaux sur la propagation acoustique sont susceptibles d'être mis en évidence. Dans ce but, différents cristaux phononiques granulaires sont étudiés théoriquement dans ce travail. L'étude se retreint à un régime linéaire.

Une chaîne phononique granulaire monoatomique dont les particules possèdent un degré de liberté en translation et un en rotation est étudiée dans le premier chapitre. L'interaction entre mouvements de rotation et de translation ainsi que l'existence de modes localisés sont en particulier analysées.

La propagation de modes volumiques dans un cristal phononique granulaire cubique 2D composé de particules cylindriques est présentée dans le troisième chapitre. Plusieurs phénomènes spécifiques à cette structure et liés à l'interaction entre les mouvements longitudinaux, transversaux et de rotation des particules sont mis en évidence.

Dans le dernier chapitre, une analyse de l'existence d'ondes propagatives et de surface dans des cristaux granulaires 3D est présentée. La description d'ondes de surface dans ces cristaux permet en particulier de comparer les résultats de la théorie discrète avec les prédictions de la théorie de Cosserat.

Bibliographie

[1] L. Brillouin. *Wave Propagation in Periodic Structures.* NY : Dover, New York, 1953.

[2] A. Yariv and P. Yeh. *Optical Waves in Crystals.* Wiley, New York, 1984.

[3] J.M. Bendickson, J.P. Dowling, and M. Scalora. Analytic expressions for the electromagnetic mode density in finite, one-dimensional, photonic band-gap structures. *Phys. Rev. E.*, page 4107, 1996.

[4] J.D. Joannopoulos, R.D. Meade, and J.N. Winn. *Photonic crystals : Modeling the Flow of Light.* Princeton University Press, Princeton, 1995.

[5] C.M. Soukoulis. *Photonic Band Gaps and Localization.* C.M. Soukoulis (Ed.), New York, 1993.

[6] C.M. Soukoulis. *Photonic Band Gaps Materials.* C.M. Soukoulis (Ed.), Dordrech, 1993.

[7] M. S. Kushwaha, P. Halevi, L. Dobrzynski, and B. Djafari-Rouhani. Acoustic band structure of periodic elastic composites. *Phys. Rev. Lett.*, 71 :2022, 1993.

[8] E.N. Economou and M.M. Sigalas. Stop bands for elastic waves in periodic composite materials. *J. Acoust. Soc. Am.*, 95 :1734, 1994.

[9] M.M. Sigalas and E.N. Economou. Band structure of elastic waves in two dimensional systems. *Solid State Commun*, 86 :141, 1993.

[10] R. Martinez-Sala, J. Sancho, J.V. Sanchez, V. Gomez, J. Llinares, and F. Meseguer. Sound attenuation by sculpture. *Nature*, 378 :241, 1995.

[11] J.O. Vasseur, P.A. Deymier, G. Frantziskonis, G. Hong, B. Djafari-Rouhani, and L. Dobrzynski. Experimental evidence for the existence of absolute acoustic band gaps in two-dimensional periodic composite media. *J. Phys. :Condens. Matter*, 10 :6051, 1998.

[12] J.V. Sanchez-Perez, D. Caballero, R. Martinez-Sala, C. Rubio, J. Sanchez-Dehesa, F. Meseguer, J. Llinares, and F. Galves. Sound attenuation by a two-dimensional array of rigid cylinders. *Phys. Rev. Lett.*, 80 :1208, 1998.

[13] X. Zhang and Z. Liu. Negative refraction of acoustic waves in two dimensional phononic crystals. *Appl. Phys. Lett.*, 85 :341, 2004.

[14] J. Bravo-Abad, T. Ochiai, and J. Sanchez-Dehesa. Anomalous refractive properties of a two-dimensional photonic band-gap prism. *Physical review*, 67 :115116, 2003.

[15] D. Prather, S. Shi, and J. Murakowski. Self-collimation in photonic crystal strucures : a new paradigm for applications and device development. *J. Appl. Phys*, 40 :2635–2651, 2007.

[16] S. Yang, J.H. Page, Z. Liu, M.L. Cowan, C.T. Chan, and P Sheng. Focusing sound in a 3D phononic crystal. *Physical review*, 341 :024301, 2004.

[17] J. Bucay, E. Roussel, J.O. Vasseur, P.A. Deymier, A-C. Hladky-Hennion, Y. Pennec, K. Muralidharan, B. Djafari-Rouhani, and B. Dubus. Positive, negative, zero refraction, and beam splitting in a solid/air phononic crystal : Theoretical and experimental study. *Phys. Rev. B*, 79(21) :214305, 2009.

[18] D. Torrent, A. Hakansson, F. Cervera, and J. Sanchez-Dehesa. Homogenization of two-dimensional cluster of rigid rods in air. *Phys. Rev. Lett.*, 96 :204302, 2006.

[19] M.M. Sigalas. Elastic wave band gaps and defect states in two-dimensional composites. *J. Acoust. Soc. Am.*, 101 :1256, 1997.

[20] M.M. Sigalas. Defect states of acoustic waves in a two dimensional lattice of solid cylinders. *J. Appl. Phys*, 84 :3026, 1998.

[21] F.G. Wu, Z.L. Hou, Z.Y. Liu, and Y.Y. Liu. Point defect states in two-dimensional phononic crystals. *Phys. Rev. Lett.*, 292 :198, 2001.

[22] J.B. Pendry. Negative refraction makes a perfect lens. *Phys. Rev. Lett.*, 85 :3966–3969, 2000.

[23] N. Fang, H. Lee, C. Sun, and X. Zhang. Sub-diffraction-limited optical imaging with a silver superlens. *Science*, 308 :534, 2005.

[24] V. F. Nesterenko. Propagation of nonlinear compression pulses in granular media. *J. Appl. Mech. Tech. Phys.*, 24 :733–743, 1983.

[25] A.N. Lazaridi and V.F. Nesterenko. Observation of a new type of solitary waves in a one-dimensional granular medium. *JAMTP*, 26(3) :405–408, 1985.

[26] V.F. Nesterenko. *Dynamics of Heterogeneous Materials*. Springer-Verlag, New York, 2001.

[27] C. Daraio, V.F. Nesterenko, E.B. Herbold, and S. Jin. Energy trapping and shock disintegration in a composite granular medium. *Phys. Rev. Lett.*, 96 :058002, 2006.

[28] V.F. Nesterenko, C. Daraio, E.B. Herbold, and S. Jin. Anomalous wave reflection at the interface of two strongly nonlinear granular media. *Phys. Rev. Lett.*, 56 :158702, 2005.

[29] C. Coste, E. Falcon, and S. Fauve. Solitary waves in a chain of beads under Hertz contact. *Phys. Rev. E.*, 56 :6104, 1997.

[30] M. de Billy. Experimental study of sound propagation in a chain of spherical beads. *J. Acoust. Soc. Am.*, 108 :1486, 2000.

[31] V. Tournat, V.E. Gusev, and B. Castagnede. Self-demodulation of elastic waves in a one-dimensional granular chain. *Phys. Rev. E.*, 70(5) :056603, 2004.

[32] V. Tournat, V.E. Gusev, V.Y. Zaitsev, and B. Castagnede. Acoustic second-harmonic generation with shear to longitudinal mode conversion in granular media. *Europhysics Letters (EPL)*, 66(6) :798–804, 2007.

[33] J. Cabaret, V. Tournat, and P. Béquin. Amplitude-dependent phononic processes in a diatomic granular chain in the weakly nonlinear regime. *Phys. Rev. E.*, 86(4) :041305, 2012.

[34] S. Job, F. Melo, A. Sokolow, and S. Sen. How Hertzian solitary waves interact with boundaries in a 1D granular medium. *Phys. Rev. Lett.*, 94 :178002, 2005.

[35] S. Job, F. Santibanez, F. Tapia, and F. Melo. Wave localization in strongly nonlinear Hertzian chains with mass defect. *Phys. Rev. E.*, 80 :025602, 2009.

[36] S. Job, F. Melo, F. Santibanez, and F. Tapia. Nonlinear waves in Hertzian granular chains : Effects of inertial and stiffness heterogeneities. *Proc. Ultrasonics*, page 1727, 2007.

[37] C. Daraio and V.F. Nesterenko. Strongly nonlinear waves in a chain of polymer coated beads. *Phys. Rev. E.*, 73 :026612, 2006.

[38] C. Daraio, V.F. Nesterenko, E.B. Herbold, and S. Jin. Strongly nonlinear waves in a chain of teflon beads. *Phys. Rev. E.*, 72 :016603, 2005.

[39] L. Ponson, N. Boechler, Y.M. Lai, M.A. Porter, P.G. Kevrekidis, and C. Daraio. Nonlinear waves in disordered diatomic granulair chains. *Phys. Rev. E.*, 82 :021301, 2010.

[40] R. Carretero-Gonzales, D. Khatri, M.A. Porter, P.G. Kevrekidis, and C. Daraio. Dissipative solitary waves in granular crystals. *Phys. Rev. Lett.*, 102 :024102, 2009.

[41] G. Theocharis, M. Kavousanakis, P.G. Kevrekidis, C. Daraio, M.A. Porter, and G. Kevrekidis. Localized breathing modes in granular crystals with defects. *Phys. Rev. E.*, 80 :066601, 2009.

[42] G. Theocharis, N. Boechler, P.G. Kevrekidis, S. Job, M.A. Porter, and C. Daraio. Intrinsic energy localization through discrete gap breathers in one-dimensional diatomic granular crystals. *Phys. Rev. E.*, 82(5) :056604, November 2010.

[43] N. Boechler, G. Theocharis, S. Job, P.G. Kevrekidis, M.A. Porter, and C. Daraio. Discrete breathers in one-dimensional diatomic granular crystals. *Phys. Rev. Lett.*, 104(24) :244302, June 2010.

[44] N. Boechler, G. Theocharis, and C. Daraio. Bifurcation-based acoustic switching and rectification. *Nature Materials*, 10 :665–668, 2011.

[45] Y.B. Jeon, R. Sood, J. h. Jeong, and S.-G. Kim. {MEMS} power generator with transverse mode thin film {PZT}. *Sensors and Actuators A : Physical*, 122(1) :16 – 22, 2005. {SSSAMW} 04 Special Section of the Micromechanics Section of Sensors and Actuators based on contributions revised from the Technical Digest of the 2004 Solid-State Sensor, Actuator and Microsystems Workshop.

[46] A.-C. Hladky-Hennion and M. de Billy. Experimental validation of band gaps and localization in a one-dimensional diatomic phononic crystal. *The Journal of the Acoustical Society of America*, 122(5) :2594, 2007.

[47] A.-C. Hladky-Hennion, G. Allan, and M. de Billy. Localized modes in a one-dimensional diatomic chain of coupled spheres. *Journal of Applied Physics*, 98(5) :054909, 2005.

[48] A.-C. Hladky-Hennion, F. Cohen-Tenoudji, A. Devos, and M. de Billy. On the existence of subresonance generated in a one-dimensional chain of identical spheres. *J. Acoust. Soc. Am.*, page 054850, 2002.

[49] E.V. Shevchenko, D.V. Talapin, C.B. Murray, and S.O'Brien. Structural characterisation of self-assembled multifunctional binary nanoparticles. *Journal of the American Chemical Society*, 128 :3620–3637, 2006.

[50] K.E. Mueggenburg, X.-M Lin, R.H. Goldslith, and H.M. Jaeger. Elastic membranes of close-packed nanoparticle arrays. *Nature Materials*, 6 :656–660, 2007.

[51] W. Cheng, M.J. Campolongo, J.J. Cha, S.J. Tan, C.C. Umbach, D.A. Miller, and D. Luo. Free standing nanoparticle superlattice sheets controlled by DNA. *Nature Materials*, 8 :519–525, 2009.

[52] A. Dong, J. Chen, P.M. Vora, J.M. Kikkawa, and C.B. Murray. Binary nanocrystal superlattice membranes self-assembled at the liquid-air interface. *Nature (London)*, 466 :474–477, 2010.

[53] E. Auyeun, J.I. Cutler, R.J. Macfarlane, M.R. Jones, J. Wu, G. Liu, K. Zhang, D. Osberg, and C.A. Mirkin. Synthetically programmable nanoparticle superlattices using a hollow three-dimensional spacer approach. *Nature Nanotechnologies*, 7 :24–28, 2012.

[54] A. Van Blaaderena, R. Ruel, and P. Wiltzius. Template-directed colloidal crystallisation. *Nature (London)*, 385 :321323, 1997.

[55] Z. Cheng, W.B. Russel, and P.M. Chaikin. Controlled growth of hard-sphere colloidal crystals. *Nature (London)*, 401 :893–895, 1999.

[56] J.D. Joannopoulos. Self-assembly lights up. *Nature*, 414 :257–258, 2001.

[57] H. Rossmanith and A. Shukla. Photoelastic investigation of dynamic load transfer in granular media. *Acta Mechanica*, 42 :211–225, 1982.

[58] A. Shukla, M.H. Sadd, Y. Xu, and Q.M. Tai. Influence of loading pulse duration on dynamic load transfer in a simulated granular medium. *J. Mech. Phys. Solids*, 41 :1795–1808, 1993.

[59] A. Shukla, M. Zhu, and M.H. Sadd. Angular dependence of dynamic load transfer due to explosive loading in granular aggregate chains. *Journal of strain analysis*, 23 :121–127, 1988.

[60] A. Shukla, M.H. Sadd, R. Singh, Q. Tai, and S. Vishwanathan. Role of particle shape and contact profile on the dynamic response of particulate materials. *Optics and Lasers in Engineering*, 19 :99–119, 1993.

[61] R. Singh, A. Shukla, and H. Zervas. Effect of flaws on the stress wave propagation in particulate aggregates : Near and far field observations. *International Journal of Solids and Structures*, 32(17-18) :2523–2546, 1995.

[62] F.J. Sierra-Valdez, F. Pacheco-Vázquez, O. Carvente, F. Malloggi, J. Cruz-Damas, R. Rechtman, and J.C. Ruiz-Suárez. Acoustic gaps in a chain of magnetic spheres. *Phys. Rev. E.*, 81(1) :011301, January 2010.

[63] C. Coste and B. Gilles. Sound propagation in a constrained lattice of beads : High-frequency behavior and dispersion relation. *Phys. Rev. E.*, 77 :021302, 2008.

[64] B. Gilles and C. Coste. Low-frequency behavior of beads constrained on a lattice. *Phys. Rev. Lett.*, 90 :174302, 2003.

[65] M. Nishida, Y. Tanaka, and T. Ishida. DEM simulation of wave propagation in two-dimensional ordered array of particles. *Shock waves*, 26 :815–820, 2009.

[66] M. Nishida and Y. Tanaka. DEM simulations and experiments for projectile impacting two-dimensional particle packings including dissimilar material layers. *Granular Matter*, 12 :357–368, 2010.

[67] A. Leonard and C. Daraio. Stress wave anisotropy in centered square highly nonlinear granular systems. *Phys. Rev. Lett.*, 108 :214301, 2012.

[68] A. Leonard, F. Fraternali, and C. Daraio. Directional wave propagation in a highly nonlinear square packing of spheres. *Experimental Mechanics*, 53 :327–337, 2013.

[69] F. Göncü, S. Luding, and K. Bertoldi. Exploiting pattern transformation to tune phononic band gaps in a two-dimensional granular crystal. *J. Acoust. Soc. Am.*, 131 :EL475, 2012.

[70] E. Kim and J. Yang. Wave propagation in single column woodpile phononic crystals : Formation of tunable band gaps. *Condens Mattered*, 2014.

[71] I.A. Kunin. *Elastic Media with Microstructure Three-Dimensional Models vol 2*. Springer, Berlin, 1983.

[72] J. Duffy and R.D. Mindlin. Stress-strain relations and vibrations of a granular medium. *ASME Trans. J. Appl. Mech.*, 24 :585–593, 1958.

[73] F. Gassmann. Elastic waves through a packing of spheres. *Geophysics*, 16 :673, 1951.

[74] R.D. Stroll. *Sediment acoustics*. Springer, Berlin, 1989.

[75] J.E. White. *Underground sound*. Springer, Amsterdam, 1983.

[76] C. Inserra, V. Tournat, and V.E. Gusev. A method of controlling wave propagation in initially spatially periodic media. *Europhysics Letters*, 78 :44001, 2007.

[77] V. Tournat and V.E. Gusev. Acoustics of unconsolidated granular media : an overview of recent results and several open problems. *Acta-Acustica United with Acustica*, 96 :208–224, 2010.

[78] V.E. Gusev and V. Tournat. How acoustic waves are guided in buried subsurface channels in unconsolidated granular media. *Phys. Rev. E.*, 78(3) :036602, 2008.

[79] A. Merkel, V. Tournat, and V.E. Gusev. Elastic waves in noncohesive frictionless granular crystals. *Ultrasonics*, 50(2) :133 – 138, 2009.

[80] A. Merkel, V. Tournat, and V.E. Gusev. Dispersion of elastic waves in three-dimensional noncohesive granular phononic crystals : Properties of rotational modes. *Phys. Rev. E.*, 82(3) :031305, 2010.

[81] A. Merkel, V. Tournat, and V.E. Gusev. Experimental evidence of rotational elastic waves in granular phononic crystals. *Phys. Rev. Lett.*, 107(22) :225502, 2011.

[82] V. Tournat, I. Pèrez-Arjona, A. Merkel, V. Sanchez-Morcillo, and V.E Gusev. Elastic waves in phononic monolayer granular membranes. *New Journal of Physics*, 13(7) :073042, 2011.

[83] O. Mouraille. *Sound propagation in dry granular materials : discrete element simulations, theory and experiments.* PhD thesis, University of Twente, 2009.

[84] F. Liu, Y.n Lai, X. Huang, and C. Chan. Dirac cones at k=0 in phononic crystals. *Phys. Rev. B*, 84(22) :224113, 2011.

[85] G. Wang, X. When, J. When, L. Shao, and Y. Liu. Two-dimensional locally resonant phononic crystals with binary structures. *Phys. Rev. Lett.*, 93(15) :154302, 2004.

[86] Y. Lai, Y. Whu, P. Sheng, and Z.-O. Zhang. Hybrid elastic solids. *Nature Materials*, 10 :620–624, 2011.

[87] R. Sainidou, N. Stefanou, and A. Modinos. Formation of absolute frequency gaps in three-dimensional solid phononic crystals. *Phys. Rev. B.*, 66 :212301, 2002.

[88] H. Zhao, Y. Liu, G. Wang, J. Wen, D. Yu, X. Han, and X. Wen. Resonance modes and gap formation in a two-dimensional solid phononic crystal. *Phys. Rev. B.*, 72 :012301, 2005.

[89] P. Peng, J. Mei, and Y. Wu. Lumped model for rotational modes in phononic crystals. *Phys. Rev. B.*, 86 :134304, 2012.

[90] E. Cosserat and F. Cosserat. *Théorie des corps déformables.* Herman et Fils, Paris, 1909.

[91] L. Limat. Percolation and Cosserat elasticity : exact results on a deterministic fractal. *Phys. Rev. B.*, 37(1) :672–675, 1988.

[92] H.B. Mühlaus and F. Oka. Dispersion and wave propagation in discrete and continous models for granular materials. *International Journal of Solids and Structures*, 33 :2841, 1996.

[93] E. Pasternak and H.-B. Muhlhaus. *Cosserat and non-local continuum models for problems of wave propagation in fractured materials.* Pergamon, Amsterdam, 2000.

[94] A.K. Noor. Continuum modelling for repetitive lattice structures. *Appl. Mech. Rev.*, 41 :285–296, 1988.

[95] R. Lakes. Deformation mechanisms in negative poisson's ratio materials : structural aspects. *J. Mater. Sci.*, 26 :2287–2292, 1991.

[96] A. Spadoni and M. Ruzzene. Numerical and experimental analysis of static compliance of chiral truss-core airfoils. *J. Mech. Mater. Struct.*, 2 :965–981, 2007.

[97] J. Pouget, A. Askar, and G.A. Maugin. Lattice model for elastic ferroelectric crystals : continuum approximation. *Phys. Rev. B.*, 33 :6320–6325, 1986.

[98] A. Askar. *Lattice dynamical foundations of continuum theories.* World Scientific, Singapore, 1986.

[99] W. Nowacki. *Theory of Asymmetric Elasticity.* Pergamon, Oxford, 1986.

[100] A. Eringen. *Microcontinuum Field Theories. I.Foundations and Solids.* Springer, New York, 1999.

[101] E.F. Grekova, M.A. Kulesh, and Herman G.C. Waves in linear elastic media with microrotations, part 2 : Isotropic reduced Cosserat model. *Bulletin of the seismological society of America*, 99 :1423–1428, 2009.

[102] M.A. Kulesh, E.F. Grekova, and I.N. Shardakov. Rayleigh wave in the isotropic and linear, reduced Cosserat continuum. *Advanced Problems in Mechanics*, pages 53–54, 2006.

[103] M.A. Kulesh, E.F. Grekova, and I.N. Shardakov. The problem of surface wave propagation in a reduced Cosserat medium. *Acoustics of structurally inhomogeneous solid media*, 55(2) :218–226, 2007.

[104] A.S.J. Suiker, R. de Borst, and C. S. Chang. Micro-mechanical modelling of granular material. part 1 : Derivation of a second-gradient micro-polar constitutive theory. *Acta Mechanica*, 149 :161–180, 2001.

[105] A.S.J. Suiker, R. de Borst, and C. S. Chang. Micro-mechanical modelling of granular material. part 2 : Plane wave propagation in infinite media. *Acta Mechanica*, 149(Part2) :181–200, 2001.

[106] I.S. Pavlov, A.I. Potapov, and G.A. Maugin. A 2D granular medium with rotating particles. *International Journal of Solids and Structures*, 43(20) :6194 – 6207, 2006.

[107] A.A. Vasiliev, A.E. Miroshnichenko, and M. Ruzzene. Multifield model for Cosserat media. *Journal of mechanics of materials and structures*, 3 :1365, 2008.

[108] H. Hertz. On the contact of elastic solids. *J. Reine Angew. Math*, 92 :1, 1881.

[109] K.L. Johnson. *Contact Mechanics*. Cambridge University Press, Cambridge, 1985.

[110] R.D. Mindlin. Compliance of elastic bodies in contact. *ASME J. Appl. Mech.*, 16 :259–268, 1949.

[111] R.D. Mindlin and H. Deresiewicz. Elastic spheres in contact under varying oblique forces. *ASME J. Appl. Mech.*, 75 :327–342, 1953.

[112] T. Harris. *Rolling Bearing Analysis*. Wiley, New York, 2001.

[113] D. Khatri, D. Ngo, and C. Daraio. Highly nonlinear solitary waves in chains of cylindrical particles. *Granular Matter*, 14 :63–69, 2011.

[114] N.W. Ashcroft and N.D. Mermin. *Solid States Physics*. Saunders College Publishing, Philadelphia, 1976.

[115] H. Lamb. On the vibration of an elastic sphere. *Proc. Lond. Math. Soc.*, 13 :61–68, 1882.

Chapitre 2

Localized transversal-rotational modes in linear chains of equal masses

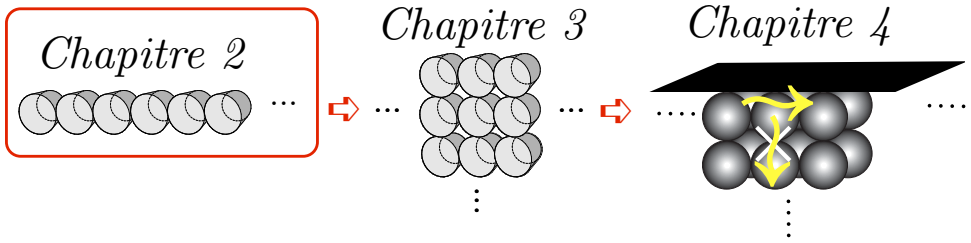

Une grande partie des études réalisées précédemment par notre équipe sur le sujet a porté sur des cristaux phononiques tridimensionnels [1–4]. C'est pourquoi, dans un premier temps, afin d'analyser plus précisément l'interaction entre les différents mouvements des particules, en particulier l'influence des mouvements de rotation sur les mouvements transversaux, nous nous sommes intéressés à une chaîne de cylindres ayant deux degrés de liberté. Par ailleurs, la mise en évidence de modes localisés dans une telle structure constitue un premier pas vers l'étude d'ondes de surfaces dans des cristaux phononiques granulaires présentant des degrés de liberté supplémentaires.

Ce chapitre, rédigé en anglais, est la transcription d'un article paru dans le journal Physical Review E [5]. La propagation d'ondes de volume et l'existence d'ondes localisées dans une chaîne monoatomique de particules possédant deux degrés de liberté est analysée. Les particules sont cylindriques et possèdent un degré de liberté en translation et un degré de liberté en rotation. Le contact entre les particules est modélisé par des ressorts de cisaillement et de flexion. Deux modes propagatifs, pour lequels les mouvements transversaux et de rotation sont couplés, existent dans la structure. Ces deux modes sont séparés par une bande interdite. Lorsque la chaîne est considérée semi-infinie, l'existence de modes localisés est discutée en fonction des conditions aux limites appliquées. Les modes localisés obtenus sont une combinaison de deux modes évanescents et sont mis en évidence dans une chaîne monoatomique. Ceci est une importante différence avec les modes localisés étudiés dans des chaînes diatomiques excitées longitudinalement. En effet, dans ces chaînes diatomiques où les particules ne possèdent qu'un degré de liberté, seul un mode, propagatif ou évanescent, peut exister à une fréquence donnée.

Abstract

The propagation and localization of transversal-rotational waves in a two-dimensional granular chain of equal masses are analyzed in this study. The masses are infinitely long cylinders possessing one translational and one rotational degree of freedom. Two dispersive propagating modes are predicted in this granular crystal. By considering the semi-infinite chain with a boundary condition applied at its beginning, the analytical study demonstrates the existence of localized modes, each mode composed of two evanescent modes. Their existence, position (either in the gap between the propagating modes or in the gap above the upper propagating mode) and structure of spatial localization are analyzed as a function of the relative strength of the shear and bending inter particle interactions and for different boundary conditions. This demonstrates the existence of a localized mode in a semi-infinite monatomic chain when transversal-rotational waves are considered, while it is well known that these types of modes do not exist when longitudinal waves are considered.

2.1 Introduction

Many investigations have been devoted to the propagation of acoustic and elastic waves in periodic samples, such as superlattices, multilayered structures, and phononic crystals in particular because of the presence of frequency band gaps, in which only non propagating waves can be excited. These waves, called evanescent waves, are particular solutions of the wave equation that decay or increase exponentially with distance. They are involved in many physical phenomena including coupling in and out of waveguides and resonators [6], near-field optics [7], tunneling [8, 9], sub wavelength focusing [10], or surface waves [11, 12]. The question of the existence or nonexistence of localized vibrations and surface acoustic waves is of large interest in mechanics and acoustics because of the important role played by these modes in various physical processes [13–15]. It was shown that localized modes may be excited and associated with local defects of periodicity or with the ends of the lattice. The case of a localized mode occurring in one-dimensional (1D) monatomic [16, 17] and diatomic [17–19] lattices has been studied previously for compressional waves. The localized modes engendered by an impurity of mass and force constant different from those of the atom it replaces in the chain have been characterized. As a results of these works, it is well known that in a semi-infinite linear chain of atoms, the vibrations cannot be localized near the free edge if all the masses and interactions between the neighboring atoms are equal. However, in this 1D lattice with a single degree of freedom, the localized vibrations exist near the first mass of the chain when the masses take alternatively two different values and the chain starts from a lighter mass. By modifying also the force constant of the impurity, the frequency of the localized mode can lie either in the forbidden frequency band between optical and acoustic branches or above the optical branch [18].

The localized vibration modes in periodically layered infinite and semi-infinite superlattices (SLs) have also attracted increasing attention over the years. In particular, an inhomogeneity embedded in a SL with perfect periodicity (e.g., a defect, a free surface, or an interaction with a substrate) is shown to cause localized vibrations within the frequency gaps induced by the periodicity of a SL. Evidence of these modes has been demonstrated both theoretically [20, 21] and experimentally via Raman spectroscopy [22], a phonon reflection experiment [23], and picosecond ultrasonic measurements [24, 25].

More recently, the understanding and control of these localized modes have been reported in a 1D diatomic granular chain excited longitudinally. The granular chain consists of closely packed ensembles of elastically interacting particles. In these diatomic chains, where the beads are coupled by a spring responding to compression and dilatation, a band gap exists between the optical and acoustic propagating branches. Under certain conditions, depending on the parity of the number and on the characteristics (mass and diameter) of the beads in the chain, it was shown both theoretically [26–28] and experimentally [27–29] that one or two localized modes exist in these forbidden bands. Intrinsic localized modes, which are also known as discrete breathers, have also been reported in compressed 1D nonlinear diatomic granular crystals [30–32].

Here we demonstrate theoretically that a localized mode exists in a 2D monatomic granular phononic crystal composed of infinitely long cylinders with equal masses. The considered mechanical system possesses one translational and one rotational degree of freedom and the contacts between the cylinders are provided by linear shear and linear bending rigidities. In these granular crystals the elastic contacts between adjacent particles occur over a surface that is much smaller than the particle dimensions and much softer than the particles themselves. This enables the propagation of elastic waves at frequencies much lower than the acoustic resonance frequencies of the individual particles [2, 33]. The problem considered could be realized experimentally, for instance, using a chain composed of short magnetic cylinders. To investigate the vibrational response of the chain, it can be excited at one of its ends by a shaker. The attractive magnetic force between cylinders causes in this case the prestress of the contacts between the cylinders, initiating their shear and bending contact rigidities [34]. Two dispersive propagating acoustic modes, in which the rotational and transversal motions are mixed, are predicted in this granular phononic crystal. These modes are separated by a gap of forbidden frequencies. By considering a semi-infinite chain with different boundary conditions, we establish the necessary criteria for the existence of a localized mode. Simple analytical expressions are obtained for the propagating and localized modes, which provide the opportunity for a straightforward evaluation of the existence and the frequency of the localized mode. With the use of free boundary condition and when the structure is not composed of empty cylindrical shells, the frequency of the localized vibration, composed of the two evanescent acoustic modes, is located inside the low frequency gap for waves propagation. Localization is also demonstrated with the use of more rigid boundary conditions. In this case the frequencies of the localized modes lie either in the forbidden band between the two propagating modes or above the upper propagating mode. It is worth mentioning that each of the localized coupled transversal and rotational modes in the evaluated chain of cylinders is composed of two evanescent modes. This is an important difference from earlier studied cases of longitudinal localized modes in linear chains of beads [26–28] and in layered structures [16, 17], where at each frequency only a single evanescent mode could exist.

The results of our research are complementary to the recent theoretical [1, 2, 4] and experimental [3] investigations of the acoustic waves in 3D granular crystals possessing rotational degrees of freedom. The Cosserat theory predicts the existence of additional rotational bulk elastic modes [35, 36] and the existence of additional surface acoustic waves with purely horizontal polarization of shear displacements [37], which are absent in the classical theory of elasticity of isotropic solids. Recently, the experimental observation of the coupled rotational-translational bulk modes in a non cohesive granular

phononic crystal [3] was reported. It was also demonstrated that the Cosserat theory in general fails to predict correctly the dispersion relations of the bulk elastic modes in granular crystals even in the long-wavelength limit because it does not account for all effects of the material inhomogeneity on its elastic behavior.

The theoretical analysis of the propagation in an infinite chain of a cylinder is presented in Sec. 2.2. Then the study focuses on the search for the possible localized modes in the chain. Their existence, general position (within the gap between the propagating modes or the gap above the upper propagating mode) and localization structure are analyzed in Sec. 2.3 for different boundary conditions applied at the beginning of the chain.

2.2 Infinite linear granular chain

2.2.1 Theory

The 2D linear chain under consideration is made of infinitely long cylinders with a circular cross-section, as depicted in Fig. 2.1(a). The structure is characterized by a lattice constant $a = 2R_c$, where R_c is the radius of the cylinders. Each cylinder possesses one translational and one rotational degree of freedom. The shear force at the contact between two adjacent particles is described by a spring of constant rigidity ξ^s. The elongation of the springs introduces forces and momenta that induce the motion of the particles: the displacement w along the y axis and the rotation φ around the z axis, Fig. 2.1(b). Here T and R indicate purely transversal and rotational motions, respectively, and TR and RT refer to coupled transversal-rotational modes with a predominance of translation or with a predominance of rotation, respectively.

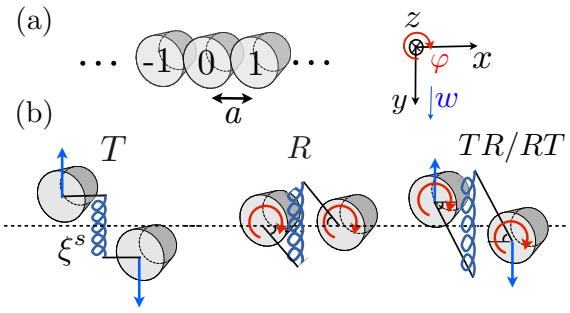

Figure 2.1 – (a) Representation of the infinite linear granular chain, (b) illustration of different possible motions.

The equations of motion of the zeroth particle obtained by applying the Lagrange principle [38] are

$$m\ddot{w}_0 = -\xi^s(\delta s_{-1} - \delta s_1) \ , \tag{2.1a}$$

$$I\ddot{\varphi}_0 = -\xi^s R_c(\delta s_{-1} + \delta s_1) \ , \tag{2.1b}$$

where m is the mass of the cylinder and I is its inertia momentum. The shear spring elongations, i.e., the relative displacements between the zeroth particle and its neighboring particles at the contact points, are denoted by δs_n, with n the particle number, and are explicitly given by

$$\delta s_{-1} = w_0 - w_{-1} + R_c(\varphi_0 + \varphi_{-1}) \ , \tag{2.2a}$$

$$\delta s_1 = w_1 - w_0 + R_c(\varphi_1 + \varphi_0) \ . \tag{2.2b}$$

The bending rigidity at the contacts of radius r is described by two additional springs with normal rigidities ξ^B, Fig. 2.2. They are located at the edge points of the contacts and are oriented orthogonally to the contact surface. The resulting additional momenta acting on the zeroth particle are described by $M_{0n} = -\dfrac{(R_c\theta)^2}{2}\xi^B(\varphi_0 - \varphi_n)$, with $n = -1, 1$ and θ the angular contact dimension. The radius of the contact is defined by $r = \dfrac{R_c\theta}{2}$.
The equation of motion for the rotation (2.1b) is then modified to account for all additional momenta $\Delta M = -\dfrac{(R_c\theta)^2}{2}\xi^B(2\varphi_0 - \varphi_{-1} - \varphi_1)$ applied on the zeroth particle.

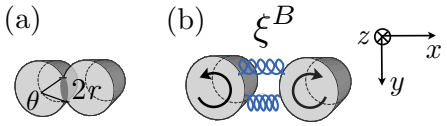

Figure 2.2 – Schematic representation of the bending rigidity, (a) contact geometry and (b) bending coupling.

The equations of motion become

$$m\ddot{w}_0 = -\xi^s\left[2w_0 - w_{-1} - w_1 + R_c(\varphi_{-1} - \varphi_1)\right] \ , \tag{2.3}$$

$$I\ddot{\varphi}_0 = -\xi^s R_c\left[w_1 - w_{-1} + R_c(2\varphi_0 + \varphi_{-1} + \varphi_1)\right] - \frac{(R_c\theta)^2}{2}\xi^B(2\varphi_0 - \varphi_{-1} - \varphi_1) \ . \tag{2.4}$$

Their solutions are sought in the form of plane waves

$$\mathbf{V}_n = \begin{pmatrix} w_n(x,t) \\ \Phi_n(x,t) \end{pmatrix} = \mathbf{v}e^{\mathrm{i}\omega t - \mathrm{i}k_x x_n} \ , \tag{2.5}$$

with the new variable $\Phi = R_c\varphi$, k_x the complex wave number in the x direction and $\mathbf{v} = \begin{pmatrix} A_w \\ A_\Phi \end{pmatrix}$ the amplitude vector. Equation (2.5) is developed around the equilibrium position x_0 of the central particle $\mathbf{V}_n = \mathbf{v}e^{\mathrm{i}\omega t - \mathrm{i}k_x x_0}e^{-\mathrm{i}k_x \Delta x_n}$, where $\Delta x_n = x_n - x_0$ is the relative coordinate between the central particle and the nth particle, and ω is the angular frequency.

Finally, the substitution of Eq. (2.5) into the set of Eqs. (2.3) and (2.4) leads to the eigenvalue problem

$$\mathbf{S}\mathbf{v} = -\Omega^2\mathbf{v} \ , \tag{2.6}$$

where $\Omega = \omega/\omega_0$ is the reduced frequency with $\omega_0 = 2\sqrt{\xi^s/m}$, and $\mathbf{S}$ is the dynamical matrix defined by

$$\mathbf{S} = \begin{pmatrix} -\sin^2 q & -\mathrm{i}\sin q\cos q \\ \mathrm{i}p\sin q\cos q & -p(\cos^2 q + p_B\sin^2 q) \end{pmatrix} \ ,$$

where $p_B = \dfrac{\theta^2}{2}\dfrac{\xi^B}{\xi^s}$ is the bending rigidity parameter, $p = \omega_1^2/\omega_0^2 = mR_c^2/I$ with $\omega_1 = 2R_c\sqrt{\xi^s/I}$, and $q = k_x a/2$ is the normalized wave number. Physically, the value of the parameter p is equal to or larger than 1. Depending on the mass distribution, the cylinders can be radially inhomogeneous ($I \leq mR^2$), and the limit case of $p = 1$ corresponds to a chain made of cylindrical infinitely thin shells.

The eigenvalue problem (2.6) can be solved for either Ω or $\sin q$. When Ω is the unknown, the solution of this eigenvalue problem gives the dispersion curves $\Omega = \Omega(q)$. There exist two possible values of $\Omega_\pm^2$ for a given wave number q, i.e., two modes defined by the square roots of the mathematical expression

$$\Omega_\pm^2 = \frac{1}{2}\left[\sin^2 q + p(\cos^2 q + p_B \sin^2 q) \pm \sqrt{[\sin^2 q + p(\cos^2 q + p_B \sin^2 q)]^2 - 4p_B p \sin^4 q}\right] . \qquad (2.7)$$

Alternatively, when $\sin^2 q$ is the unknown, there exists two values of $S_\pm^2 = \sin^2 q_\pm$, and thus two wave numbers $q_\pm$ for a given frequency Ω

$$S_\pm^2 = \sin^2 q_\pm = \Omega^2 \frac{1 + p(p_B - 1)}{2p_B p}\left(1 \pm \sqrt{1 - \frac{4p_B p(\Omega^2 - p)}{\Omega^2(1 + p(p_B - 1))^2}}\right), \quad \text{with} \quad p_B \neq 0 . \qquad (2.8)$$

The displacement and rotation of the two modes can then be written in the form

$$\begin{pmatrix} w_{n_\pm} \\ \Phi_{n_\pm} \end{pmatrix} = \begin{pmatrix} A_{w_\pm} \\ A_{\Phi_\pm} \end{pmatrix} e^{-\mathrm{i}2q_\pm n} e^{\mathrm{i}\omega t} = A_{\Phi_\pm} \begin{pmatrix} \alpha_\pm \\ 1 \end{pmatrix} e^{-\mathrm{i}2q_\pm n} e^{\mathrm{i}\omega t} , \qquad (2.9)$$

with $\alpha_\pm$ the ratio between the transversal $A_{w_\pm}$ and rotational $A_{\Phi_\pm}$ amplitudes of the modes defined by

$$\alpha_\pm = \frac{A_{w_\pm}}{A_{\Phi_\pm}} = \frac{\mathrm{i}S_\pm C_\pm}{\Omega^2 - S_\pm^2} , \qquad (2.10)$$

where $C_\pm^2 = \cos^2 q_\pm$ and n the particle number.

Equation (2.7) describes the $\Omega = \Omega(q)$ dispersion of the propagative and evanescent waves in the structure. When the solutions for the wave number q, determined by Eq. (2.8), are purely real, the waves are propagative. Evanescent waves whose frequency lies in the forbidden band for propagating waves are characterized by a complex-valued wave number in such a way that the amplitude of the mode should decay when it penetrates the chain. In this case, Eq. (2.7) describes the dispersion of waves that are attenuated to the right when n increases and to the left when n decreases.
Equation (2.7) is periodic and can be limited to a normalized wave number q value lying between 0 and $\frac{\pi}{2}$. In this study, the analysis is restricted to the first Brillouin zone and waves propagating to the right ($q > 0$).

2.2.2 Dispersion curves of the propagating modes

Figure 2.3 describes the $\Omega = \Omega(q)$ dispersion curves of the propagating modes depending on the value of the bending rigidity parameter p_B. The dispersion curves are restricted to a real wave number, i.e., to a wave propagating to the right (the positive direction). The eigenmodes of the granular chain motion are composed of two components, the transversal motion T and the rotational motion R. In Fig. 2.3, the plotted eigenvalues are colored relative to the type of associated eigenvectors that have been classified and the nature of the modes is labeled. Coupled transversal-rotational modes propagate in the chain: the solid red lines correspond to the modes with a predominance of rotation (RT) and the dashed blue lines correspond to the modes with a predominance of translation (TR). The frequencies of the modes at the edge of the Brillouin zone, i.e., at normalized wave numbers $q = 0$ and $q = \pi/2$, are found analytically and are indicated to emphasize the dependence of these characteristic frequencies on

p and p_B. Without bending rigidity, i.e., with $p_B = 0$, Fig. 2.3(a), a counterbalance between rotational and transversal motions takes place, resulting in a zero-frequency mode called also a soft mode. As illustrated in Fig. 2.3(b), this mode propagates when the bending rigidity parameter p_B increases, i.e., $p_B > 0$. In fact, this counterbalance disappears due to the additional momenta ΔM acting between the particles. Two band gaps are noticed in this structure, one between the two propagating modes and one above the upper mode. The width of the band gap between the two propagating modes is described analytically. As illustrated in Fig. 2.3(b), when $0 < p_B < 1/p$ the lower and upper limits of the first band gap are $\sqrt{p_B p}$ and 1, respectively. When $p_B = 1/p$ the band gap closes, Fig. 2.3(c). When $1/p < p_B < 1$ the boundaries of the band gap are specified by 1 and $\sqrt{p_B p}$, Fig. 2.3(d). Finally, when $p_B > 1$, the band gap is located between 1 and $\sqrt{p}$, Fig. 2.3(e). Note that, by definition, p is always greater than or equal to 1.

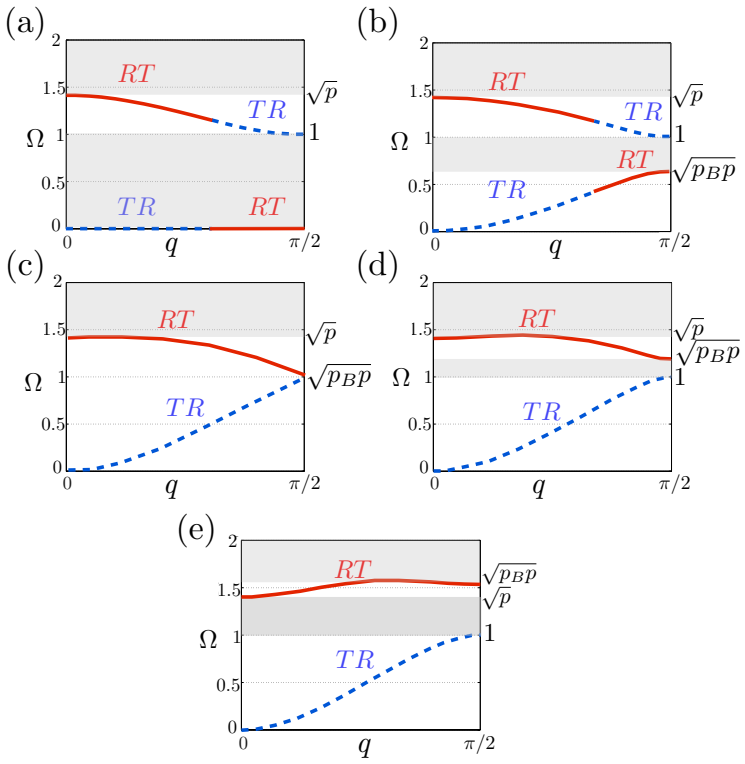

Figure 2.3 – Different possible dispersion curves depending on the value of the bending rigidity parameter: $p = 2$ and (a) $p_B = 0$, (b) $0 < p_B < 1/p$ ($p_B = 0.2$), (c) $p_B = 1/p$ ($p_B = 0.5$), (d) $1/p < p_B < 1$ ($p_B = 0.7$) and (e) $p_B > 1$ ($p_B = 1.2$).

To know the lower limit of the upper band gap, the extremum of the upper propagative band Ω_+ must be determined. The bending rigidity has an important influence on the structure of this mode. For low bending rigidities $p_B < 1 - 1/p$, the second propagating mode is monotonic with a negative group velocity and its maximum is equal to $\sqrt{p}$, Fig. 2.4(a). For the values of p_B between $1 - 1/p$ and $1 + 1/p$ this mode becomes nonmonotonic with a zero-group-velocity point and its maximum is equal to

$$\Omega_{\text{ZGVP}} = \left[\frac{4p_B p^2}{4p_B p - (1 + p_B p - p)^2}\right]^{1/2},$$

Fig. 2.4(b). Finally, for the values of p_B above $1 + 1/p$ the second mode is monotonic with a positive group velocity and its maximum frequency is equal to $\sqrt{p_B p}$, Fig. 2.4(c).

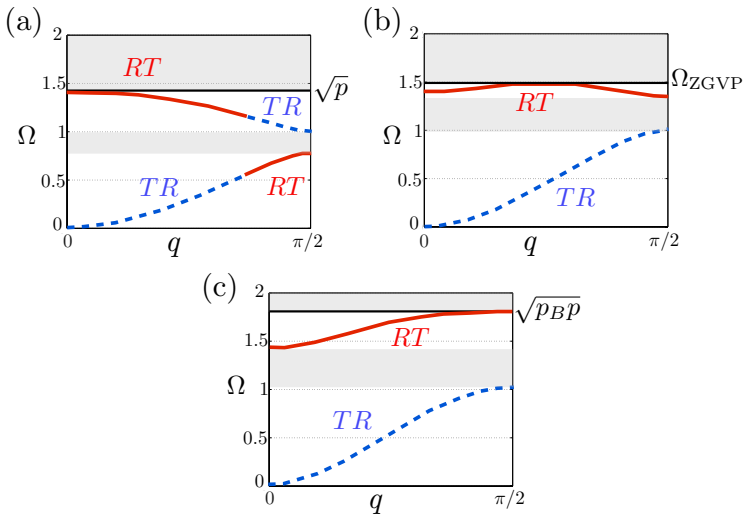

Figure 2.4 – Upper limit of the second propagative band depending on the value of the bending rigidity parameter: (a) $p_B < 1 - 1/p$ ($p = 2$ and $p_B = 0.3$), (b) $1 - 1/p < p_B < 1 + 1/p$ ($p = 2$ and $p_B = 0.9$), and (c) $p_B > 1 + 1/p$ ($p = 2$ and $p_B = 1.7$).

2.3 Localized modes

The study focuses now on the search for localized modes in the chain. With the aim of inducing localized modes, the linear chain is considered semi-infinite and a boundary condition is applied at its beginning. The analysis shows that to satisfy the boundary condition for one given frequency, two waves must be combined. As noted in Eq. (2.7), these two waves have wave numbers q_+ and q_-, respectively. The localized modes are, by definition, the modes whose amplitude decreases away from the boundary. Therefore, the localized wave is a combination of two evanescent waves and its decay is related to the imaginary parts of the wave numbers q_+ and q_-. Since the analysis is restricted to modes with an amplitude that decreases when n increases (to the right), the imaginary parts of the wave numbers must be negative.

In order to know at which frequency and for which parameters p and p_B the two wave numbers q_+ and q_- of the two combined waves are complex with a negative imaginary part, a description of the band structure is presented in Sec. 2.3.1. The general method to determine the frequency of the mode induced by the boundary conditions is presented in Sec. 2.3.2 and the way to determine the profiles of the transversal and rotational displacements as a function of the cylinder positions is presented in Sec. 2.3.3. This method is applied to different boundary conditions in Sec. 2.3.4 and the range of parameters p_B and p for which localization takes place is defined and the spatial structure of the modes is described.

2.3.1 General description of the dispersion curves

In the considered linear chain of cylinders, exhibiting two degrees of freedom each, there exist two allowed wave numbers for one single frequency, Eq. (2.8). Depending on the value of the frequency, these wave numbers can be both complex, both purely real, or one complex and the other purely real. This is illustrated in Fig. 2.5(a), where the real and imaginary parts of S_+^2 and S_-^2 are plotted as a function of the frequency where $p = 2$ and $p_B = 0.9$. Figure 2.5(b) represents the corresponding

dispersion curves. This description provides information about the wave numbers. On the one hand, if

$$0 \leq \sin^2 q \leq 1 \ , \tag{2.11}$$

a real solution for the wave number q exists and the corresponding mode is propagative. On the other hand, if

$$\sin^2 q < 0 \ , \quad \text{or} \quad \sin^2 q > 1 \ , \quad \text{or} \quad \sin^2 q = \beta^{'} + \mathrm{i}\beta^{''} \ , \tag{2.12}$$

no purely real solution for q exists and the corresponding mode is evanescent.
When at least one of $S_{\pm}^2$ satisfies Eq. (2.11), the corresponding frequency Ω lies in a propagative band. When both S_{+}^2 and S_{-}^2 satisfy one of the inequalities of Eq. (2.12), the corresponding frequency lies in a band gap. Thus, as can be seen in Fig. 2.5, for example, there is one propagative and one evanescent mode in the first propagative band, i.e., when $\Omega \in [0, 1]$, or two evanescent modes in the first band gap, i.e., when $\Omega \in [1, \sqrt{p}]$. See annexe A for a more detailed description of S_{+}^2 and S_{-}^2 as a function of the parameters p and p_B.

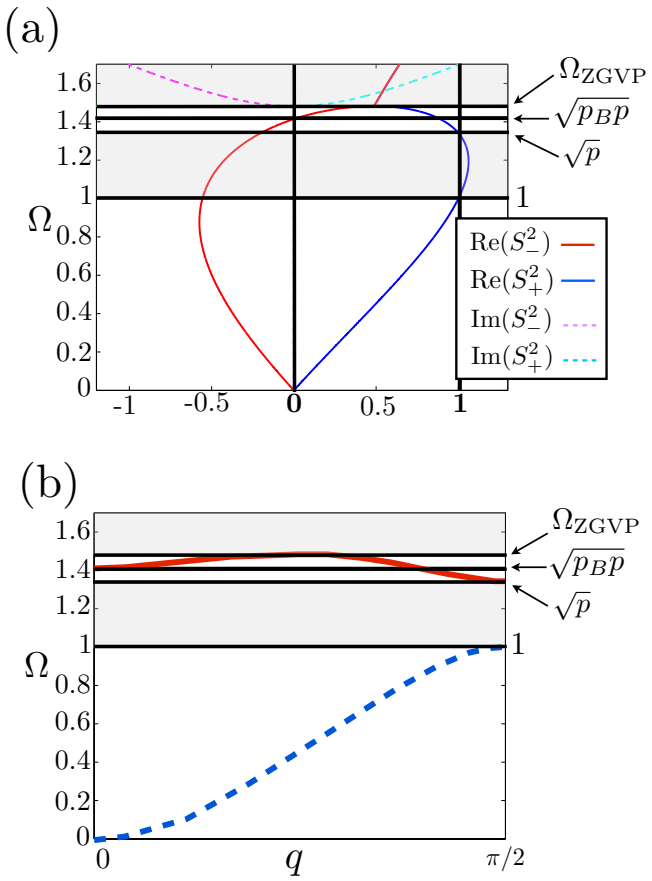

Figure 2.5 – (a) Real and imaginary parts of S_{+}^2 and S_{-}^2 as a function of the frequency Ω for a homogeneous cylinder ($p = 2$) when $p_B = 0.9$, (b) corresponding dispersion curves $\Omega = \Omega(q)$.

Localization occurs when the frequency lies in a band gap, i.e., when the two corresponding wave numbers are complex with a negative imaginary part. If $\sin^2 q < 0$, the wave takes the form of a simple exponentially decreasing function because the wave number has an imaginary value

$$q_1 = -\mathrm{i}\,\mathrm{arcsinh}(|H|) \ , \tag{2.13}$$

where H is the square root of the right-hand side of Eq. (2.8). If $\sin^2 q > 1$, the wave takes the form of decaying function with additional oscillation

$$q_2 = -\frac{\pi}{2} - \mathrm{i}\,\mathrm{arccosh}(|H|) \ . \tag{2.14}$$

If $\sin^2 q$ is complex, it takes the form

$$q_3 = q_3^{'} - \mathrm{i}\, q_3^{''} \ , \tag{2.15}$$

with $q_3^{'} = \mathrm{Re}[\mathrm{arcsinh}(|H|)]$ and $q_3^{''} = \mathrm{Im}[\mathrm{arcsinh}(|H|)]$, which corresponds to an exponentially decaying wave with additional oscillations. See annexe A for a detailed way to determine these wave functions.

2.3.2 Determination of the frequency of the modes induced by the boundary condition

We are interested in analyzing the existence of the localized modes when the chain of cylinders is semi-infinite and one of its ends is either mechanically free or attached to an absolutely rigid wall by springs. The rigidities of these springs are, in general, different from those of the chain. Formally, both situations can be mathematically accessed by modifying the rigidities between the first negative and the zeroth particles in the infinite chain from $-\infty$ to ∞ for completely blocking the motion of the first negative cylinder and looking for the vibrations localized on the cylinders with non-negative n.
The shear and bending forces at the contact between the first negative and the zeroth particles are described by springs of constant rigidity $\xi^{s'}$ and ξ^{B}, respectively. As above, the other contacts are described with spring rigidities ξ^{s} and ξ^{B}. The new equations of motion for the particle $n = 0$ become

$$m\ddot{w}_0 = -\xi^{s'}[w_0 - w_{-1} + R_c(\varphi_0 + \varphi_{-1})] + \xi^{s}[-w_0 + w_1 + R_c(\varphi_0 + \varphi_1)] \ , \tag{2.16}$$

$$\begin{aligned} I\ddot{\varphi}_0 = &-\xi^{s'} R_c[w_0 - w_{-1} + R_c(\varphi_0 + \varphi_{-1})] - \frac{(R_c\theta)^2}{2}\xi^{B'}(\varphi_0 - \varphi_{-1}) \\ &- \xi^{s} R_c[-w_0 + w_1 + R_c(\varphi_0 + \varphi_1)] - \frac{(R_c\theta)^2}{2}\xi^{B}(\varphi_0 - \varphi_1) \ . \end{aligned} \tag{2.17}$$

Then the motion of the $n{=}{-}1$ particle is completely blocked, i.e., $w_{-1} = 0$ and $\varphi_{-1} = 0$, which mimics the absolutely rigid wall. So if $\xi^{s'} = \xi^{B'} = 0$ the beginning of the chain, starting with the zeroth particle, is mechanically free and if $\xi^{'s} \neq 0$ and $\xi^{B'} \neq 0$, the chain is attached to an absolutely rigid wall by the springs of different rigidities $\xi^{s'}$ and $\xi^{B'}$. By varying the ratio between these rigidities and those between the other cylinders of the chain, the boundary conditions are modified.

When $w_{-1} = 0$ and $\varphi_{-1} = 0$, Eqs. (2.16) and (2.17) become

$$m\ddot{w}_0 = -\xi^{s'}(w_0 + R_c\varphi_0) + \xi^{s}(-w_0 + w_1 + R_c(\varphi_0 + \varphi_1)) \ , \tag{2.18}$$

$$\begin{aligned} I\ddot{\varphi}_0 = &-\xi^{s'} R_c(w_0 + R_c\varphi_0) - \frac{(R_c\theta)^2}{2}\xi^{B'}\varphi_0 \\ &- \xi^{s} R_c(-w_0 + w_1 + R_c(\varphi_0 + \varphi_1)) - \frac{(R_c\theta)^2}{2}\xi^{B}(\varphi_0 - \varphi_1) \ . \end{aligned} \tag{2.19}$$

Note that all the modes in the chain, i.e., both propagating and evanescent modes, satisfy the equations of motions (2.3) and (2.4). Then, the difference between Eqs. (2.3) and (2.18) leads to

$$(\xi^{s'} - \xi^{s})(-w_0 - \Phi_0) - \xi^{s}(w_{-1} - \Phi_{-1}) = 0 \ . \tag{2.20}$$

Likewise, the difference between Eqs. (2.4) and (2.19), leads to

$$-\Phi_0\xi^{B'} + \Phi_0\xi^B - \Phi_{-1}\xi^B = 0 \ . \tag{2.21}$$

Finally, these two boundary conditions can be rewritten as

$$\begin{cases} (l_1-1)(w_0+\Phi_0) + w_{-1} - \Phi_{-1} = 0 \\ (l_2-1)\Phi_0 + \Phi_{-1} = 0 \end{cases} , \tag{2.22}$$

with $l_1 = \dfrac{\xi^{s'}}{\xi^s}$ and $l_2 = \dfrac{\xi^{B'}}{\xi^B}$.

To satisfy the system (2.22) two evanescent waves must be combined. The resulting mode has a displacement w_n and a rotation Φ_n of the form

$$w_n = w_{n_+} + w_{n_-} = A_+\alpha_+ e^{-\mathrm{i}2q_+ n}e^{\mathrm{i}\omega t} + A_-\alpha_- e^{-\mathrm{i}2q_- n}e^{\mathrm{i}\omega t}, \tag{2.23}$$

$$\Phi_n = \Phi_{n_+} + \Phi_{n_-} = A_+ e^{-\mathrm{i}2q_+ n}e^{\mathrm{i}\omega t} + A_- e^{-\mathrm{i}2q_- n}e^{\mathrm{i}\omega t} \ . \tag{2.24}$$

The expressions (2.23) and (2.24) are then substituted into the two conditions (2.22), which gives the system of equations

$$\begin{pmatrix} (l_1-1)(\alpha_+ +1) + \alpha_+ e^{\mathrm{i}2q_+} - e^{\mathrm{i}2q_+} & (l_1-1)(\alpha_- +1) + \alpha_- e^{\mathrm{i}2q_-} - e^{\mathrm{i}2q_-} \\ l_2 - 1 + e^{\mathrm{i}2q_+} & l_2 - 1 + e^{\mathrm{i}2q_-} \end{pmatrix} \begin{pmatrix} A_+ \\ A_- \end{pmatrix} = \begin{pmatrix} 0 \\ 0 \end{pmatrix} \ . \tag{2.25}$$

Solutions exist if the determinant of the matrix in the left-hand-side of Eq. (2.25) is equal to zero. Thus the following relation between the frequency of the modes induced by the boundary condition, the ratios of the rigidities l_1 and l_2 and the wave numbers $q_\pm$, is obtained

$$\frac{l_1\left[(C_+ - \mathrm{i}S_+)\dfrac{\mathrm{i}S_+C_+}{\Omega^2 - S_+^2}\right] - 2C_+\dfrac{\Omega^2}{\Omega^2 - S_+^2}}{l_1\left[(C_- - \mathrm{i}S_-)\dfrac{\mathrm{i}S_-C_-}{\Omega^2 - S_-^2}\right] - 2C_-\dfrac{\Omega^2}{\Omega^2 - S_-^2}} = \frac{l_2\,(C_+ - \mathrm{i}S_+) + 2\mathrm{i}S_+}{l_2\,(C_- - \mathrm{i}S_-) + 2\mathrm{i}S_-} \ . \tag{2.26}$$

When the ratios between the shear rigidities and the bending rigidities are the same, i.e., $l_1 = l_2 = l^{'}$, the relation (2.26) becomes

$$\frac{\mathrm{i}S_+C_+}{\Omega^2 - S_+^2} + \frac{l^{'}(C_+ - \mathrm{i}S_+) - 2C_+}{l^{'}(C_+ - \mathrm{i}S_+) + 2\mathrm{i}S_+} = \frac{\mathrm{i}S_-C_-}{\Omega^2 - S_-^2} + \frac{l^{'}(C_- - \mathrm{i}S_-) - 2C_-}{l^{'}(C_- - \mathrm{i}S_-) + 2\mathrm{i}S_-} \ . \tag{2.27}$$

Finally, for a given $l^{'}$, the frequency of the possible oscillations in the chain when a boundary condition is applied at its beginning, can be determined by substituting Eq. (2.8) into Eq. (2.27). Since the calculation of the general expression (for all $l^{'}$) of this frequency is too cumbersome, only expressions for particular values of $l^{'}$, i.e., for particular boundary conditions, will be given. The case of free boundary conditions ($l^{'} = 0$) is studied in Sec. 2.3.4.1 and results by considering the link to the infinitely rigid wall to be more and more rigid ($l^{'} > 0$) are presented in Sec. 2.3.4.2.

2.3.3 Determination of the transversal and rotational displacements of the localized modes

According to Eq. (2.9), the amplitudes of the transversal w_n and rotational Φ_n displacements of the localized modes as a function of the particle number n can be determined by combining two evanescent

modes

$$\begin{pmatrix} w_n \\ \Phi_n \end{pmatrix} = A_+ \begin{pmatrix} \alpha_+ \\ 1 \end{pmatrix} e^{-\mathrm{i}2q_+ n} e^{\mathrm{i}\omega t} + A_- \begin{pmatrix} \alpha_- \\ 1 \end{pmatrix} e^{-\mathrm{i}2q_- n} e^{\mathrm{i}\omega t} \ . \tag{2.28}$$

From Eq. (2.25), the discrete displacements (2.28), can be rewritten in the form

$$\begin{pmatrix} w_n \\ \Phi_n \end{pmatrix} = A_- \left[Z \begin{pmatrix} \alpha_+ \\ 1 \end{pmatrix} e^{-\mathrm{i}2q_+ n} e^{\mathrm{i}\Omega t} + \begin{pmatrix} \alpha_- \\ 1 \end{pmatrix} e^{-\mathrm{i}2q_- n} e^{\mathrm{i}\Omega t} \right] \ , \tag{2.29}$$

with $Z = \dfrac{A_+}{A_-} = -\dfrac{l_2 - 1 + e^{2\mathrm{i}q_-}}{l_2 - 1 + e^{2\mathrm{i}q_+}}$. In the following, the normalized displacements are calculated with $A_- = 1$.

The structure of these displacements (2.29) as a function of the particle number depends on the wave numbers q_+ and q_- of the combined evanescent waves. The forms of these wave numbers depend on the position and value of localized mode frequency. They can take a form that corresponds to a simple exponential decaying function or to a decaying function with few oscillations. The results for different boundary conditions are presented in the next section. The existence or nonexistence of localization is described as a function of the parameters p and p_B and the profiles of the displacements are illustrated. Note that the localized modes are plotted with a dotted line to clearly show and compare the frequency value of this mode with the frequencies of the propagating modes in the following dispersion curves. However, it is important to keep in mind that the localized mode contains two components with two different complex wave numbers.

2.3.4 Results for different boundary conditions

In this section, we analyze the localization phenomena for several different particular boundary conditions applied at the beginning of the chain. In all the considered cases it is convenient to present the boundary condition (2.27) in the form

$$\frac{\alpha_+}{\alpha_-} = f(S_+, S_-) \ , \tag{2.30}$$

where $\alpha_\pm$ are defined by Eq. (2.10) and f is a function dependent on the considered boundary conditions. With the notation introduced in Eq. (2.30), the ratio w_n/Φ_n, which provides information on the relative changes in regard to the depth n of the displacements and rotations in the localized mode, can be written as

$$\frac{w_n}{\Phi_n} = \alpha_- \frac{Z f(S_+, S_-) e^{-\mathrm{i}2(q_+ - q_-)n} + 1}{Z e^{-\mathrm{i}2(q_+ - q_-)n} + 1} \ . \tag{2.31}$$

Analytically, it is convenient to search for the frequencies that satisfy $(\alpha_+/\alpha_-)^2 = f^2(S_+, S_-)$ rather than Eq. (2.30). So when the solutions are found, we choose among them those that satisfy Eq. (2.30) and not $\alpha_+/\alpha_- = -f(S_+, S_-)$.

2.3.4.1 Free boundary condition

When $l' = 0$ and $\xi^{s'} = \xi^{B'} = 0$, the boundary of the chain is mechanically free because there is no link between the particle $n = -1$ and the particle $n = 0$. Equation (2.30) becomes

$$\frac{\alpha_+}{\alpha_-} = \frac{S_+^2}{S_-^2} \ . \tag{2.32}$$

By substituting the expression of $S_{\pm}^2$, Eq. (2.8), into Eq. (2.32) squared, the solutions for the mode frequencies are $\Omega_{L1_{free}}^2 = \dfrac{p_B p^2}{p(p_B+1)-1}$ and $\Omega_{L2_{free}}^2 = 1$. These solutions satisfy the boundary conditions (2.32) and thus provide the possible frequencies of the localized modes if $p_B > 1/p$.

The simple analytical expressions obtained for the propagating and localized modes provide the opportunity for a straightforward evaluation of the existence and the frequency of the localized mode depending on the relative strength of the shear and bending inter particle interactions. For a localized mode to exist, the solutions $\Omega_{L1_{free},L2_{free}}$ should not cross the dispersion curves of the propagating modes of the infinite chain $\Omega_{\pm}$.

When the chain is composed of empty cylindrical shells ($p = 1$), the solutions $\Omega_{L1_{free}}$ and $\Omega_{L2_{free}}$ are equal to 1 and cannot provide localization because for all value of p_B these frequencies lie in a propagative band, Fig. 2.3.
When $p > 1$, if a band gap exists between the two propagating modes ($p_B \neq 1/p$), the frequency $\Omega_{L1_{free}}$ always lies in the first band gap. Thus the localized vibration, composed of the two evanescent acoustic modes, exists near the mechanically free end of the chain when $p > 1$ and $p_B > 1/p$.
For the waves localized in the first band gap it is straightforward to show that w_n/Φ_n, Eq. (2.31), is always real. For this particular boundary condition $f(S_+, S_-) \neq 1$ (Eq. (2.32)). Consequently, w_n/Φ_n depends on n. In the case of the mechanically free boundary condition, in the derived localized mode, the oscillations are in anti-phase ($w_n/\Phi_n < 0$) independently of n and the ratio of their amplitudes $|w_n|/|\Phi_n|$ varies with depth.
In Fig. 2.6 the profiles of the displacements are plotted on the right of the considered dispersion curves for homogeneous cylinders ($p = 2$) and two different values of p_B. The amplitudes of the rotational and transversal displacements of the localized mode are always a combination of a simple decaying function and a decaying function with few oscillations. As expected from a physical background, the mode is more localized, i.e., its amplitude decays more rapidly, when its frequency is far away from the two band edges. In Fig. 2.6(b), for $p_B > 1$, the contribution to the rotational motion of the simple exponentially decaying function is more important than the contribution of the decaying function with additional oscillations.

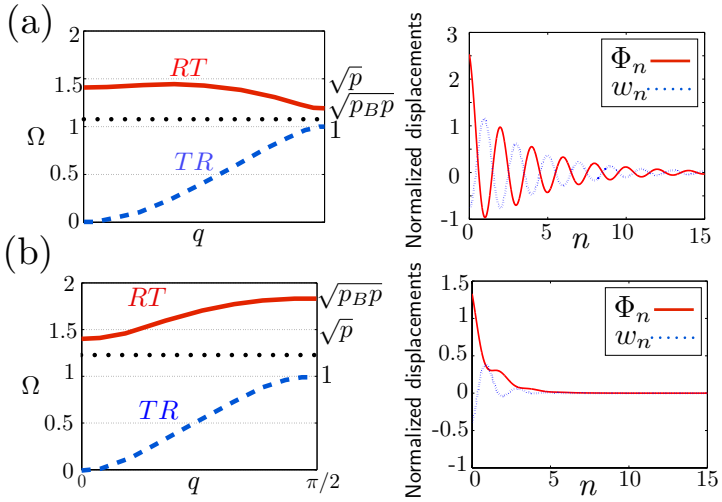

Figure 2.6 – Dispersion curves and corresponding discrete displacement profiles of the localized mode in the case of free boundary conditions and for a homogenous cylinder ($p = 2$): (a) $1/p < p_B < 1$ ($p_B = 0.7$) and (b) $p_B > 1$ ($p_B = 1.7$). The solid red curves correspond to the RT mode, the dashed blue curves correspond to the TR mode, and the dotted black lines indicate the frequency value $\Omega_{L1_{free}}$.

2.3.4.2 Chain in contact with rigid substrate

When $l' = 1$, the link between the chain and the rigid wall is performed via the same springs as the springs between all the other cylinders, i.e., $\xi^s = \xi^{s'}$ and $\xi^B = \xi^{B'}$. Equation (2.30) becomes

$$\frac{\alpha_+}{\alpha_-} = 1 \ . \tag{2.33}$$

By substituting Eq. (2.8) into Eq. (2.33) squared, the solutions for the mode frequencies are $\Omega^2_{L1_{l'=1}} = \dfrac{p}{1+p-p_B p}$ and $\Omega^2_{L2_{l'=1}} = 1$. These solutions satisfy the boundary conditions (2.33) and thus provide the possible frequencies of the localized modes if $p_B < 1/p$. For frequency $\Omega_{L2_{l'=1}} = 1$, the mode is not localized for any values of p and p_B because this frequency always crosses a propagative band.
For $p_B < 1/p$ and for all $p \geq 1$, the frequency $\Omega_{L1_{l'=1}}$ is located in the first band gap. Thus, for this boundary condition, localization exists when $p_B < 1/p$ and $p \geq 1$ and when the frequency lies in the first band gap. Figure 2.7(a) and 2.7(b) present the dispersion curves and the corresponding profiles of the displacements in the cases of a homogeneous cylinder ($p = 2$) and an empty cylindrical cylinder ($p = 1$), respectively.
For these particular boundary conditions $f(S_+, S_-) = 1$ and Eq. (2.31) reduces to $w_n/\Phi_n = \alpha_-$, with $\alpha_- > 0$. Consequently, neither the relative phase nor the ratio of the amplitudes of displacements and rotations depends on n. The oscillations w_n and Φ_n are found to be in phase at all depths ($w_n/\Phi_n > 0$).

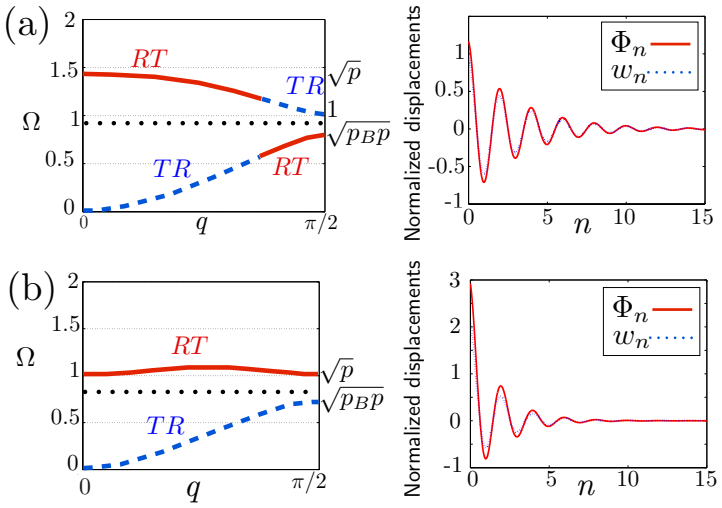

Figure 2.7 – Dispersion curves and corresponding discrete displacement profiles of the localized mode when $l' = 1$, for (a) homogeneous cylinders ($p = 2$) with $p_B = 0.3 < 1/p$ and (b) empty cylindrical shells ($p = 1$) with $p_B = 0.2 < 1/p$. The solid red curves correspond to the RT mode, the dashed blue curves correspond to the TR mode, and the dotted black lines correspond to $\Omega_{L1_{l'=1}}$.

By increasing l', the link to the rigid wall becomes more rigid. For intermediate value of l' between 1 and $+\infty$, analytical expressions of the localized mode become cumbersome and the description of the existence of localization cannot be reported in details analytically. However, it is possible to study the localization and corresponding displacements numerically. For example, with $l' = 2$, Eq. (2.30) becomes

$$\frac{\alpha_+}{\alpha_-} = \frac{1 - S_+^2}{1 - S_-^2} \ . \tag{2.34}$$

By substituting Eq. (2.8) into Eq. (2.34) squared, the solutions for the mode frequencies are found

$$\Omega^2_{L1_{l'=2}} = \frac{-p(p_B+1) + p^2\left(p_B^2+p_B+1\right) + \sqrt{p^2\left(p^2\left(p_B^2+p_B+1\right)^2 - 2p\left(p_B^3+1\right) + (p_B-1)^2\right)}}{2(p_B p + p - 1)} \ ,$$

$$\Omega^2_{L2_{l'=2}} = \frac{-p(p_B+1) + p^2\left(p_B^2+p_B+1\right) - \sqrt{p^2\left(p^2\left(p_B^2+p_B+1\right)^2 - 2p\left(p_B^3+1\right) + (p_B-1)^2\right)}}{2(p_B p + p - 1)} \ .$$

These solutions satisfy the boundary conditions (2.34) and thus provide the possible frequencies of the localized modes for all values of p and p_B.

The frequency $\Omega_{L2_{l'=2}}$ is not real and the frequency $\Omega_{L1_{l'=2}}$ can be found in the upper band gap when $p_B > 0$ and for different values of p. The description of S_+^2 and S_-^2 in the upper band gap, annexe A, provides an opportunity to describe the profiles of the displacements depending on the value of the parameters.

Three different cases are possible: either $S_+^2 < 0$ and $S_-^2 < 0$, or S_+^2 and S_-^2 are complex or $S_+^2 > 1$ and $S_-^2 > 1$. See annexe A for a description of the values of the parameters p and p_B corresponding to these three cases.

Examples of dispersion curves and corresponding profiles of displacements are depicted in Fig. 2.8 for these three cases. Figure 2.8(a) corresponds to the case where $S_+^2 < 0$ and $S_-^2 < 0$. In this case, the wave numbers q_+ and q_- constituting the localized mode are both in the form of Eq. (2.13),

which corresponds to a simple exponentially decreasing wave function. The oscillations are in phase ($w_n/\Phi_n > 0$ and real) independently of n and the ratio of their amplitudes $|w_n|/|\Phi_n|$ varies with depth. Figure 2.8(b) corresponds to the case where S_+^2 and S_-^2 are complex. The wave numbers are both in the form of Eq. (2.15), which corresponds to a decaying wave function with additional oscillations. The values of w_n/Φ_n are complex and depend on n, i.e., the relative phase and the ratio of the amplitudes depend on n. .

Figure 2.8(c) corresponds to the case where $S_+^2 > 1$ and $S_-^2 > 1$. The wave numbers constituting the localized mode are both in the form of Eq. (2.14), which corresponds to a decaying wave function with additional oscillations. The oscillations are in anti-phase ($w_n/\Phi_n < 0$ and real) independently of n and the ratio of their amplitudes $|w_n|/|\Phi_n|$ varies with depth. When the bending rigidity increases, Fig. 2.8(c), the transversal displacement vanishes and the rotational motion is dominant.

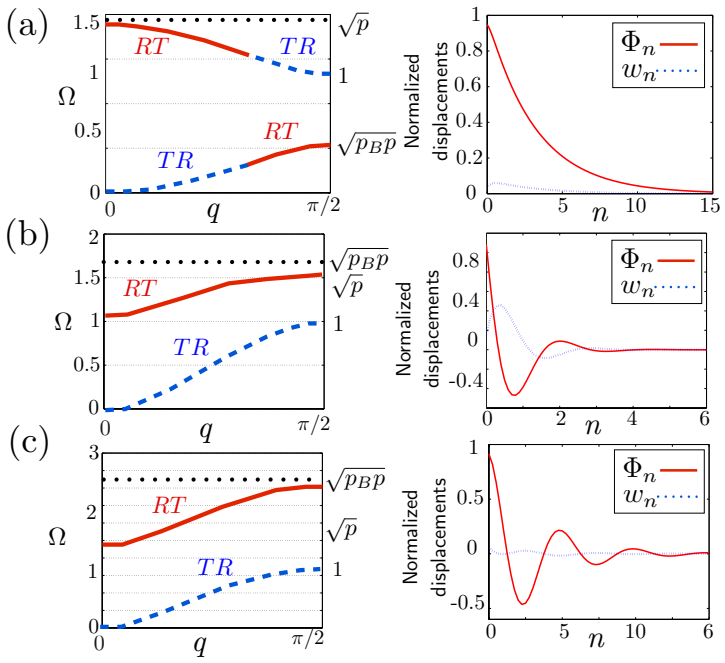

Figure 2.8 – Dispersion curves and discrete rotational and transversal displacements when $l' = 2$ and (a) $p = 2$ and $p_B = 0.08$, (b) $p = 1.2$ and $p_B = 2$ and (c) $p = 2$ and $p_B = 2.95$.

When $l' \to +\infty$, Eq. (2.30) becomes

$$\frac{\alpha_+}{\alpha_-} = \frac{S_+^2}{S_-^2}.$$

This case is identical to the one with $l' = 1$, except that the localization will start from the $n = 1$ particle. In fact, increasing l' the link to the wall at the $n = -1$ particle becomes more and more rigid and finally, when $l' \to +\infty$, the motion of the 0th particle is completely blocked and the 0th cylinder becomes a part of the rigid wall.

2.4 Conclusions

In this work we have demonstrated that localized modes can be exhibited in a 2D monatomic granular crystal when transversal and rotational motions are considered. The chain is composed of cylinders of equal mass, which possess one translational and one rotational degree of freedom. The interaction between transversal and rotational waves leads to two dispersive propagating acoustic

modes, separated by a gap of forbidden frequencies. By modifying the bending and shear rigidities between the end of the chain and a rigid wall, we have established the required conditions for the existence of a localized mode in the semi-infinite chain of cylinders. The special feature of the evaluated linear chain of cylinders, exhibiting two degrees of freedom each, is that the localized mode is composed of two evanescent modes. This is an important difference from earlier studied cases of longitudinal localized modes in linear chains of beads and in layered structures where at each frequency only a single evanescent mode could exist. The advantage of this theoretical evaluation of discrete granular crystal, is to obtain simple analytical expressions for the propagating and localized modes. Depending on the ratio between the rigidities of the springs connecting the first cylinder in the chain to the rigid wall and the rigidities between the other cylinders of the chain, the frequency of the localized mode can lie either in the forbidden band between the two propagating modes or above the upper propagating mode. We have examined the profiles of the rotational and transversal displacements of the localized mode as a function of the particle number and for different boundary conditions. Depending on the position of the localized mode frequency with respect to the propagating bands, these profiles and the degree of localization are various. The results of our research, the mode localization in a chain with cylinder of equal masses are complementary to the recent theoretical [1, 2, 4] and experimental [3] investigations of the acoustic waves in 3D granular crystals where the roles of the rotational degrees of freedom of the beads on the wave propagation have been analyzed.

In the future, this investigation should be extended to two- and three-dimensional granular crystals in terms of the wedge and the surface waves characterizing these structures and also to comparison of these surface waves with the prediction of surface modes existing within the Cosserat continuum. In the experimental investigations of these localized modes the considered configuration would be realized using a chain composed of magnetic cylinders. To investigate the vibrational response of the chain, it can be excited at one of its ends by a shaker. The attractive magnetic force between cylinders causes in this case the prestress of the contacts between the cylinders, initiating their shear and bending contact rigidities.

Bibliography

[1] A. Merkel, V. Tournat, and V.E. Gusev. Elastic waves in noncohesive frictionless granular crystals. *Ultrasonics*, 50(2):133 – 138, 2009.

[2] A. Merkel, V. Tournat, and V.E. Gusev. Dispersion of elastic waves in three-dimensional noncohesive granular phononic crystals: Properties of rotational modes. *Phys. Rev. E.*, 82(3):031305, 2010.

[3] A. Merkel, V. Tournat, and V.E. Gusev. Experimental evidence of rotational elastic waves in granular phononic crystals. *Phys. Rev. Lett.*, 107(22):225502, 2011.

[4] V. Tournat, I. Pèrez-Arjona, A. Merkel, V. Sanchez-Morcillo, and V.E Gusev. Elastic waves in phononic monolayer granular membranes. *New Journal of Physics*, 13(7):073042, 2011.

[5] H. Pichard, A. Duclos, J-P. Groby, V. Tournat, and V.E. Gusev. Localized transversal-rotational modes in linear chains of equal masses. *Phys. Rev. E.*, 89:1–10, January 2014.

[6] M. Cai, O. Painter, and K.J. Vahala. Observation of critical coupling in a fiber taper to a silica-microsphere Whispering-Gallery Mode System. *Phys. Rev. Lett.*, 85:74–77, July 2000.

[7] F. de Fornel. *Evanescent Waves: From Newtonian Optics to Atomic Optics*. Springer, New York, 2001.

[8] Ch. Spielmann, R. Szipöcs, A. Stingl, and F. Krausz. Tunneling of optical pulses through photonic band gaps. *Phys. Rev. Lett.*, 73:2308–2311, October 1994.

[9] S. Yang, J.H. Page, Z. Liu, M.L. Cowan, C.T. Chan, and P. Sheng. Ultrasound tunneling through 3D phononic crystals. *Phys. Rev. Lett.*, 88(10):104301, February 2002.

[10] J.B. Pendry. Negative refraction makes a perfect lens. *Phys. Rev. Lett.*, 85:3966–3969, October 2000.

[11] D.M. Profunser, O.B. Wright, and O. Matsuda. Imaging ripples on phononic crystals reveals acoustic band structure and Bloch harmonics. *Phys. Rev. Lett.*, 97(5):055502, August 2006.

[12] R.J.P. Engelen, D. Mori, T. Baba, and L. Kuipers. Subwavelength structure of the evanescent field of an optical Bloch wave. *Phys. Rev. Lett.*, 102(2):023902, January 2009.

[13] J. Mahanty, A.A. Maradudin, and G.H. Weiss. Vibrational thermodynamic properties of lattices with defects. *Progress of theoretical physics*, 20:1–26, September 1958.

[14] V. Keppens, D. Mandrus, B.C. Sales, B.C. Chakoumakos, P. Dai, R. Coldea, M.B. Maple, D.A. Gajewski, E.J. Freeman, and S. Bennington. Localized vibrational modes in metallic solids. *Nature*, 395:876–878, 1998.

[15] J. Mock, T. Hill, Y.-J. Tsai, A. Chilkoti, and D.R. Smith. Probing dynamically tunable localized surface plasmon resonances of film-coupled nanoparticles by evanescent wave excitation. *Nano Letters*, 12(4):1757–1764, April 2012.

[16] E.W. Montroll and R.B. Potts. Effect of defects on lattice vibrations. *Physical review*, 100:525–543, October 1955.

[17] R.F. Wallis and A.A. Maradudin. Impurity induced infrared lattice vibration absorption. *Progress of theoretical physics*, 24:1055–1077, November 1960.

[18] R.L. Bjork. Impurity-induced localized modes of lattice vibration in a diatomic chain. *Physical review*, 105:456–459, January 1957.

[19] R.F. Wallis. Effect of free ends on the vibration frequencies of one-dimensional lattices. *Physical review*, 540:1–6, July 1957.

[20] R.E. Camley, B. Djafari-Rouhani, L. Dobrzynski, and A.A. Maradudin. Transverse elastic waves in periodically layered infinite and semi-infinite media. *Phys. Rev. B*, 27:7318, December 1983.

[21] E.H. Boudouti, B. Djafari-Rouhani, A. Akjouj, and L. Dobrzynski. Theory of surface and interface transverse elastic waves in *N-layer* superlattices. *Phys. Rev. B*, 54:1–14, November 1996.

[22] H.J. Trodahl, P.V. Santos, G.V.M. Williams, and A. Bittar. Raman scattering from surface and bulk acoustic phonons in capped superlattices. *Phys. Rev. B*, 40:8577, June 1989.

[23] S. Mizuno and S.I. Tamura. Resonant interaction of phonons with surface vibrational modes in a finite-size superlattice. *Phys. Rev. B*, 53:4549–4552, February 1996.

[24] H.T. Grahn, J. Maris, J. Tauc, and B. Abeles. Time-resolved study of vibrations of a-GE:H/a-Si:H multilayers. *Phys. Rev. B*, 38:6066, March 1988.

[25] N.-W. Pu and J. Bokor. Study of surface and bulk acoustic phonon excitations in superlattices using picosecond ultrasonics. *Phys. Rev. Lett.*, 91(7):076101, August 2003.

[26] S. Aubin, P.B. Allen, and R.B. Doak. Surface phonons and other localized excitations. *American Journal of Physics*, 68:228, February 2000.

[27] A.-C. Hladky-Hennion, A. Devos, and M. de Billy. Quantitative analysis of the vibration modes in a finite set of coupled spheres. *The Journal of the Acoustical Society of America*, 116(1):117, 2004.

[28] A.-C. Hladky-Hennion, G. Allan, and M. de Billy. Localized modes in a one-dimensional diatomic chain of coupled spheres. *Journal of Applied Physics*, 98(5):054909, 2005.

[29] A.-C. Hladky-Hennion and M. de Billy. Experimental validation of band gaps and localization in a one-dimensional diatomic phononic crystal. *The Journal of the Acoustical Society of America*, 122(5):2594, 2007.

[30] G. Theocharis, N. Boechler, P.G. Kevrekidis, S. Job, M.A. Porter, and C. Daraio. Intrinsic energy localization through discrete gap breathers in one-dimensional diatomic granular crystals. *Phys. Rev. E.*, 82(5):056604, November 2010.

[31] N. Boechler, G. Theocharis, S. Job, P.G. Kevrekidis, M.A. Porter, and C. Daraio. Discrete breathers in one-dimensional diatomic granular crystals. *Phys. Rev. Lett.*, 104(24):244302, June 2010.

[32] C. Hoogeboom, G. Theocharis, and P.G. Kevrekidis. Discrete breathers at the interface between a diatomic and a monoatomic granular chain. *Phys. Rev. E.*, 82(6):061303, December 2010.

[33] V.F. Nesterenko. *Dynamics of Heterogeneous Materials.* Springer-Verlag, New York, 2001.

[34] K.L. Johnson. *Contact Mechanics.* Cambridge University Press, Cambridge, 1985.

[35] A. Eringen. *Microcontinuum Field Theories. I.Foundations and Solids.* Springer, New York, 1999.

[36] W. Nowacki. *Theory of Asymmetric Elasticity.* Pergamon, Oxford, 1986.

[37] M.A. Kulesh, V. P. Matveenko, and I.N. Shardakov. Propagation of surface elastic waves in the Cosserat medium. *Acoustical Physics*, 52:186, 2006.

[38] A.S.J. Suiker, A.V. Metrikine, and R. de Borst. Comparison of wave propagation characteristics of the Cosserat continuum model and corresponding discrete lattice models. *International Journal of Solids and Structures*, 38(9):1563 – 1583, 2001.

Chapitre 3

Two-dimensional discrete granular phononic crystal for shear wave control

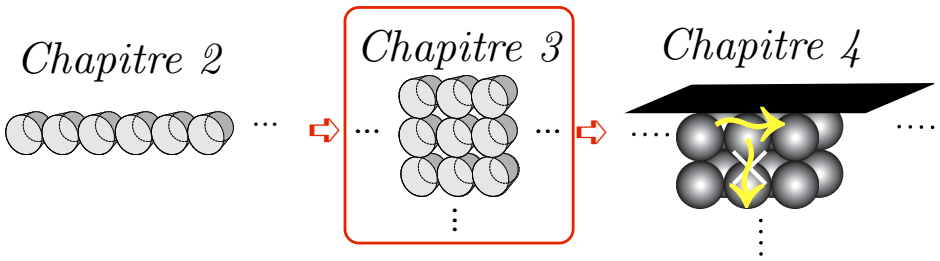

Ce chapitre, rédigé en anglais, est la transcription d'un article paru dans le journal Physical Review B [1]. Suite à l'analyse de modes propagatifs et localisés dans une chaîne granulaire monoatomique exposée dans le chapitre précédent, la propagation d'ondes de volume dans un cristal phononique granulaire bidimensionnel est analysée. Le passage d'une chaîne à un cristal bidimensionnel introduit la prise en compte d'un degré de liberté supplémentaire. Les particules possèdent alors deux degrés de liberté en translation et un degré de liberté en rotation. L'interaction entre ondes de translation et ondes de rotation dans le cristal est analysée. Selon les valeurs des différentes forces de contact entre les particules, une large variété de structure de bandes est obtenue. Sont révélées en particulier une bande interdite complète, la présence d'un cône de Dirac ainsi que l'existence d'un point de vitesse de groupe nulle résultant en un phénomène de double réfraction. L'intérêt de ce travail théorique est d'obtenir des expressions analytiques simples des fréquences des modes de propagation aux différents points de la zone de Brillouin. Ceci permet de décrire précisément les diagrammes de dispersion en fonction des paramètres contrôlant le cristal. Aussi, cette analyse détaillée de la structure de bandes du cristal phononique granulaire permettra d'étudier, dans le dernier chapitre, l'existence de modes de surface. Dans ce but, il est en particulier intéressant de connaître la position des bandes interdites correspondant aux zones autorisées pour les ondes de surface dans le cristal.

Abstract

The phononic properties of a two-dimensional discrete phononic crystal, made of circular cross-section infinitely long contacting elastic cylinders arranged on a simple square lattice, are described analytically. The significant interaction between shear and rotational waves is demonstrated in such granular phononic crystals. Controlling these interactions provides an opportunity for shear wave band design in metamaterials. The phononic band structure presents typical features of a square elementary cell of discrete phononic materials and also of continuous (composite) two-dimensional phononic materials with identical elementary cells. The theoretical analysis provides a clear physical explanation for the existence of a zero-group velocity point of the lowest-energy acoustic mode in particular directions of the phononic crystal and demonstrates the birefraction phenomenon.

3.1 Introduction

Two-dimensional models of granular media with spatially periodic distribution of particles were developed earlier [2–4] to extract, from the long-wavelength limit, the microstructural physical origin of the elastic constants appearing in the Cosserat and micro polar theories [5–7] of continuum elasticity. More elaborate three-dimensional discrete micro-mechanical models of disordered granular material have also been proposed [3, 8] to improve existing generalized theories of the continuum elasticity through homogenization methods. These generalized theories could be used to predict weak velocity dispersion of acoustic waves in micro inhomogeneous materials in the long-wavelength limit. Such effective medium theories are either a combination of the Cosserat and higher-order deformation gradient theories [8] or a second-gradient micro-polar constitutive theory [9].

Despite the seminal publication 30 years ago [10] researchers started only recently to apply the discrete lattice models to describe the phononic band structure of granular crystals. These discrete models do not only apply for the long-wavelength limit, and they provide elastic eigenmodes for all possible wavelengths, which can be used to predict, in particular, the frequency forbidden bands for wave propagation [11–18]. The revival of interest in discrete lattice models has been largely stimulated by the recent progress in manufacturing new materials made of periodically arranged micro- and nano-grains, such as colloidal crystals [19–21], nanoparticle superlattices [22–24] and nanoparticle membranes [25, 26]. Recently, the propagation of elastic stress waves in centered square highly nonlinear granular systems has been studied experimentally and numerically [27] and the transformation of the band gap of a two dimensional (2D) bidisperse granular crystal with deformation has been investigated numerically [28]. A two-dimensional discrete lattice model with particles possessing one translational and two rotational degrees of freedom has been applied recently to the analysis of a monolayer granular phononic membrane [17]. A three-dimensional discrete lattice model with rotating particles [18] has demonstrated that the Cosserat theory [5–7] fails to predict correctly the dispersion of the elastic waves in granular crystals even in the long-wavelength limit and should be combined with higher-gradient theories [8, 9]. Even more importantly, this discrete model has been successfully applied for the description of cut off frequencies and dispersion relations of coupled rotational-translational elastic waves observed for the first time in granular crystals. Thus, the results presented in Ref. [18] demonstrate the usefulness of discrete lattice models for both the prediction of phononic properties of granular

crystals and the evaluation (in the long-wavelength limit) of the effective/homogenized properties of micro-inhomogeneous/composite materials.

Here we present a theoretical evaluation of the elastic eigenmodes of a two-dimensional granular crystal made of circular cross-section infinitely long cylinders distributed periodically on a square lattice. Each particle possesses two translational and one rotational degrees of freedom similar to earlier studied models [2–4]. Our analysis provides the description of elastic eigenmodes not only near the Γ point but in the complete first Brillouin zone. In these granular crystals the elastic contacts between adjacent particles occur over a surface that is much smaller than the particle dimensions and are much softer than the particles themselves. This enables the propagation of elastic waves at frequencies much lower than the acoustic resonance frequencies of the individual particles. Propagation of translational waves at these low frequencies is strongly affected by their interactions with rotational waves. Two mixed transversal/rotational modes are actually propagating even in the high-symmetry directions of these phononic crystals. The interactions between the longitudinal, transversal and rotational motions of the particles can produce a variety of possible phononic band structures. These band structures could either present or not present forbidden frequency bands depending on the relative strength of the different inter-particle forces, which are due to normal, shear and bending rigidities of the contacts. Thus, the particles can be natural "bricks" for the design of granular metamaterials with phononic properties required for the control of shear wave propagation.

The developed theory revealed a remarkable coupling between shear and rotational waves in the lowest-frequency band along the ΓM direction. Along this direction, two group velocity regions, separated by a zero-group velocity point, exist for a single acoustic mode. A nonmonotonous dependence of the frequency on the wave number for the lowest energy mode propagating along the ΓM direction was numerically predicted earlier by computation of the phononic properties of two-dimensional metamaterials. These metamaterials were made of cylinders distributed on a square lattice surrounded by a host matrix [29–33]. These cylinders were either composed of a material different from the one of the host matrix [29, 30, 34] or empty [29, 31]. However, the physical nature of the possible unusual refraction of this lowest-energy mode was not revealed because the theoretical analysis was focused on understanding the physics of the band-gap formation. The simple analytical theory developed in this paper provides insight not only into the physical origin of the nonmonotonous dispersion curves for the lowest-frequency mode in the discrete granular phononic crystal but also into two-dimensional periodic composites. The theory relates the nonmonotonous lowest-energy mode to the existence of zero-energy rotational vibrations and to hybridization of transversal and rotational modes. This is important from a general theoretical point of view and also in view of currently growing interest in negative refraction [33, 35–37] and birefraction [35] phenomena in phononic crystals and metamaterials. Until now these phenomena have only been studied theoretically [38] and demonstrated experimentally for the eigenmodes belonging to higher-order ("optical") allowed frequency bands [33, 35, 36]. It is worth noting that the discrete lattice model of the granular crystals is obviously similar in its application to the evaluation of the periodic composite materials in the frame of the lumped-mass-spring model proposed for the study of band structures in two-dimensional phononic crystals some years ago [32]. The crucial difference lies in the fact that the lumped-mass-spring model [32] did not account for the rotational degrees of freedom of microinhomogeneous/composite media and, as a consequence, failed

to predict the effects related to the interactions between the translational and rotational elastic motions.

This chapter is organized as follows. The discrete model and the resulting dispersion curves are presented in Sec. 3.2. The influence of the different interparticle forces on these dispersion curves is discussed in Sec. 3.3. In particular, a possible realization of the Dirac-like cones is demonstrated. Finally, the propagation of the lowest transversal/rotational mode along the ΓM direction, exhibiting a nonmonotonous dispersion relation with a zero-group velocity point, is studied in Sec. 3.4.

3.2 Theory

3.2.1 Longitudinal and shear rigidities at the contacts

The two-dimensional granular crystal under consideration is made of circular cross-section infinitely long cylinders distributed periodically on a square lattice, as depicted in Fig. 3.1(a). The structure is characterized by a lattice constant $a = 2R_c$, where R_c is the radius of the cylinders. The corresponding first Brillouin zone of this phononic crystal is defined in Fig. 3.1(c).

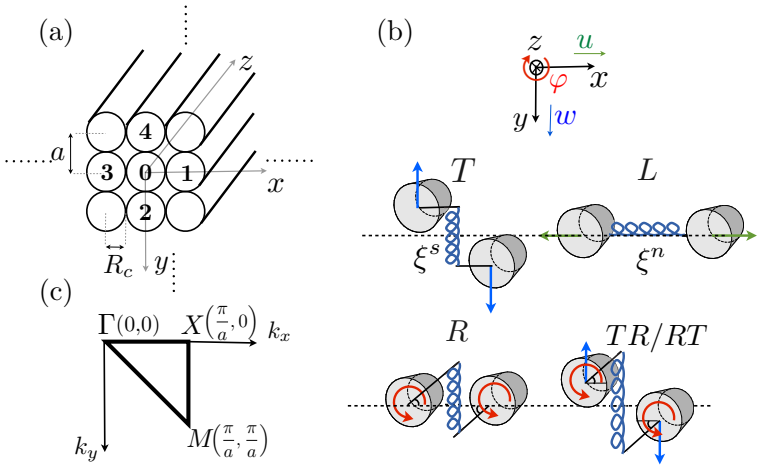

Figure 3.1 – (a) Representation of the periodic arrangement of cylinders and the coordinate axes, (b) illustration of different possible motions, (c) definition of the first Brillouin zone.

Each particle, i.e., each cylinder, possesses two translational and one rotational degrees of freedom. Normal and shear forces at the contacts between two adjacent particles are described with springs of constant rigidity, ξ^n and ξ^s, respectively. The elongation of the springs introduces forces and momenta that induce the motion of the particles: the displacements u along the x axis and w along the y axis and the rotation φ around the z axis. Different possible motions of two neighbor particles are illustrated in Fig. 3.1(b). T, L, R, and T/R represent the transversal, longitudinal, rotational and combined transversal/rotational motions, respectively. Note that on R and TR/RT motions, it is still shear rigidity which works, i.e., as on the T one. As presented in Fig. 3.3 (Sec. 3.2.3), attention will be given to the combination of these three motions.

The equations of motion of the central particle denoted by 0, obtained by applying the Lagrange

principle [3], are

$$m\ddot{u}_0 = \xi^n \left[\delta l_1 - \delta l_3\right] + \xi^s \left[\delta s_4 - \delta s_2\right] \ , \tag{3.1a}$$

$$m\ddot{w}_0 = \xi^n \left[\delta l_2 - \delta l_4\right] + \xi^s \left[\delta s_1 - \delta s_3\right] \ , \tag{3.1b}$$

$$I\ddot{\varphi}_0 = -\xi^s R_c \left[\delta s_1 + \delta s_2 + \delta s_3 + \delta s_4\right] \ , \tag{3.1c}$$

where m is the mass of the particle and I is its momentum of inertia. The spring elongation in the normal and transversal directions between the central and the ith particles, i.e., the relative displacement between the zeroth and the ith particle at the contact point, are denoted, respectively, by δl_i and δs_i. These relative displacements are explicitly given by

$$\begin{aligned}
\delta l_1 &= u_1 - u_0 \ , \\
\delta l_2 &= w_2 - w_0 \ , \\
\delta l_3 &= u_0 - u_3 \ , \\
\delta l_4 &= w_0 - w_4 \ , \\
\delta s_1 &= w_1 - w_0 + R_c(\varphi_1 + \varphi_0) \ , \\
\delta s_2 &= u_0 - u_2 + R_c(\varphi_2 + \varphi_0) \ , \\
\delta s_3 &= w_0 - w_3 + R_c(\varphi_3 + \varphi_0) \ , \\
\delta s_4 &= u_4 - u_0 + R_c(\varphi_4 + \varphi_0) \ .
\end{aligned} \tag{3.2}$$

The equations of motion are solved in the form of plane waves

$$\mathbf{V_i} = \begin{pmatrix} u_i(x,y,t) \\ w_i(x,y,t) \\ \Phi_i(x,y,t) \end{pmatrix} = \mathbf{v} e^{i\omega t - ik_x x_i - ik_y y_i} \ , \tag{3.3}$$

with the new variable $\Phi = R_c\varphi$ and $\mathbf{v} = \begin{pmatrix} u \\ w \\ \Phi \end{pmatrix}$ being the amplitude vector.
Equation (3.3) is then developed around the equilibrium position (x_0,y_0) of the central particle, $\mathbf{V_i}$=$\mathbf{v}e^{i\omega t - ik_x x_0 - ik_y y_0} e^{-ik_x \Delta x_i - ik_y \Delta y_i}$, where $\Delta x_i = x_i - x_0$ and $\Delta y_i = y_i - y_0$ are the relative coordinates between the central particle and the ith particle and ω is the angular frequency.

Finally, substituting Eq. (3.3) into the set of Eqs. (3.1) and (3.2) leads to the eigenvalue problem

$$\mathbf{S}\mathbf{v} = -\Omega^2 \mathbf{v} \ , \tag{3.4}$$

where $\Omega = \omega/\omega_0$ is the reduced frequency with $\omega_0 = 2\sqrt{\xi^s/m}$, and $\mathbf{S}$ is the dynamical matrix defined by

$$\mathbf{S} = \begin{pmatrix} -\eta \sin^2 q_x - \sin^2 q_y & 0 & i \sin q_y \cos q_y \\ 0 & -\eta \sin^2 q_y - \sin^2 q_x & -i \sin q_x \cos q_x \\ -ip \sin q_y \cos q_y & ip \sin q_x \cos q_x & -p(\cos^2 q_x + \cos^2 q_y) \end{pmatrix} \ , \tag{3.5}$$

where $p = \omega_1^2/\omega_0^2 = mR_c^2/I$ with $\omega_1 = 2R_c\sqrt{\xi^s/I}$, $\eta = \xi^n/\xi^s$, and $q_{x,y} = k_{x,y}a/2$.
The solution of this eigenvalue problem gives the $\Omega - k$ dispersion curves.

The dispersion curves are controlled by the ratio $\eta = \xi^n/\xi^s$ between the normal rigidity ξ^n and the shear rigidity ξ^s of the individual contacts and by the ratio $p = mR_c^2/I$ between the momentum of inertia of empty cylindrical shell mR_c^2 and the one of the cylinders I. Depending on the mass distribution, the cylinders can be radially inhomogenous ($I \leq mR_c^2$) and in the limit case of $p = 1$, the dispersion curves of a 2D granular crystal made of cylindrical shells of infinitely small thickness can be theoretically studied.

3.2.2 Bending rigidity at the contacts

The bending rigidity of the contact of the radius r is described [17] by two additional springs with normal rigidity ξ^B. They are located at the edge points of the contacts and are oriented along the vector connecting the centers of the contacting beads, Fig. 3.2. In this simplified model of bending rigidity, rotations of the neighbor particles in opposite directions with the same angle will induce elongation of one of the springs and contraction of the other. The corresponding forces have nonzero momenta and cause the particles to return to their equilibrium state. As a consequence, momenta exist along the z axis even if the particles rotate with exactly opposite angles. These additional momenta acting on the zeroth particle can be described by $M_{0i} = -\dfrac{(R_c\theta)^2}{2}\xi^B(\varphi_0 - \varphi_i)$, with i=1,2,3,4 and θ being the angular contact dimension.
The equation of motion for the rotation, Eq. (3.1c), is then modified to account for all additional momenta ΔM applied on the particle 0

$$\Delta M = \sum_{i=1}^{4} M_{0i} = -\frac{(R_c\theta)^2}{2}\xi^B(4\varphi_0 - \varphi_1 - \varphi_2 - \varphi_3 - \varphi_4) \ .$$

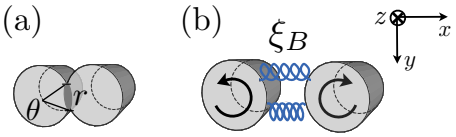

Figure 3.2 – Schematic representation of the bending rigidity, (a) contact geometry, (b) bending coupling.

The matrix $\mathbf{S}$, Eq. (3.5), is modified and becomes $\mathbf{S}'$ by adding the extra term ΔS_{33} to S_{33} in the following way, $S'_{33} = S_{33} + \Delta S_{33}$, with $\Delta S_{33} = -4p_B p(\sin^2 q_x + \sin^2 q_y)$ and p_B being the bending rigidity parameter defined as $p_B = \dfrac{\theta^2}{2}\dfrac{\xi^B}{\xi^s}$.

3.2.3 Dispersion curves

Figure 3.3 depicts $\Omega - k$ dispersion curves following the $M\Gamma XM$ path of the first Brillouin zone, and the solution of the eigenvalue problem, Eq. (3.4), with η=2.5, p=1.2, and p_B=0, i.e., without bending rigidity. From the eigenvalues and eigenvectors, the dispersion relations of the different modes can be found analytically and can be described within the complete Brillouin zone. The eigenmodes of the granular phononic crystal motion are composed of three components, the longitudinal motion L, the transversal motion T, and the rotational motion R. In Fig. 3.3, the plotted eigenvalues have been colored relative to the eigenvectors that have been classified, and the nature of the modes is labeled. The continuous red-orange lines correspond to coupled displacement-rotation modes with

a predominance of rotation (RT, RLT), the dashed blue lines correspond to coupled displacement-rotation modes with a predominance of displacement (TR, LTR), and the dotted green lines correspond to pure displacement modes (L, TL).

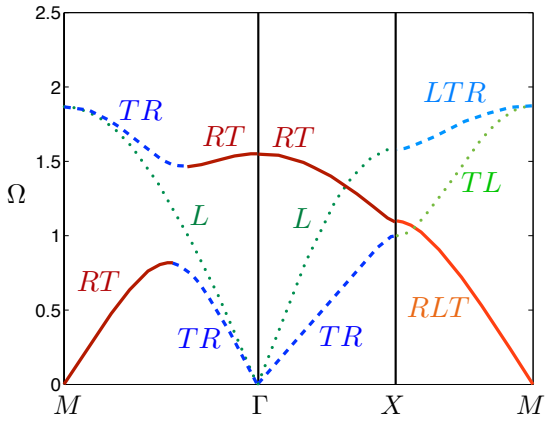

Figure 3.3 – Dispersion curves for η=2.5, p=1.2 and p_B=0. Solid curves correspond to coupled displacement-rotation modes (with a predominance of rotation), dashed curves correspond to coupled displacement-rotation modes (with a predominance of displacement), and dotted curves correspond to pure displacement modes. The resonance vibrational frequencies of the individual cylinders are assumed to be at much higher frequencies and are not represented here.

Along the principal directions ΓX and ΓM, transversal waves strongly interact with rotational waves and two-mixed transversal/rotational TR and RT modes propagate even along the symmetry axis of this phononic crystal. A pure acoustic-type longitudinal mode L propagates at frequencies $\Omega_{LA}=\sqrt{\eta}\sin q_x$ and $\Omega_{LA}=\sqrt{\eta+1}\sin q_x$ along the ΓX and ΓM directions, respectively. This pure longitudinal mode is not coupled to the mixed transversal/rotational modes TR and RT. Along the XM direction, the lowest and highest frequency modes are composed of all three possible motions, i.e., L, T, and R. These bands are intercepted by a pure displacement mode TL. The interaction between the longitudinal, transversal and rotational motions of the particles can produce a variety of phononic band structures, which are controlled by the parameters η, p, and p_B. The influence of parameters η and p on the band structure will be discussed in Sec. 3.3.1; attention will be given in Sec. 3.3.2 to the case of a cylindrical shell of infinitely small thickness (p=1) where the band structure exhibits a Dirac singularity. The influence of the bending parameter p_B will be presented in Sec. 3.3.3.

A remarkable feature of the lowest transversal/rotational mode along the ΓM direction is the existence of two group velocity regions separated by a zero-group velocity point, resulting from a birefraction phenomenon. The position of this zero-group velocity point strongly depends on the parameters p, η and p_B. The description and the physical nature of these nonmonotonous modes and of the zero-group velocity point, as well as their dependence on the bending rigidity parameter p_B, will be presented in Sec. 3.4.

3.3 Influence of the parameters on the dispersion curves

3.3.1 Without bending rigidity

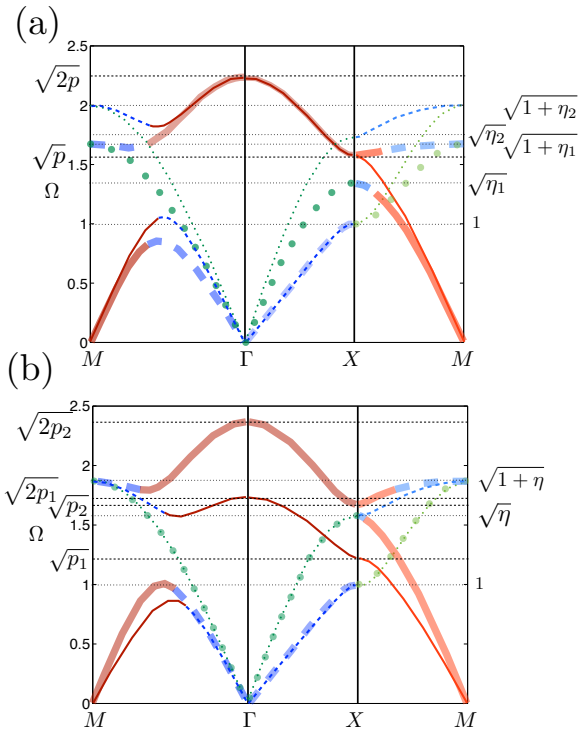

Figure 3.4 – Dispersion curves obtained with different values of the parameters η and p. (a) p=2.5, $\eta_1 = 1.8$ (thick line) and $\eta_2 = 3$ (thin line), (b) η=2.5, p_1=1.5 (thin line) and p_2=2.8 (thick line). Solid curves correspond to coupled displacement-rotation modes (with a predominance of rotation), dashed curves correspond to coupled displacement-rotation modes (with a predominance of displacement), and dotted curves correspond to pure displacement modes. The resonance vibrational frequencies of the individual cylinders are assumed to be at much higher frequencies and are not represented here.

When the bending rigidity is neglected, the dispersion curves in this granular crystal are controlled only by the ratio $\eta = \xi^n/\xi^s$ between the normal rigidity ξ^n and the shear rigidity ξ^s of the individual contacts and by the ratio $p = mR_c^2/I$ between the momentum of inertia of the empty cylindrical shell mR_c^2 and the one of the cylinders I, which can be radially inhomogeneous ($I \leq mR_c^2$). These curves can be strongly modified by varying one of these parameters. Figure 3.4 presents dispersion curves with different values of parameters η and p. The analytical values corresponding to characteristic points of the Brillouin zone are also plotted to emphasize the dependence of the eigenvalues on η and p. In the principal directions ΓX and ΓM, forbidden band gaps stand between the low-frequency transversal/rotational TR and high-frequency rotational/transversal RT propagation modes. These forbidden gaps are crossed only by a pure longitudinal mode L, which interacts neither with transversal nor with rotational modes. These forbidden gaps are encountered for different interactions between the transversal and rotational motions of the particles, i.e., for different values of η and p. However, no absolute band gap is noticed, i.e., a gap in all directions, because all three motions (shearing, rotation, and compression/dilatation) can be coupled within the individual plane eigenmodes aside the principal directions.

3.3.2 Dirac-like point

Intriguing transport properties, partly due to linear dispersion at the six corners of the hexagonal Brillouin zone, have been observed in graphene [39]. Such a feature in the dispersion relations, where two modes touch as a pair of cones, is referred to as Dirac cones, and the touching point is called a Dirac point. As recently developed in [40], the linear dispersion can have different physical origin. Dirac singularities have been reported in photonic [41, 42] and phononic crystals [43] at the corner of the Brillouin zones of triangular and honeycomb lattices where two bands meet. Similar to the graphene, the Dirac cones exist naturally as a consequence of lattice symmetry in these crystals. The Dirac cones possess a Berry phase [44] of $\pm\pi$, and therefore can give rise to antilocalization effects. It was reported that linear dispersions can also occur at the Brillouin zone center of a square lattice photonic crystal, induced by simultaneous zero permittivity and permeability, and the linear dispersion can be understood from an effective medium perspective [45]. Different from the Dirac cones in triangular/honeycomb lattice, which are a result of double degeneracy, the existence of linear dispersion due to triple degeneracy has been found in phononic crystals [46] and in metamaterial with simple cubic lattice [47]. This type of dispersion occurs by tuning the microstructure of the crystals and is called Dirac-like cones. As demonstrated by Mei et al. [40], it is important to distinguish the physical origin of Dirac and Dirac-like cones. For example, the Dirac-like cones with triple degeneracy cannot be mapped into the massless Dirac Hamiltonian and carry no Berry phase. Therefore, the structures are expected to exhibit normal localization behavior rather than antilocalization in the presence of disorder.

In this granular crystal, when the particles are cylindrical empty shells, i.e., p=1, with η=1 and $p_B = 0$, the dispersion relations exhibit a singularity at the X point: the dispersion relations of the lowest and highest modes become linear in the neighborhood of the X point, Fig. 3.5. In this case, the linear dispersion arises from triple degeneracy of the modes near the X point of the Brillouin zone and is then referred as a Dirac-like cone. To illustrate such Dirac-like cone visually, the 3D dispersion curves around the X point are presented in Fig. 3.5(b). Another characteristic here is that the Dirac-like cone modes exhibit super-anisotropic [46, 48] behavior. The Dirac-like cone modes have equi-frequency contours [36] (EFCs) that are almost circular; i.e., the system appears to be isotropic, but the eigenmodes are superanisotropic as only transverse modes are allowed to propagate along certain directions, while only longitudinal modes are allowed along other directions. As presented in Fig. 3.5(c), only transversal/rotational (TR/RT) waves are allowed along the ΓX direction, while only longitudinal/rotational (LR/RL) waves are allowed along the XM direction. This analytical model demonstrates that this 2D phononic granular crystal can exhibit super-anisotropy near the X point when p=1 and η=1.

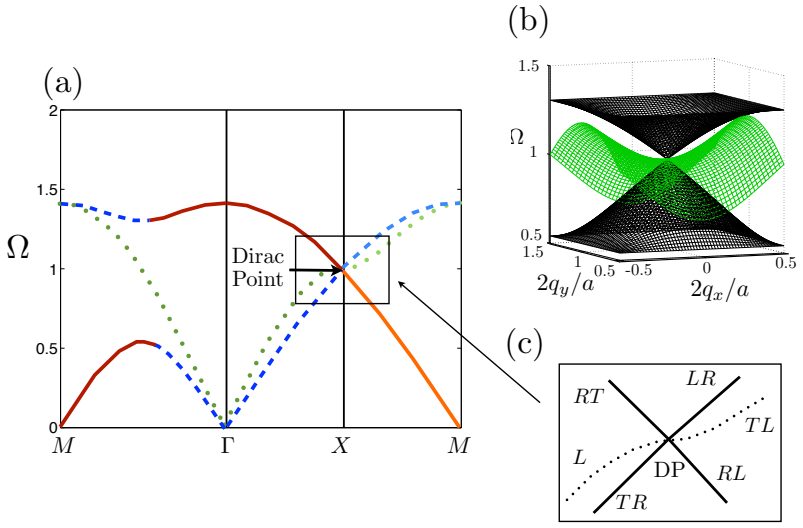

Figure 3.5 – (a) Dispersion curves obtained with p=1 and η=1, (b) three-dimensional dispersion surfaces near the Dirac-like point. The lowest and highest bands form Dirac-like cones, (c) enlarged view of the dispersion curves near the Dirac-like point (DP). The resonance vibrational frequencies of the individual shells are assumed to be at much higher frequencies and are not represented here.

It is worth recalling to remind here that in the theory under development the resonance frequencies of the cylinders are assumed to be much higher than the frequencies of the propagating modes (see the caption of Fig. 3.4). Thus the hybridization phenomenon between the propagating modes under evaluation and the resonances of the individual beads is suppressed. The most difficult challenge could be to satisfy this assumption in the case of crystals constructed from thin shells because their resonance frequencies could be much smaller than those of homogeneous cylinders.

To avoid possible hybridization between the propagating modes and the resonance of the cylindrical shells, the following condition must be respected

$$\frac{\omega_{shell}}{\omega_0} \gg \frac{\omega_{max}}{\omega_0} = \Omega_{max} \ , \tag{3.6}$$

where Ω_{max} is the maximum value of the normalized frequency. By substituting the first resonance frequency of an individual shell [49] $f_{shell} = \dfrac{\omega_{shell}}{2\pi} = \dfrac{1}{2\pi}\sqrt{E^*}\dfrac{h}{R_c^2}$ in Eq. (3.6), the condition becomes $\sqrt{E^*}\dfrac{h}{2R_c^2}\sqrt{m/\xi^s} \gg \Omega_{max}$, with $m \simeq 2\pi R_c h\rho$ being the mass of the shells and, $E^* = \dfrac{E}{12\rho(1-\nu^2)}$ where E is Young's modulus, ν is Poisson's ratio, ρ is the mass density, h is the thickness, and R_c the radius of the shells.

The material characteristics (E, ρ, ν) being fixed, the parameters that can be modified to respect the condition are the radius R_c, the thickness h of the cylindrical shells, and the shear rigidity ξ^s at the contact between the shells. According to Eq. (3.6), the shear rigidity must satisfy $\xi^s \ll \dfrac{h^3 E^* \rho\pi}{2R_c^3\Omega_{max}^2}$.

Experimental works have investigated the viscoelastic properties of a thin polymer film sheared between a bead and an ultrasonic resonator [50]. By depositing a layer of spherical beads on top of a quartz-crystal resonator [51] coated with a polymer, the properties and the influence of the film were determined. In particular, it was shown that the deposition of the film lowers the resonance of the quartz resonator, which attests of a decrease in the shear rigidity between the beads and the quartz resonator due to the additional film between them. Similarly, the boundary lubrication in weakly adhering molecularly thin films deposited between a sphere and a plane has been investigated exper-

imentally [52]. It has been demonstrated that the shear rigidity can be reduced by increasing the thickness of the film and by changing its nature. It is also possible to increase the shear rigidity limit $\xi^s_{lim} = \dfrac{h^3 E^* \rho \pi}{2R_c^3 \Omega^2_{max}}$ by increasing the ratio between the thickness and the radius h/R_c of the cylinders.

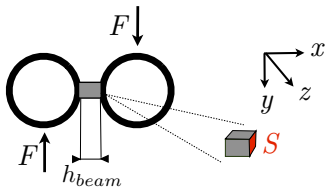

Figure 3.6 – Schematic view of the cylindrical shells with a beam made of polymer rigidly attached to them.

Theoretically, the rigidity induced by some additional coupling material can be estimated by considering a contact in the form of a beam rigidly attached to the shells, Fig. 3.6. The shear stress τ is related to the shear strain γ by the following equation [53]: $\tau = G\gamma = G\dfrac{\Delta w_{beam}}{h_{beam}}$, where $G = \dfrac{E}{2(1+\nu)}$ is the shear modulus of the material constituting the beam, Δw_{beam} is the beam displacement, and h_{beam} is the thickness of the beam. The pure shear stress and the shear stress in the case of bending are given by $\tau_{pure} = \dfrac{F}{S}$ and $\tau_b = \dfrac{3F}{2S}$, respectively, with F being the shear force and S being the surface of contact between the beam and the cylinders. The shear and bending rigidities of the coupling contact can be deduced

$$\xi^s_{pure} = \frac{F}{\Delta w_{beam}} = \frac{SG}{h_{beam}}, \quad \xi^s_b = \frac{2SG}{3h_{beam}} \ .$$

Therefore, the characteristics of the beam (material E, ν, thickness h_{beam}, and surface S) can be adequately chosen to respect the required condition (3.6).

3.3.3 With bending rigidity

Figures 3.7(a) and 3.7(b) depict the dispersion curves with η=2 and p=2.5 obtained for p_B=0.07 and p_B=0.35, respectively. For convenience, results obtained for these parameters without bending rigidity ($p_B = 0$) are plotted with thin lines. The frequencies of all the modes in the M, Γ, and X points can be found analytically. They are unchanged with and without the bending rigidity for the modes with a predominance of displacement (dotted and dashed curves), i.e., $\Omega = \sqrt{1+\eta}$ in M, $\Omega = 0$ in Γ, and $\Omega = 1$ and $\Omega = \sqrt{\eta}$ in X, and for the mode with a predominance of rotation in Γ where $\Omega = \sqrt{2p}$ (the values are indicated on the right side of the dispersion curves in Fig. 3.7). For the modes with a predominance of rotation (solid lines), the frequencies are modified by the bending rigidity at the characteristic M and X points. At the X point the bending parameter appears in the term $\sqrt{p}$, which becomes $\sqrt{p(1+4p_B)}$, and at the M point the rotational mode does not vanish any longer; i.e., the zero value at the M point becomes to $2\sqrt{2p_B p}$. The values are indicated on the left side of the dispersion curves in Fig. 3.7. The modes with a predominance of rotation are shifted to higher frequencies at the M and X points when the bending rigidity parameter p_B increases. An absolute band gap opens when $2\sqrt{2p_B p} > \sqrt{1+\eta}$ and $\sqrt{2p} > \sqrt{1+\eta}$ as shown in Fig. 3.7(b). To summarize, the upper limit of the complete band gap is shifted to high frequencies with increasing p and p_B and the lower limit is shifted to low frequencies with decreasing η.

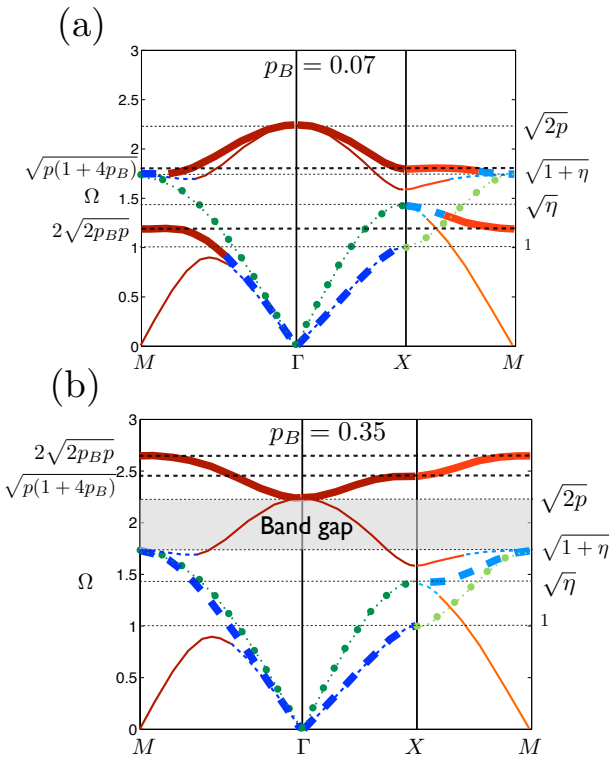

Figure 3.7 – Dispersion curves obtained with $\eta = 2$ and $p = 2.5$ for different values of the parameter p_B of bending rigidity : (a) p_B=0.07 ($2\sqrt{2p_Bp} < \sqrt{1+\eta}$) and (b) p_B=0.35 ($2\sqrt{2p_Bp} > \sqrt{1+\eta}$). Thin curves correspond to the identical case without bending rigidity. The complete band gap is shown by the gray shaded zone. The resonance vibrational frequencies of the individual cylinders are assumed to be at much higher frequencies and are not represented here.

This theoretical analysis demonstrates that the interactions between the longitudinal, transversal and rotational motions of the particles can produce a variety of possible phononic band structures, which can contain a Dirac-like point when p=1 and η=1 or a complete band gap when the bending rigidity is introduced. The position and the width of this complete band gap depend on the relative strength of the different inter-particle forces, which are due to normal, shear, and more importantly, bending rigidities.

3.4 Description of the nonmonotonous modes along the ΓM direction

3.4.1 Birefraction phenomenon

The developed theory reveals a remarkable coupling between transversal and rotational motions at the lowest frequencies along the ΓM direction. Indeed, along this direction two group velocity regions, separated by a zero-group velocity point, exist for a single mode, Fig. 3.3 and 3.4. Birefraction in the same band can be observed in this structure as in annular photonic crystals [38]. In order to understand the propagation behavior of the waves within the crystal, the band structure and corresponding EFCs [36] are examined for p=1, η=1.2 and p_B=0 in the lowest mode identified in Fig. 3.8(a). Using a 3D representation of the dispersion curves, Fig. 3.8(b), the EFCs are obtained from the intersection of the 3D dispersion curves with a horizontal plane, i.e., at fixed frequency. Figure 3.9 represents the EFCs for the studied crystal in the normalized K-space and the surrounding medium contour (dashed

contour) at $\Omega_m = 0.55$. The wave vector of the refracted beam should obey the $\mathbf{k}_{//}$-conservation relation: $\mathbf{k}^i_{//} = \mathbf{k}^{ref}_{//} + \mathbf{G}_{//}$, where $\mathbf{k}^i_{//}$ and $\mathbf{k}^{ref}_{//}$ are the wave-vector components parallel to the interface for the incident and refracted beams, respectively, and $\mathbf{G}_{//}$ is the parallel component of any reciprocal lattice vector. The group velocity (and hence the direction of energy propagation) of sound waves inside the crystal is given by the gradient of the angular frequency with respect to the wave vector, i.e., $\mathbf{v_g} = \nabla\Omega(\mathbf{k})$. This group velocity is always perpendicular to the EFCs and points toward the increasing frequencies. In our case, dual EFCs can be found for a single frequency, one around the Γ point and the other around the M point; then the $\mathbf{k}_{//}$-conservation line intersects the EFCs at two points, where the direction of the group velocity points inside the crystal. So, for a single frequency, two positive waves are transporting energy from the crystal surface toward the depth of the crystal (see the schematic representation in Fig. 3.10).

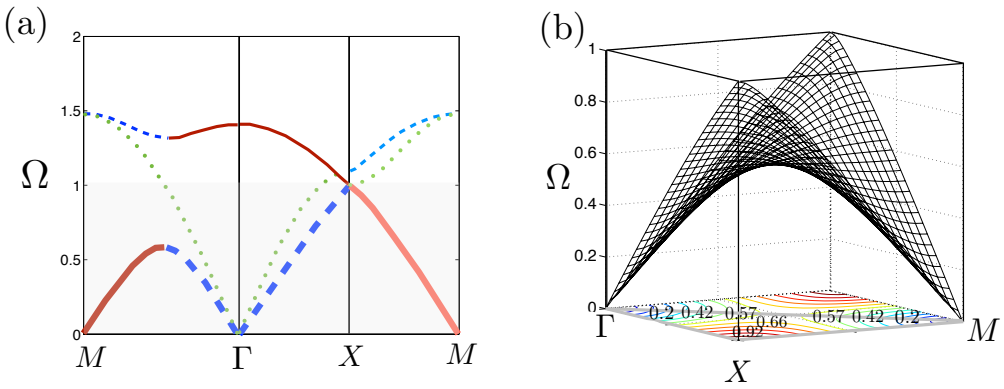

Figure 3.8 – (a) 2D dispersion curves; the lowest mode is identified, (b) 3D dispersion curves and equifrequency contours for the lowest mode (p=1, η=1.2 and p_B=0).

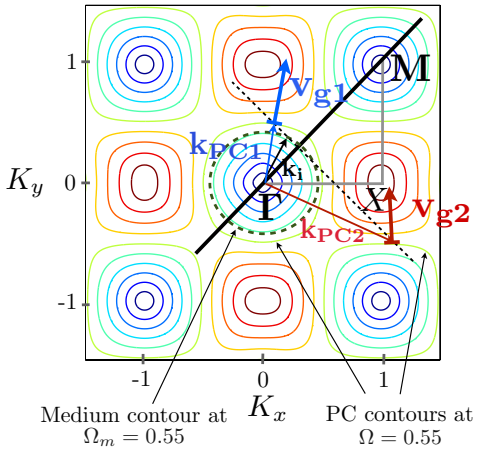

Figure 3.9 – (a) Equifrequency contours for the lowest mode in the PC (solid contour lines) and in a surrounding medium (dotted contour line) for $\Omega_m = 0.55$. The black dotted line shows the $\mathbf{k}_{//}$-conservation line, thin arrows denote the wave vectors, and thick arrows represent the group velocities.

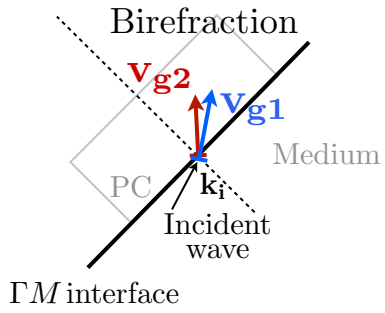

Figure 3.10 – Schematics of the birefraction process. The black dotted line shows the $\mathbf{k}_{//}$-conservation line, thin arrows denote the wave vectors and thick arrows represent the group velocities. $\mathbf{v_{g1}}$ is the group velocity vector of the wave with the dominance of the shear component, and $\mathbf{v_{g2}}$ is the group velocity vector of the wave with the dominance of the rotational component.

To our knowledge, birefraction for a single mode has not been observed in phononic crystals at low frequencies. The existence conditions for these nonmonotonous modes as a function of parameters p, η, and p_B are discussed in the next section. A physical explanation is also proposed for the origin of these nonmonotonous modes.

3.4.2 Hybridization of the modes

To investigate the behavior of the nonmonotonous modes along the ΓM direction, the interaction between pure rotational and pure transversal modes is studied along this direction. We impose, respectively, $I \to \infty$ and $m \to \infty$ in the analytical dispersion relations corresponding to the transversal/rotational modes. These assumptions formally avoid either the rotation or the translation of the cylinders. Therefore, when $p = \dfrac{mR_c^2}{I} \underset{I\to\infty}{\to} 0$, a pure transversal mode exists, and when $p = \dfrac{mR_c^2}{I} \underset{m\to\infty}{\to} \infty$, a pure rotational mode exists.
The dispersion relations of the different modes are found analytically by solving the eigenvalue problem, Eq. (3.4), with $q_x = q_y = q$ (ΓM direction). By imposing $p \to 0$ and $p \to \infty$, the dispersion relations of pure transversal Ω^T and pure rotational Ω^R modes along the ΓM direction are obtained: $\Omega^T = \sin q\sqrt{1+\eta}$ and $\Omega^R = \sqrt{2p\cos^2 q + 8p_B p \sin^2 q}$.

Figure 3.11(a) depicts the dispersion curves and the frequencies at the Γ and M points of the pure transversal and pure rotational modes in the absence of bending rigidity. The modes intersect inevitably because the frequency of the rotational mode is $\Omega_R = 0$ at the M point and the one of the transversal mode is $\Omega_T = 0$ at the Γ point. In other words, the intersection is due to $\Omega_R < \Omega_T$ at the M point and $\Omega_R > \Omega_T$ at the Γ point. Thus, repulsion occurs between the two modes around this intersection point, resulting in a hybridization of these two modes in the real crystal, as can be seen in Fig. 3.11(b).

As presented in Fig. 3.12(a) for two values of the bending rigidity parameter (p_{B1}=0.05 and p_{B2}=0.3), the frequency of the pure rotational mode is shifted to higher frequencies at the M point with increasing bending rigidity parameter. Therefore, for sufficiently large values of p_B (for instance, p_{B2}=0.3 in Fig. 3.12(a)) the pure rotational and pure transversal modes do not intersect any longer and the nonmonotonous modes disappear, Fig. 3.12(b). The existence of these nonmonotonous modes

and thus of the zero-group velocity point depends on the relative strength of the different interparticle forces, which are due to normal, shear, and bending rigidities at the contacts.

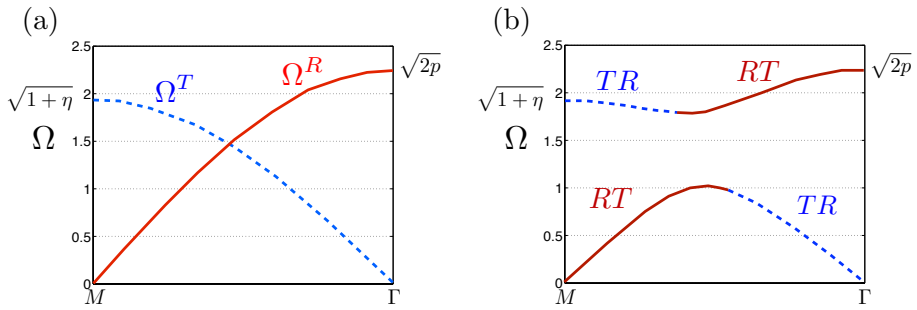

Figure 3.11 – (a) Dispersion curves of pure transversal ($p \to 0$) and pure rotational ($p \to \infty$) modes in the absence of bending rigidity (p_B=0) with p=2.5 and η=2.7, (b) corresponding dispersion curves.

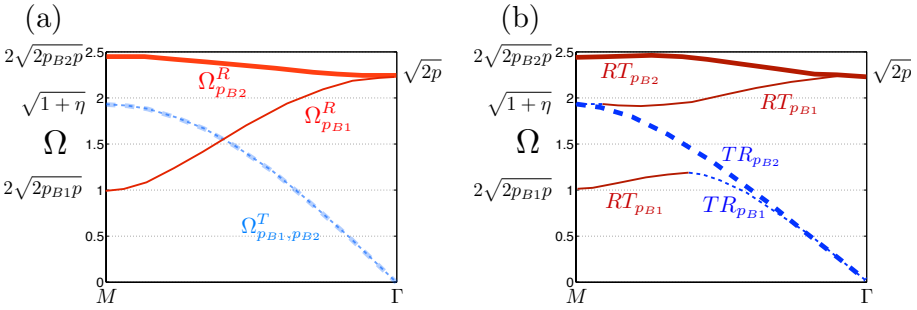

Figure 3.12 – (a) Dispersion curves of pure transversal ($p \to 0$) and pure rotational ($p \to \infty$) modes with p=2.5, η=2.7 and for two values of bending rigidity, p_{B1}=0.05 (thin line) and p_{B2}=0.3 (thick line), (b) corresponding dispersion curves.

3.4.3 Influence of the parameters η, p and p_B on the zero-group velocity point

In order to analyze the influence of the parameters on the position of the zero-group velocity point (ZGVP), the analytical expression of the lowest mode Ω_1 along the ΓM direction is obtained by solving the eigenvalue problem, Eq. (3.4), and it reads

$$\Omega_1^2 = \frac{1}{2}[2p\cos^2 q + 8p_B p \sin^2 q + \sin^2 q(1+\eta) - \sqrt{[2p\cos^2 q + \sin^2 q(1+\eta) + 8p_B p \sin^2 q]^2 - 8p\eta \sin^2 q(1-\sin^2 q) - 32 p_B p \sin^4 q(1+\eta)}] \,, \tag{3.7}$$

with $q = q_x = q_y$.

In the absence of bending rigidity, the wave number q_{zgvp} of the ZGVP is defined by solving

$$\left.\frac{\partial \Omega_1^2}{\partial \sin^2 q}\right|_{q=q_{zgvp}} = 0 \,. \tag{3.8}$$

The resolution of Eq. (3.8) leads to

$$\sin^2(q_{zgvp}) = \frac{\sqrt{2p}\left[\sqrt{2p}(2p-1+\eta) - (2p-1-\eta)\right]}{(2p-1+\eta)^2 + 4\eta} \,. \tag{3.9}$$

The position of this ZGVP as a function of parameters η and p can be estimated with Eq. (3.9). As illustrated in Fig. 3.13, the ZGVP moves toward the M point ($\sin q_{zgvp} \to 1$) with increasing p (for different values of η) and toward the Γ point ($\sin q_{zgvp} \to 0$) with increasing η (for different values of p). This can also be demonstrated analytically through

$$\left.\frac{\partial \sin^2(q)}{\partial \eta}\right|_{q=q_{zgvp}} < 0 \ , \tag{3.10}$$

$$\left.\frac{\partial \sin^2(q)}{\partial p}\right|_{q=q_{zgvp}} > 0 \ . \tag{3.11}$$

For $\eta \gg p \geqslant 1$, Eq. (3.9) reduces to

$$\sin^2(q_{zgvp}) \simeq \frac{\sqrt{2p}(\sqrt{2p}-1)}{\eta} \ll 1 \ , \tag{3.12a}$$

$$q_{zgvp} \simeq \sqrt{\frac{\sqrt{2p}(\sqrt{2p}-1)}{\eta}} \ . \tag{3.12b}$$

For $p \gg (\eta, 1)$, it reduces to

$$\sin^2(q_{zgvp}) \simeq 1 - \frac{1}{\sqrt{2p}} \ , \tag{3.13a}$$

$$q_{zgvp} \simeq \frac{\pi}{2} - \left(\frac{1}{2p}\right)^{1/4} \ . \tag{3.13b}$$

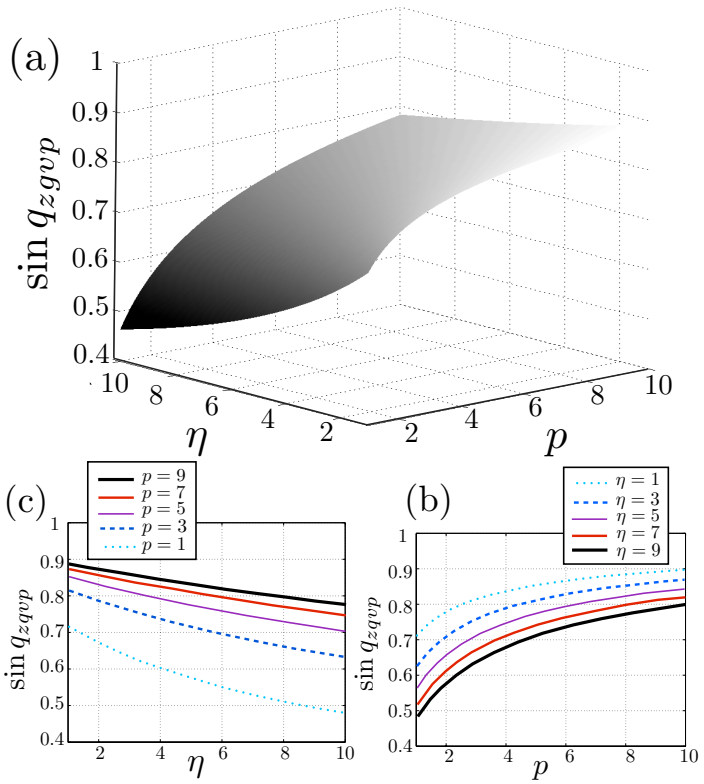

Figure 3.13 – (a) Position of the ZGVP as a function of p and η, $p_B = 0$, (b) sections of (a) at different values of p, (c) sections of (a) at different values of η.

These results were expected from the analysis of the hybridization leading to the ZGVP point. Equation (3.10) and the asymptotic case $\eta \gg p \geqslant 1$, Eq. (3.12), emphasize the influence of η on the

ZGVP, while Eq. (3.11) and the asymptotic case $p \gg (\eta, 1)$ demonstrate a very slow shift of the position of the ZGVP to the M point with increasing p, Eq. (3.13b).

With an increasing bending rigidity parameter, the ZGVP moves toward the M point, i.e., $\left.\frac{\partial \sin^2(q)}{\partial p_B}\right|_{q=q_{zgvp}} > 0$, and a part of the mode dominated by rotation is shifted to higher frequencies. Thus, when the maximum of the frequency of the lowest mode is at the M point, the ZGVP disappears. It is then possible to find a condition of disappearance of the ZGVP by solving the equation determining the extremum value of the lowest mode Ω_1, Eq. (3.7), at the M point

$$\left.\frac{\partial \Omega_1^2}{\partial \sin^2 q}\right|_{q=\pi/2} = 0 \ . \tag{3.14}$$

The resolution of Eq. (3.14) leads to $p_B^{Lim} = \frac{p + \eta + 1 - \sqrt{p^2 + 4p}}{8p}$ and indicates that when $p_B > p_B^{Lim}$, the ZGVP disappears.

This analytical demonstration shows that the position of the ZGVP changes with the ratio between p, η, and p_B. The nonmonotonous modes are encountered for a large interval of the parameters, characterizing the relative magnitude of bending, shear, and normal rigidities of the interparticle contacts, which provides a large variety of innovative granular metamaterial designs. The existence of this ZGVP is related to zero-energy rotational vibrations at the M point, when the bending rigidity is negligible, and can be explained physically.

3.4.4 Physical explanation

To better understand how the short-wavelength motions near the M point can occur at very low frequencies, it is insightful to analyze the spatial structure of the predicted lowest-energy TR/RT mode propagating along the ΓM direction when $\Omega \to 0$. When $\Omega < \Omega_{ZGVP}$, three propagating waves can be excited at each frequency. The first wave is a pure longitudinal wave of acoustical type, which does not interact with TR/RT mode. At $\Omega \ll \Omega_{ZGVP}$ this mode is nondispersive, $\Omega = \Omega_{LA} = \sqrt{1+\eta}\sin q \simeq \sqrt{1+\eta}\, q$. Due to the nonmonotonous dispersion relation of the TR/RT mode, two other waves can be excited at the same frequency. The first of them, with a dominance of transversal motion compared to the rotational one, is also of the acoustic type. When $\Omega \to 0$, this wave becomes a purely transversal nondispersive wave $\Omega = \Omega_{TR} = \sqrt{\eta}\sin q \simeq \sqrt{\eta} q \equiv \Omega_{TA}$. The dispersion relation of the second of the TR/RT waves is $\Omega_{RT}^2 \simeq \left(\frac{2p\eta}{1+\eta}\right)\cos^2 q$, which formally describes highly dispersive waves with $q \simeq \pi/2$ and with opposite directions of phase and group velocities, as is obvious in Fig. 3.3. The elastic field created by this counter-propagating RT wave can be presented in the form

$$C_+ e^{i(\omega t - 2qn)} + C_- e^{i(\omega t + 2qn)} \ , \tag{3.15}$$

where an integer number n accounts for the consecutive neighboring layers/rows of beads along the ΓM direction (see Fig. 3.14). The normalized wave number $q = (k_{11} a_{11})/2$ involves the wave number $k_{11} = \sqrt{2} k_x$ and the distance between the layers $a_{11} = a/\sqrt{2}$ along the ΓM direction.

While the form of the field in Eq. (3.15) indicates a highly dispersive acoustic-type wave with a normalized phase velocity defined by $v_{ph}^{RT} = \Omega/2q$, it can be rewritten in the low-frequency limit (for $q \simeq \pm\pi/2 \mp \Delta q$ and $\Delta q \to 0$) in the form

$$C_+(-1)^n e^{i\Omega\left(t+\frac{n}{v_{RT}(\Delta q)}\right)} + C_-(-1)^n e^{i\Omega\left(t-\frac{n}{v_{RT}(\Delta q)}\right)}, \tag{3.16}$$

where the velocity $v_{RT}(\Delta q) = \sqrt{\frac{p\eta}{2(1+\eta)}}$ is defined by $v_{RT}(\Delta q) = \Omega/2\Delta q$ and is frequency independent. The solution in Eq. (3.16) demonstrates that the RT elastic field can be viewed at low frequencies as a superposition of nondispersive optical-type waves, i.e., waves for which the neighboring beads are moving in opposite directions. The optical character of the RT mode is described by the factors $(-1)^n$ in Eq. (3.16). The revealed above optical-type waves are long wavelength in the sense that the spatial modulation of the beads motion, which is additional to the one described by the $(-1)^n$ factors, takes place at distances much longer than the lattice period.
In the limit $\Omega \to 0$ the RT mode is purely rotational. The structure of the mode in this case, when the displacements of the beads are negligible compared with their rotations, is illustrated in Fig. 3.14.

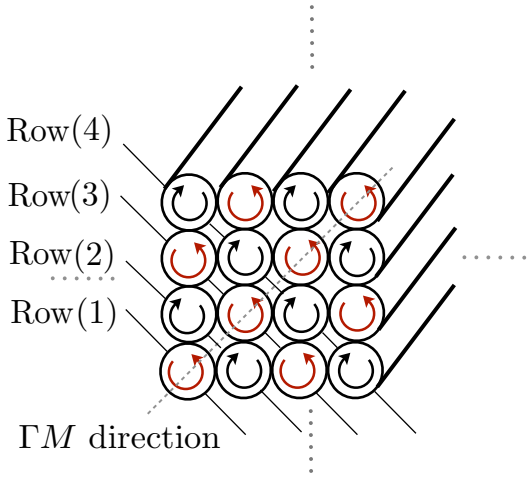

Figure 3.14 – Illustration of the purely rotational motion when $\Omega \to 0$. The displacements of the beads are negligible compared with their rotations.

It can be seen that a plane RT wave, with the phase front normal to the ΓM direction, can propagate. This motion is possible because of the absence of contact between the beads situated along the wave front, i.e., between the beads belonging to the same row in Fig. 3.14. Because of this, these beads all can rotate in the same direction and with the same magnitude, even in presence of shear rigidity of the contact. Thus, a plane phase front homogeneous in amplitude is possible. In the absence of the bending rigidity the beads/cylinders in the nearest-neighbor rows along the ΓM direction can freely rotate in opposite directions as shown in Fig. 3.14. This motion requires no energy, when in the vibrational motion illustrated in Fig. 3.14, no spatial modulation is added to the one described by $(-1)^n$.

The existence of both TR and RT waves at low frequencies leads to the prediction of a peculiar phenomenon of the elastic field polarization rotation, which is usually forbidden for the fields propagating along the directions of high symmetry. In fact, if we assume that a layer of beads normal to the ΓM direction is oscillating with rotational amplitude Φ_A and that the amplitude of the transversal (in-plane) displacement is U_T, then the RT and TR waves will be emitted by the layer in both positive and negative directions. The polarization of the field at each point of the lattice can be characterized by the phase delay between the rotations and the transversal vibrations of the beads. The polarization of the emitted elastic field will vary with the distance from the emitter because the transversal vibra-

tions are predominantly propagated by the TR wave while the rotations are predominantly propagated by the RT wave at $\Omega \ll \Omega_{ZGVP}$ and because these two waves propagate, in general, with different velocities.

3.5 Conclusions

Our experience with theoretical evaluation and experimental realization of granular phononic crystals [16–18] gives us an opportunity to highlight the important advantages of granular discrete metamaterials. Compared with composite metamaterials [32, 48, 54, 55], they allow analytical solutions for the dispersion relations and the possibility to efficiently control the relative importance of stresses and momentum stresses [5–7] by varying the dimensions of the interparticle contacts. Granular phononic crystals can exhibit enhanced interactions between transversal and rotational waves that provide opportunities for shear wave band design in phononic metamaterials. The specific features of the phononic band structure of the considered granular crystals indicate that rotation of wave polarization could occur even when the transversal/rotational mode propagates along the principal direction, i.e., along a high-symmetry axis. Dirac-like cones, composed of the dispersion bands with the rotational component, are possible in the discrete granular phononic crystals built of cylindrical shells.
This study shows that complete band gap and birefraction in the same single band at low frequencies can be encountered in this granular phononic crystal. If birefraction is realized, this could provide interesting applications in anti-seismic devices, for example. Our theoretical model indicates that nonmonotonous dispersion could exist for the lowest eigenmode belonging to the first lowest-frequency band in not only two-dimensional but also three-dimensional granular crystals (with a simple cubic lattice) as well as in periodic elastic composites. In fact, due to the absence of contacts between beads situated along the wave front in the 2D granular crystal, the rotations of these beads are possible without resistance; these beads all can rotate in the same direction and with the same magnitude. Then, the situation in the [111] direction for a 3D granular crystal is similar to the situation in the [11] direction for a 2D granular crystal. We have verified this statement analytically. Nonmonotonous dispersion relations of the lowest elastic mode also exist in 3D granular crystals.

Thus, the theory of two-dimensional phononic granular crystals could be useful for the description of innovative granular materials [19–26] and also for understanding wave phenomena in periodic structured composites [56–58]. However, the interaction between the translational and rotational degrees of freedom could be not the only reason for the existence of nonmonotonous low-frequency modes in periodic composite. If we imagine that the granular phononic crystal, depicted in Fig. 3.14, is transformed into a composite material by filling the space between the cylinders with another material (for example by a polymer), then the interaction between the non-nearest-neighbor rows of cylinders (i.e, between n and $n+1$ rows along the ΓM direction) is activated by this filling. From the theory of the crystal lattice [59] it is known that the non-nearest-neighbor interaction can also result in nonmonotonous dispersion curves even for the lowest-energy band. Also, the coupling between scattering resonances and propagating waves in the surrounding medium can lead to the formation of band gaps, often referred to hybridization gaps. The theory of this hybridization phenomenon has been developed in Refs. [60, 61]. Such gaps originate, in general, from level repulsion when two bands of the same symmetry cross each other. In addition, indications that the lowest mode in the colloidal crystals exhibits a zero-group velocity point have been found in the experiments [62–64] and confirmed by theoretical modeling [61, 65, 66].

However, in the granular crystals considered in our studies [14, 16–18], the resonances of the individual cylinders are assumed to be at a much higher frequency than the propagation modes, and the interaction/repulsion of the transversal and rotational motions, leading to hybridized rotational/translational modes, is the only reason for the possible existence of the nonmonotonous low-frequency dispersion band and of the zero-group velocity point.

Bibliography

[1] H. Pichard, A. Duclos, J-P. Groby, V. Tournat, and V.E. Gusev. Two-dimensional discrete granular phononic crystal for shear wave control. *Phys. Rev. B.*, 86:134307, 2012.

[2] A. Askar and A.S. Cakmak. A structural model of a micropolar continuum. *International Journal of Engineering Science*, 6(10):583 – 589, 1968.

[3] A.S.J. Suiker, A.V. Metrikine, and R. de Borst. Comparison of wave propagation characteristics of the Cosserat continuum model and corresponding discrete lattice models. *International Journal of Solids and Structures*, 38(9):1563 – 1583, 2001.

[4] I.S. Pavlov, A.I. Potapov, and G.A. Maugin. A 2D granular medium with rotating particles. *International Journal of Solids and Structures*, 43(20):6194 – 6207, 2006.

[5] E. Cosserat and F. Cosserat. *Théorie des corps déformables.* Herman et Fils, Paris, 1909.

[6] A. Eringen. *Microcontinuum Field Theories. I.Foundations and Solids.* Springer, New York, 1999.

[7] W. Nowacki. *Theory of Asymmetric Elasticity.* Pergamon, Oxford, 1986.

[8] H.B. Mühlaus and F. Oka. Dispersion and wave propagation in discrete and continous models for granular materials. *International Journal of Solids and Structures*, 33:2841, 1996.

[9] A. S. J. Suiker, R. de Borst, and C. S. Chang. Micro-mechanical modelling of granular material. *Acta Mechanica*, 149:161–181, 2001.

[10] L.M. Schwartz, D.L. Johnson, and S. Feng. Vibrational modes in granular media. *Phys. Rev. Lett.*, 52:831–834, 1984.

[11] V.F. Nesterenko. *Dynamics of Heterogeneous Materials.* Springer-Verlag, New York, 2001.

[12] C. Inserra, V. Tournat, and V. Gusev. A method of controlling wave propagation in initially spatially periodic media. *Europhysics Letters*, 78:44001, 2007.

[13] V.E. Gusev and V. Tournat. How acoustic waves are guided in buried subsurface channels in unconsolidated granular media. *Phys. Rev. E.*, 78(3):036602, 2008.

[14] A. Merkel, V. Tournat, and V.E. Gusev. Elastic waves in noncohesive frictionless granular crystals. *Ultrasonics*, 50(2):133 – 138, 2009.

[15] O. Mouraille. *Sound propagation in dry granular materials: discrete element simulations, theory and experiments.* PhD thesis, University of Twente, 2009.

[16] A. Merkel, V. Tournat, and V.E. Gusev. Dispersion of elastic waves in three-dimensional noncohesive granular phononic crystals: Properties of rotational modes. *Phys. Rev. E.*, 82(3):031305, 2010.

[17] V. Tournat, I. Pèrez-Arjona, A. Merkel, V. Sanchez-Morcillo, and V.E Gusev. Elastic waves in phononic monolayer granular membranes. *New Journal of Physics*, 13(7):073042, 2011.

[18] A. Merkel, V. Tournat, and V.E. Gusev. Experimental evidence of rotational elastic waves in granular phononic crystals. *Phys. Rev. Lett.*, 107(22):225502, 2011.

[19] A. Van Blaaderena, R. Ruel, and P. Wiltzius. Template-directed colloidal crystallisation. *Nature (London)*, 385:321323, 1997.

[20] Z. Cheng, W.B. Russel, and P.M. Chaikin. Controlled growth of hard-sphere colloidal crystals. *Nature (London)*, 401:893–895, 1999.

[21] J.D. Joannopoulos. Self-assembly lights up. *Nature*, 414:257–258, 2001.

[22] E.V. Shevchenko, D.V. Talapin, C.B. Murray, and S.O'Brien. Structural characterisation of self-assembled multifunctional binary nanoparticles. *Journal of the American Chemical Society*, 128:3620–3637, 2006.

[23] W. Cheng, M.J. Campolongo, J.J. Cha, S.J. Tan, C.C. Umbach, D.A. Miller, and D. Luo. Free standing nanoparticle superlattice sheets controlled by dna. *Nature Materials*, 8:519–525, 2009.

[24] E. Auyeun, J.I. Cutler, R.J. Macfarlane, M.R. Jones, J. Wu, G. Liu, K. Zhang, D. Osberg, and C.A. Mirkin. Synthetically programmable nanoparticle superlattices using a hollow three-dimensional spacer approach. *Nature Nanotechnologies*, 7:24–28, 2012.

[25] K.E. Mueggenburg, X.-M Lin, R.H. Goldslith, and H.M. Jaeger. Elastic membranes of close-packed nanoparticle arrays. *Nature Materials*, 6:656–660, 2007.

[26] A. Dong, J. Chen, P.M. Vora, J.M. Kikkawa, and C.B. Murray. Binary nanocrystal superlattice membranes self-assembled at the liquid-air interface. *Nature (London)*, 466:474–477, 2010.

[27] A. Leonard and C. Daraio. Stress wave anisotropy in centered square highly nonlinear granular systems. *Phys. Rev. Lett.*, 108:214301, 2012.

[28] F. Göncü, S. Luding, and K. Bertoldi. Exploiting pattern transformation to tune phononic band gaps in a two-dimensional granular crystal. *J. Acoust. Soc. Am.*, 131:EL475, 2012.

[29] Y. Tanaka, Y. Tomoyasu, and S. Samura. Band structure of acoustic waves in phononic lattices: Two-dimensional composites with large acoustic mismatch. *Phys. Rev. B.*, 62:7387–7392, 2000.

[30] C. Goffaux, J. Sanchez-Dehesa, A. Levy Yeyati, Ph. Lambin, A. Khelif, J.O. Vasseur, and B. Djafari-Rouhani. Evidence of fano-like interference phenomena in locally resonant materials. *Phys. Rev. Lett.*, 88:225502, 2002.

[31] P.St.J. Russel, E. Marin, A. Diez, S. Guenneau, and A.B. Movchan. Sonic band gaps in pcf preforms: enhancing the interaction of light. *Optics Express*, 11:2555–2560, 2003.

[32] G. Wang. Lumped-mass method for the study of band structure in two-dimensional phononic crystals. *Phys. Rev. B.*, 69(18):184302, 2004.

[33] L. Feng. Acoustic backward-wave negative refractions in the second band of a sonic crystal. *Phys. Rev. Lett.*, 96:1, 2006.

[34] G. Wang, X. When, J. When, L. Shao, and Y. Liu. Two-dimensional locally resonant phononic crystals with binary structures. *Phys. Rev. Lett.*, 93(15):154302, 2004.

[35] M.-H. Lu, C. Zhang, I. Feng, J. Zhao, Y.-F. Chen, Y.W. Mao, J. Zi, Y.-Y Zhu, S.-N Zhu, and N.-B Ming. Negative birefraction of acoustic waves in a sonic crystal. *Nature Materials*, 6:744–748, 2007.

[36] J. Bucay, E. Roussel, J.O. Vasseur, P.A. Deymier, A-C. Hladky-Hennion, Y. Pennec, K. Muralidharan, B. Djafari-Rouhani, and B. Dubus. Positive, negative, zero refraction, and beam splitting in a solid/air phononic crystal: Theoretical and experimental study. *Phys. Rev. B*, 79(21):214305, 2009.

[37] A. Sukhovich, L. Jing, and J.H. Page. Negative refraction and focusing of ultrasound in two-dimensional phononic crystals. *Phys. Rev. B*, 77(1):014301, January 2008.

[38] Y. Zhang, Y. Shen, J. Zhou, Y. Wang, F. Wu, J. Sun, and C. Guo. Positive-negative birefraction phenomenon for TM polarization in annular photonic crystal. *Chin. Opt. Lett.*, 9(2):022601, 2011.

[39] M. Koshino and T. Ando. Transport in bilayer graphene: Calculations within a self-consistent born approximation. *Phys. Rev. B*, 73(24):033412, June 2006.

[40] J. Mei, Y. Wu, C.T. Chan, and Z-Q. Zhang. First-principles study of Dirac and Dirac-like cones in phononic and photonic crystals. *Phys. Rev. B.*, 86:035141, 2012.

[41] R.A. Sepkhanov, Ya B. Bazaliy, and C.W.J. Beenakker. Extremal transmission at the Dirac point of a photonic band structure. *Physical Review A*, 75:063813, June 2007.

[42] F.D.M. Haldane. Possible realization of directional optical waveguides in photonic crystals with broken time-reversal symmetry. *Phys. Rev. Lett.*, 100:013904, 2008.

[43] D. Torrent and J. Sánchez-Dehesa. Acoustic analogue of graphene: Observation of Dirac cones in acoustic surface waves. *Phys. Rev. Lett.*, 108(17):174301, April 2012.

[44] J.J. Sakurai. *Modern quantum mechanics.* Addison-Wesley, 1994.

[45] X. Huang. Dirac cones induced by accidental degeneracy in photonic crystals and zero-refractive-index materials. *Nature Materials*, 10(8):582–586, May 2011.

[46] F. Liu, Y.n Lai, X. Huang, and C. Chan. Dirac cones at k=0 in phononic crystals. *Phys. Rev. B*, 84(22):224113, December 2011.

[47] K. Sakoda. Dirac cone in two- and three-dimensional metamaterials. *Optics Express*, 20:3898–3917, 2012.

[48] Y. Lai, Y. Whu, P. Sheng, and Z.-O. Zhang. Hybrid elastic solids. *Nature Materials*, 10:620–624, 2011.

[49] W. Soedel. *Vibration of Shells and Plates.* M. Dekker, New York, 1993.

[50] J. Leopoldes and X. Jia. Probing viscoelastic properties of a thin polymer film sheared between a beads layer and an ultrasonic resonator. *Europhysics Letters*, 88:34001, 2009.

[51] G.L. Dybwad. A sensitive new method for the determination of adhesive bonding between a particle and a substrate. *J.Appl.Phys*, 58:2789, 1985.

[52] J. Leopoldes and X. Jia. Transverse shear oscillator investigation of boundary lubrication in weakly adhered film. *Phys. Rev. Lett.*, 105:266101, 2010.

[53] S. Timoshenko. *Strength of Materials*. Van Nostrand, New York, 1928.

[54] Z. Liu, X. Zhang, Y. Mao, M. Zhu, S. Yang, and P. Sheng. Locally resonant sonic materials. *Science*, 289:1734–1736, 2000.

[55] R. Sainidou, N. Stefanou, and A. Modinos. Formation of absolute frequency gaps in three-dimensional solid phononic crystals. *Phys. Rev. B.*, 66:212301, 2002.

[56] C. Jiang, S. Markutsya, Y. Pikus, and V. Tsukruk. Freely suspended nanocomposite membranes as highly sensitive sensors. *Nature Materials*, 3:721–728, 2004.

[57] A.S. Balazs, T. Emrick, and T.P. Russel. Nanoparticle polymer composites: Where two small words meet. *Science*, 314:1107, 2006.

[58] E. Hobbie, D.O. Simien, J.A. Fagan, J.Y. Huh, J.Y. Chung, S.D. Hudson, J. Obrzut, J.F. Douglas, and C.M. Stafford. Wrinkling and strain softening in single-wall carbon nanotube membranes. *Phys. Rev. Lett.*, 104(12):125505, 2010.

[59] M.T. Dove. *Structure and Dynamics, an Atomic View of Materials*. Oxford University Press, New York, 2005.

[60] J.H. Page, H.P. Schriemer, P. Sheng, I. Jones, X. Jing, and D.A. Weitz. Group velocity in strongly scattering media. *Science*, 271:1–4, February 1996.

[61] Z. Liu, C.T. Chan, P. Sheng, A.L. Goertzen, and J.H. Page. Elastic wave scattering by periodic structures of spherical objects: Theory and experiment. *Phys. Rev. B*, 62:2446, July 2000.

[62] T. Still, W. Cheng, M. Retsch, R. Sainidou, J. Wang, U. Jonas, N. Stefanou, and G. Fytas. Simultaneous occurrence of structure-directed and particle-resonance-induced phononic gaps in colloidal films. *Phys. Rev. Lett.*, 100(19):194301, May 2008.

[63] R.S. Penciu, H. Kriegs, G. Petekidis, G. Fytas, and E.N. Economou. Phonons in colloidal systems. *The Journal of Chemical Physics*, 118(11):5224, 2003.

[64] G. Tommaseo, G. Petekidis, W. Steffen, G. Fytas, A.B. Schofield, and N. Stefanou. Hypersonic acoustic excitations in binary colloidal crystals: Big versus small hard sphere control. *The Journal of Chemical Physics*, 126(1):014707, 2007.

[65] I.E. Psarobas, N. Stefanou, and A. Modinos. Scattering of elastic waves by periodic arrays of spherical bodies. *Phys. Rev. B.*, 62:5536, April 2000.

[66] I.E. Psarobas, A. Modinos, R. Sainidou, and N. Stefanou. Acoustic properties of colloidal crystals. *Phys. Rev. B*, 65(6):064307, January 2002.

Chapitre 4

Surface waves in granular phononic crystals

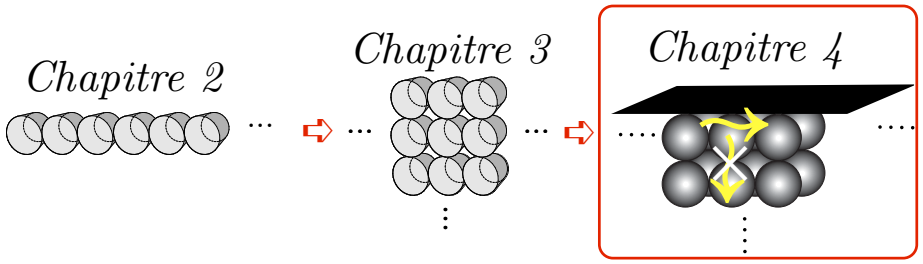

Ce chapitre, rédigé en anglais, est la transcription prochainement soumis. Une analyse de l'existence d'ondes à la surface mécaniquement libre de cristaux phononiques granulaires constitués de particules sphériques est présentée. Selon le type de degrés de liberté des particules, des ondes de type Rayleigh ou des ondes de surface de type cisaillement horizontal sont analysées. Les ondes de type Rayleigh sont étudiées à la surface d'un cristal phononique granulaire dont les particules possèdent deux degrés de liberté en translation et un en rotation. La description des diagrammes de dispersion permet de définir les zones autorisées pour les ondes de surface en fonction des paramètres contrôlant la structure. Ces paramètres dépendent des caractéristiques des particules ainsi que des ressorts longitudinal, de cisaillement et de flexion caractérisant le contact entre elles. Deux modes de surface ainsi qu'un mode plan purement longitudinal sont décrits. Le second cristal étudié est constitué de particules possédant deux degrés de liberté en rotation et un en translation. Une description des ondes volumiques se propageant dans ce cristal est tout d'abord réalisée, puis l'existence d'une onde de surface de type cisaillement horizontal est démontrée. Les profils discrets de déplacement et de rotation des différentes ondes sont également présentés. Une comparaison de la théorie développée avec les prédictions d'ondes acoustiques à la surface libre des milieux de Cosserat, ouvre la possibilité d'établir les limites de la théorie éponyme dans la description d'ondes acoustiques de surface dans les milieux micro- et nano-inhomogènes.

Abstract

The existence of surface elastic waves at a mechanically free surface of granular phononic crystals is studied. The granular phononic crystals are made of spherical particles distributed periodically on a simple cubic lattice. It is assumed that the particles are interacting by means of normal, shear and bending contact rigidities. First, Rayleigh-type surface acoustic waves, where the displacement of the particles takes place in the sagittal plane while the particles possess one rotational and two translational degrees of freedom, are analyzed. Second, shear-horizontal-type waves, where the displacement of the particles is normal to the sagittal plane while the particles possess one translational and two rotational degrees of freedom are studied. The existence of zero-group velocity surface acoustic waves of Rayleigh-type is theoretically predicted and interpreted. A comparison with surface waves predicted by the Cosserat theory is performed, and its limitations are established.

4.1 Introduction

The study of surface elastic/acoustic waves (SAWs) associated with the surface of a semi-infinite phononic crystal has attracted a lot of attention in recent years. The control of evanescent waves in periodic composites, both in photonic and phononic crystals, is promising for the design of new electromagnetic and acoustic materials for various applications [1]. An elementary volume of the medium possesses two translational degrees of freedom with the mechanical displacement vector polarized in the sagittal plane. To understand the effect of a free surface on the normal vibration modes of a crystal, continuous and discrete models have been applied to structures in one (chain), two (membrane) and three (half-space) dimensions, possessing different types of inter-atomic interactions. Investigations of surface modes of vibration using the continuum point of view have been reported for cubic crystals by Stoneley [2] and by Gazis, Herman, and Wallis [3]. A description of surface waves for discrete lattices has been given by Lifshitz and Pekar [4]. Calculations based on specific lattice models have been given by Gazis and al. [3] for diatomic one-, two-, and three-dimensional NaCI-type lattices with nearest neighbor interactions only, and by Kaplan [5] for the monatomic one-dimensional lattice with nearest and next-nearest neighbor interactions. Gazis, Herman, and Wallis treated the semi-infinite three-dimensional monatomic cubic lattice with nearest and next-nearest neighbor central forces and with angular stiffness forces. For long-wavelengths compared to the inter-atomic distance, the discrete particle theory, as to be expected, yields identical results to those of the continuum theory. When the wavelength becomes comparable to the interatomic distance the particle theory leads to dispersion, while the continuum results remain nondispersive for all wavelengths.

There are situations when the medium behavior is still elastic but the wave propagation cannot be described by the classical continuum elasticity theory because this theory does not properly describe the dispersion of the propagating long acoustic waves. To address this problem, polar (couple/asymmetric stress) elastic theories introduce supplementary and independent rotational degrees of freedom (*dofs*) of material particles, which are additional to translational *dofs* in classical continuum elasticity. Various models of this kind are widely used in continuum mechanics: Cosserat theory [6], micropolar model of Eringen [7], reduced Cosserat continuum model [8], etc. However, the lack of information on the additionally introduced physical parameters values for real materials hinders the development of these

theories and their practical applications. In the Cosserat theory, each material element possesses six *dofs*: three *dofs* for the translation and three *dofs* for the rotation. The Cosserat continuum elasticity theory predicts strong modification of the shear waves dispersion by the rotational *dofs*. One of such effects is the dispersion of the Rayleigh surface elastic wave at flat interface for long-wavelengths, while the classical theory fails to explain it [7–10]. Furthermore, the Cosserat model predicts the propagation of horizontally polarized transversal surface waves [11], which are forbidden at the surface of the homogeneous classical elastic continuum.

Recently, discrete lattice models have been developed to describe the phononic band structure of granular crystals possessing rotational *dofs* [12–17]. These discrete models provide elastic eigenmodes for all possible wavelengths. A two-dimensional (2D) discrete lattice model with particles possessing one translational and two rotational *dofs* has been applied to the analysis of a monolayer granular phononic membrane [14]. It was demonstrated theoretically that the interaction between translational and rotational motions could lead to the opening of the gaps forbidden for wave propagation, to the creation of Dirac cone, to the existence of zero-energy soft modes and zero-group-velocity bulk modes [16]. Existence of localized modes have been demonstrated theoretically in a one-dimensional (1D) monatomic granular phononic crystal composed of infinitely long cylinders with equal masses and possessing one translational and one rotational *dofs* [17]. Each of the localized coupled transversal and rotational mode existing in this studied chain is composed of two evanescent modes and is analyzed for different boundary conditions applied at the boundary of the semi-infinite chain. The experimental observation of the coupled rotational-translational bulk modes in a noncohesive granular phononic crystal was reported in [15]. It was demonstrated that the Cosserat theory generally fails to correctly predict the dispersion relations of the bulk elastic modes in granular crystals even in the long-wavelength limit because it does not account for all the effects of the material inhomogeneity. It should be combined with higher gradient elasticity theories [7, 18, 19].

This work focuses on the existence of SAWs at mechanically free surface of granular phononic crystals made of spherical particles. Rayleigh-type SAWs, where the particles possess one rotational and two translational *dofs*, and shear-horizontal-type SAWs, where particles possess one translational and two rotational *dofs*, are studied. Our analysis shows that the existence of SAWs depend on the relative strength of the different interparticle forces, which are due to normal, shear, and bending rigidities at the contacts. Interesting features of these SAWs are revealed, such as possible existence of the zero-group-velocity (ZGV) SAWs. The nature and discrete displacement profiles of the SAWs are described as a function of the parameters controlling the dispersion curves. In particular, the importance of bending rigidity is demonstrated, as the evolution of ZGV SAWs as well as the existence of SH-type SAWs strongly depend on bending interaction between beads. These analytical descriptions of SAWs dependence on the contact parameters, yield a possible comparison of the derived theoretical predictions with those of the simplest case of reduced Cosserat theory. The obtained results confirm that all effects of the material inhomogeneity are not correctly modeled in Cosserat theory because the spatial scale of the inhomogeneity, and consequently multiple scattering of the waves, are not accounted for.

In Section 4.2 Rayleigh-type waves are studied. SH-type waves are analyzed in Section 4.3. In both cases, the theoretical analysis shows the existence of SAWs propagating at the (010) surface along [100]

direction and at the (110) surface along $[1\bar{1}0]$ direction. Finally, comparison of SAWs in the granular crystals with those known predicted by the reduced Cosserat theory, is performed in Section 4.4. Some limitations of the Cosserat theory are then highlighted.

4.2 Rayleigh-type surface waves

4.2.1 Dispersion curves of the propagating modes

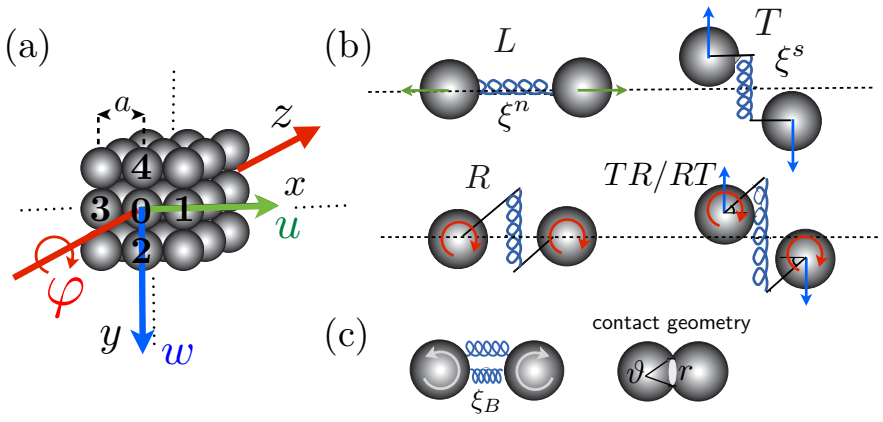

Figure 4.1 – (Color online) (a) Schematic representation of the granular phononic crystal. u denotes the longitudinal displacement along the x-axis, w denotes the translational displacement motion along the y-axis and φ denotes the rotational motion around the z-axis. (b) Illustration of the various possible motions of the beads, which are activating different contact springs/rigidities contributing to normal, shear and bending type interactions. (c) Schematic representation of the bending rigidity.

The granular phononic crystal is made of spherical particles distributed periodically on a cubic lattice with periodicity a. The radius, mass and momentum of inertia of the particles are denoted by R_c, m and I, respectively. The particles possess two translational and one rotational *dofs*, Fig. 4.1. For the analysis of the plane Rayleigh-type SAWs, which are 2D motions of the crystal, the considered crystal is equivalent to the 2D one studied in chapter 3. Normal and shear forces at the contacts between two adjacent particles are described with springs of constant rigidity ξ^n and ξ^s, respectively. The elongations of the springs introduce forces and momenta that induce the motion of the particles: the displacements u along the x-axis, w along the y-axis and the rotation φ around the z-axis. Different possible motions of two neighboring particles are illustrated in Fig. 4.1(b). The transversal, longitudinal, rotational and combined transversal/rotational motions are denoted by T, L, R, and T/R, respectively. Two spatially distinct normal springs of rigidity ξ^B are introduced in Fig. 4.1(c) to model the effect of bending rigidity at the contact, i.e., of the interaction opposing the rotation of the two contacting beads in opposite directions [14].

The complete derivation of the bulk dispersion relations for bulk acoustic waves can be found in chapter 3. The substitution of the plane wave solutions into the equations of motion leads to the eigenvalue problem

$$\mathbf{Sv} = 0 \ , \tag{4.1}$$

where $\mathbf{v} = \begin{pmatrix} A_u \\ A_w \\ A_\Phi \end{pmatrix}$ is the amplitude vector, with $\Phi = R_c\varphi$ and $\mathbf{S}$ is the dynamical matrix defined by

$$\mathbf{S} = \begin{pmatrix} -\eta\sin^2 q_x - \sin^2 q_y + \Omega^2 & 0 & \mathrm{j}\sin q_y \cos q_y \\ 0 & -\eta\sin^2 q_y - \sin^2 q_x + \Omega^2 & -\mathrm{j}\sin q_x \cos q_x \\ -\mathrm{j}p\sin q_y \cos q_y & \mathrm{j}p\sin q_x \cos q_x & -p(\cos^2 q_x + \cos^2 q_y) - 4p_B p(\sin^2 q_x + \sin^2 q_y) + \Omega^2 \end{pmatrix} , \quad (4.2)$$

wherein $\Omega = \omega/\omega_0$ is the reduced frequency with $\omega_0 = 2\sqrt{\xi^s/m}$, j is the imaginary unit, $q_{x,y} = k_{x,y}a/2$ are the normalized wave numbers, $p = mR_c^2/I$, $\eta = \xi^n/\xi^s$, $p_B = \dfrac{\vartheta^2}{2}\dfrac{\xi^B}{\xi^s}$ and ϑ is the angular contact dimension (see Fig. 4.1(c)). Note that, from classical mechanics $mR_c^2 \geq 1$ and, as consequence, $p \geq 1$. In the case of a homogeneously filled and empty sphere where all the mass is at the sphere periphery, p is equal to 2.5 and 1.5, respectively.

At any point x and y in the crystal, the displacement and rotation components of the modes are assumed to be in the form

$$\begin{pmatrix} u \\ w \\ \Phi \end{pmatrix}_{l,n} = \begin{pmatrix} A_u \\ A_w \\ A_\Phi \end{pmatrix} e^{\mathrm{j}\omega t - 2\mathrm{j}q_x l - 2\mathrm{j}q_y n} = A_\Phi \begin{pmatrix} \alpha \\ \beta \\ 1 \end{pmatrix} e^{\mathrm{j}\omega t - 2\mathrm{j}q_x l - 2\mathrm{j}q_y n} , \quad (4.3)$$

where $\alpha = \dfrac{\mathrm{j}\sin q_y \cos q_y}{\eta\sin^2 q_x + \sin^2 q_y - \Omega^2}$ is the ratio between the longitudinal A_u and rotational A_Φ amplitudes, $\beta = -\dfrac{\mathrm{j}\sin q_x \cos q_x}{\eta\sin^2 q_y + \sin^2 q_x - \Omega^2}$ is the ratio between the transversal A_w and rotational A_Φ amplitudes and l, n refers to the particle position along x-axis and y-axis, respectively, measured in integer numbers of interparticle distances.

Nontrivial solutions of Eq. (4.1) require that

$$|S_{j,i}| = 0 , \quad \text{with} \quad j, i = 1, 2, 3 . \quad (4.4)$$

For a given set of parameters p, η, p_B and wave number q_x, Eq. (4.4) constitutes a relationship between the frequency Ω and the wave number q_y, which can be written as a cubic equation for $Y = \sin^2 q_y$ and for Ω^2, see development in appendix B.1. Since it is a cubic equation in $\sin^2 q_y$ and in Ω^2, for a given frequency Ω correspond six wave numbers q_y. Each pair of wave numbers describes either two waves propagating in opposite directions or two evanescent waves with opposite directions of the amplitude decay. Figure 4.2 presents the dispersion curves of the propagating modes obtained with $\eta = 1.2$, $p = 1$ and $p_B = 0.01$. Each of the eigenmodes of the granular phononic crystal motion consists of three components, the longitudinal motion L, the transversal motion T, and the rotational motion R. The plotted eigenvalues have been colored accordingly to the eigenvectors that have been classified, and the nature of the modes is labeled. The continuous red-orange lines correspond to coupled displacement-rotation modes with a predominance of rotation (RT, RLT), the dashed blue lines correspond to coupled displacement-rotation modes with a predominance of displacement (TR, LTR), and the dotted green lines correspond to pure displacement modes (L, TL). Chapter 3 provides a complete description of the dispersion curves as a function of the parameters

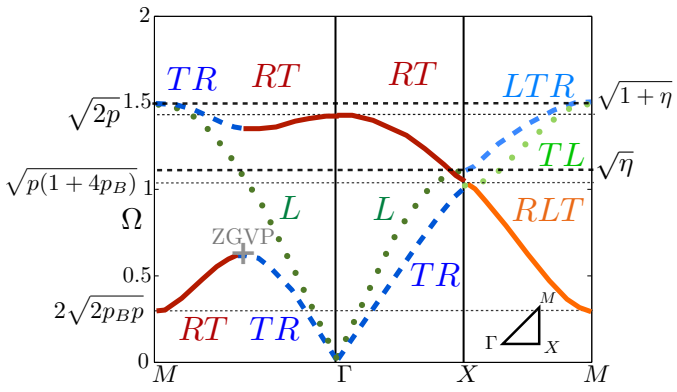

Figure 4.2 – (Color online) Dispersion curves for the plane bulk waves possessing two translational and one rotational *dofs*, obtained for $\eta = 1.2$, $p = 1$ and $p_B = 0.01$. Solid curves correspond to coupled displacement-rotation modes (with a predominance of rotation), dashed curves correspond to coupled displacement-rotation modes (with a predominance of displacement), and dotted curves correspond to pure displacement modes.

p, η and p_B. A remarkable feature of the lowest transversal/rotational mode along the ΓM direction is the existence of two group velocity regions separated by a zero-group velocity point (ZGVP, see Fig. 4.2), resulting in birefraction phenomenon. The position and existence of this ZGVP strongly depends on parameters p, η, and p_B. The developed theory explains the physical origin of these modes, which are due to interaction/repulsion of the transversal and rotational motions, leading to hybridized rotational/transversal modes. The description of the ZGVP and of these nonmonotonous modes as well as their dependence on the bending rigidity parameter p_B, is presented in details in chapter 3.

4.2.2 Boundary conditions for Rayleigh-type SAWs propagating at the (010) free surface along [100] direction

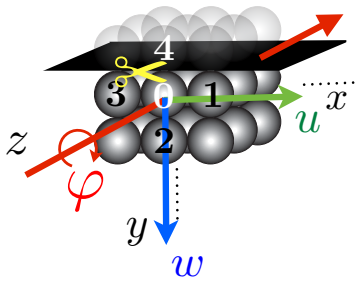

Figure 4.3 – (Color online) Schematic representation of the (010) surface and the propagation direction (x-direction) for the Rayleigh-type SAWs.

In this section we study the Rayleigh-type SAWs at the mechanically free surface of the granular crystal, which is normal to the y-axis, i.e., on (010) surface. Waves propagating along x-axis, i.e., in the [100] direction, are sought. The boundary conditions are derived from the removal of all particles on one side of the boundary layer. In this configuration, the surface modes, whose amplitudes decrease away from the boundary, i.e., along the y-axis, have an attenuation defined by the imaginary part of the

wave number q_y. Mechanically free boundary conditions are the absence of forces and of momentum between 0-th and 4-th beads, Fig. 4.3. These conditions are satisfied if the contact between the 0-th and 4-th beads is not strained, i.e., the normal and shear springs are not deformed/elongated while the beads 1 and 4 are rotating in opposite directions, preventing activation of the bending rigidity of the contact. Thus the mechanically free boundary conditions can be formulated mathematically as follows

- No longitudinal spring elongation,
$$w_0 - w_4 = 0 \ . \tag{4.5}$$
- No shear spring elongation,
$$u_4 - u_0 + (\Phi_4 + \Phi_0) = 0 \ . \tag{4.6}$$
- No rotation, which can activate bending rigidity,
$$\Phi_4 - \Phi_0 = 0 \ . \tag{4.7}$$

The boundary conditions should be satisfied by the bulk modes whose amplitudes decrease as n increases. Therefore, the localization of surface waves should operated by complex wave numbers with a negative imaginary part, i.e., by three of the six wave numbers given by Eq. (4.4). When the solutions for the wave number q_y are purely real, the waves are propagative. Three evanescent modes, whose frequency lies in the forbidden band for propagating waves, and characterized by a complex-valued wave number in such a way that the amplitude of the mode decays with increasing y-coordinate, should be coupled to satisfy the derived boundary conditions.

If A_{Φ_i} are the amplitudes of Φ in the 3 modes, the displacement and rotation components of the modes can be written in the following form

$$u_{l,n} = \sum_{i=1}^{3} A_{\Phi_i}\, \alpha_i\, e^{\mathrm{j}\omega t} e^{-2\mathrm{j}lq_x} e^{-2\mathrm{j}nq_{y_i}} \ , \tag{4.8a}$$

$$w_{l,n} = \sum_{i=1}^{3} A_{\Phi_i}\, \beta_i\, e^{\mathrm{j}\omega t} e^{-2\mathrm{j}lq_x} e^{-2\mathrm{j}nq_{y_i}} \ , \tag{4.8b}$$

$$\Phi_{l,n} = \sum_{i=1}^{3} A_{\Phi_i}\, e^{\mathrm{j}\omega t} e^{-2\mathrm{j}lq_x} e^{-2\mathrm{j}nq_{y_i}} \ , \tag{4.8c}$$

with $\alpha_i = \dfrac{\mathrm{j}\sin q_{y_i}\cos q_{y_i}}{\eta\sin^2 q_x + \sin^2 q_{y_i} - \Omega^2}$ and $\beta_i = -\dfrac{\mathrm{j}\sin q_x \cos q_x}{\eta\sin^2 q_{y_i} + \sin^2 q_x - \Omega^2}$, with $i = 1, 2, 3$ for the first, second and third mode, respectively, while q_x has the physical meaning of a surface wave number.

The substitution of these amplitudes, Eqs. (4.8), into the boundary conditions, Eqs. (4.5) - (4.7), leads to

$$\sum_{i=1}^{3} A_{\Phi_i}\, \beta_i (1 - e^{2\mathrm{j}q_{y_i}}) = 0 \ , \tag{4.9a}$$

$$\sum_{i=1}^{3} \left[A_{\Phi_i}\, \alpha_i (e^{2\mathrm{j}q_{y_i}} - 1) + A_{\Phi_i} (1 + e^{2\mathrm{j}q_{y_i}}) \right] = 0 \ , \tag{4.9b}$$

$$\sum_{i=1}^{3} A_{\Phi_i}\, (e^{2\mathrm{j}q_{y_i}} - 1) = 0 \ , \tag{4.9c}$$

which can be rewritten in the following form,

$$\mathbf{S_2 v_2} = 0 \ , \tag{4.10}$$

with $\mathbf{v_2} = \begin{pmatrix} A_{\Phi_1} \\ A_{\Phi_2} \\ A_{\Phi_3} \end{pmatrix}$ and

$$\mathbf{S_2} = \begin{pmatrix} \beta_1(1-e^{2\mathrm{j}q_{y_1}}) & \beta_2(1-e^{2\mathrm{j}q_{y_2}}) & \beta_3(1-e^{2\mathrm{j}q_{y_3}}) \\ \alpha_1(e^{2\mathrm{j}q_{y_1}}-1)+1+e^{2\mathrm{j}q_{y_1}} & \alpha_2(e^{2\mathrm{j}q_{y_2}}-1)+1+e^{2\mathrm{j}q_{y_2}} & \alpha_3(e^{2\mathrm{j}q_{y_3}}-1)+1+e^{2\mathrm{j}q_{y_3}} \\ e^{2\mathrm{j}q_{y_1}}-1 & e^{2\mathrm{j}q_{y_2}}-1 & e^{2\mathrm{j}q_{y_3}}-1 \end{pmatrix} . \tag{4.11}$$

In order to have nontrivial solutions of Eq. (4.10), the following equation must be satisfied

$$|S_{2_{j,i}}| = 0 \quad j,i = 1,2,3 \ . \tag{4.12}$$

For a set of parameters p, p_B, η and for a propagation wave number specified by q_x, the solutions Ω and the corresponding q_{y_i} of the surface modes are obtained from the simultaneous solutions of Eqs. (4.4) and (4.12). These surface modes are discussed in the following section.

According to Eqs. (4.8), the amplitudes of the longitudinal $u_{l,n}$, transversal $w_{l,n}$ and rotational $\Phi_{l,n}$ discrete displacements of the modes as a function of the particle position (l,n) in the crystal can be determined by combining the bulk modes with projections of the wave vector along the y-axis, q_{y_1}, q_{y_2} and q_{y_3}

$$\begin{pmatrix} u_i \\ w_i \\ \Phi_i \end{pmatrix}_{l,n} = A_\Phi \left[Z_1 \begin{pmatrix} \alpha_1 \\ \beta_1 \\ 1 \end{pmatrix} e^{\mathrm{j}\omega t} e^{-2\mathrm{j}lq_x} e^{-2\mathrm{j}nq_{y_1}} + Z_2 \begin{pmatrix} \alpha_2 \\ \beta_2 \\ 1 \end{pmatrix} e^{\mathrm{j}\omega t} e^{-2\mathrm{j}lq_x} e^{-2\mathrm{j}nq_{y_2}} + \begin{pmatrix} \alpha_3 \\ \beta_3 \\ 1 \end{pmatrix} e^{\mathrm{j}\omega t} e^{-2\mathrm{j}lq_x} e^{-2\mathrm{j}nq_{y_3}} \right] , \tag{4.13}$$

with $Z_1 = \dfrac{A_u}{A_\Phi} = -1 - Z_2$ and $Z_2 = \dfrac{A_w}{A_\Phi} = \dfrac{(\beta_1-\beta_3)(1-e^{2\mathrm{j}q_{y_3}})}{(\beta_1-\beta_2)(e^{2\mathrm{j}q_{y_2}}-1)}$.

The domain of the admissible wave numbers and frequencies where SAWs could be sought, through the solution of Eqs. (4.4) and (4.12), could be importantly reduced by presenting the dispersion curves of the bulk modes in the granular crystal in projected band diagram [20]. As illustrated in Fig. 4.4, to construct a band diagram projected onto the q_x direction, i.e., on the direction of SAWs propagation, the value of q_x is fixed and the frequencies corresponding to all possible real projections of the wave number q_y, i.e., of the bulk modes on the y-axis, are plotted in the same graph. For example, the obtained projected band diagram in the case of $p = 2$, $\eta = 2$ and $p_B = 0.4$ is represented in Fig. 4.4(b). In this band diagram, gray shaded regions define allowed/propagating phononic bands, while empty regions define band gaps. Note that the reprensentation along the $\Gamma XM\Gamma$ directions involves only the solutions for bulk modes on the edge of an irreductible Brillouin zone (1D calculation), while the band diagram of Fig. 4.4(b) requires computation of all the solutions inside an irreductible Brillouin zone (2D calculation). Although the $\Gamma XM\Gamma$ representation gives consistent definitions of complete band gaps the projected band diagram in Fig. 4.4(b) is preferred when detailed information is required. To determine the regions allowed for surface waves, the projected bands diagram along the q_x direction are chosen in the following analyses. In fact, it is necessary to use the projected diagram for the analysis of possible surface waves, because the surface waves cannot lie in a propagative band and should be

located between them. Otherwise SAWs emit bulk modes and are evanescent, i.e., decay along their propagation path, x-axis.

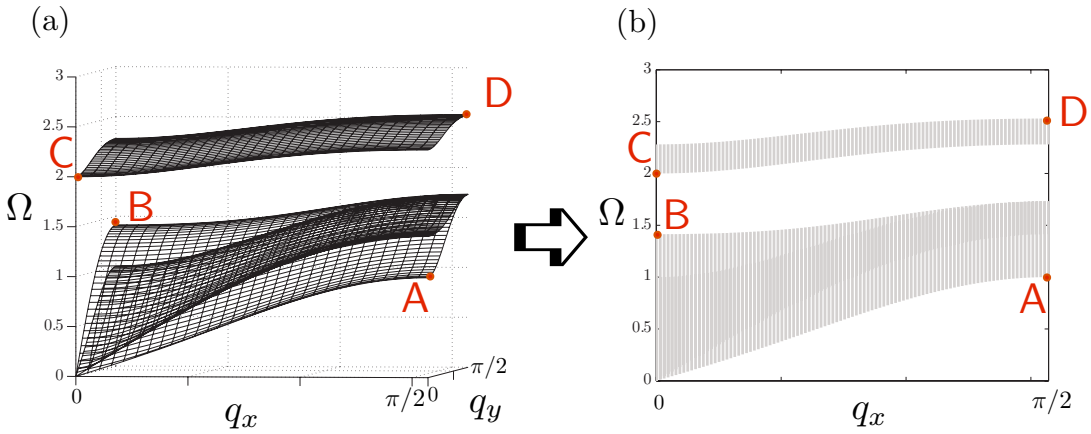

Figure 4.4 – (Color online) (a) 3D dispersion curves of the crystal for $\eta = 2$, $p = 2$ and $p_B = 0.4$. (b) Projected bulk bands along [100] direction, i.e., x direction.

4.2.3 Pure longitudinal mode

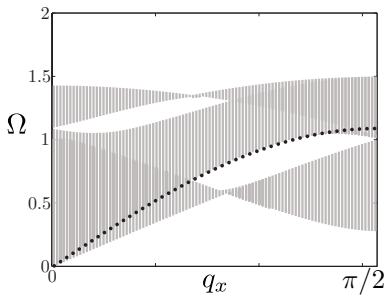

Figure 4.5 – (Color online) Dispersion curves along the q_x direction of the crystal for $\eta = 1.2$, $p = 1$ and $p_B = 0.01$. The shaded areas represent the projected bulk bands along [100], i.e., x direction. The dotted black curve represents the mode $\Omega^2 = \eta \sin^2 q_x$.

From the development of the boundary conditions determinant Eq. (4.12), it follows that a pure longitudinal mode $\Omega^2 = \eta \sin^2 q_x$ propagating along the x-axis satisfies the boundary conditions at the considered mechanically free surface of the cubic crystal (the development can be found in appendix B.2). The dispersion curve of this mode is shown in black dotted curve in Fig. 4.5. This is a pure longitudinal mode skimming along the surface ($A_\Phi = A_w = 0$), which exhibits the same dispersion than the pure longitudinal mode propagating along the ΓX direction of the crystal. This mode is not coupled with the rotational and transverse waves because the same relative motion of the neighbor particles along the x-axis at all distances from the surface does not lead to deformation of shear springs. Physically, this corresponds to a wave propagating in a material with a zero Poisson coefficient, showing no expansion/contraction in the direction orthogonal to the axis of its compression.

4.2.4 Surface modes description

Surface waves are calculated for fixed sets of parameters q_x, p, p_B and η by simultaneous solutions of Eqs. (4.4) and Eqs. (4.12). Fig. 4.6 presents the evolution of the obtained surface modes for $p = \eta = 2$ by increasing the bending rigidity parameter p_B. Example of discrete displacement profiles of the surface modes along the y-axis are given in Fig. 4.7, for two fixed wave numbers q_x. The projected bulk bands along [100], i.e., x direction, are represented by shaded areas. The surface modes are represented in dashed orange curves, and the pure longitudinal mode $\Omega^2 = \eta \sin^2 q_x$ propagating along the surface is drawn in dotted black curve.

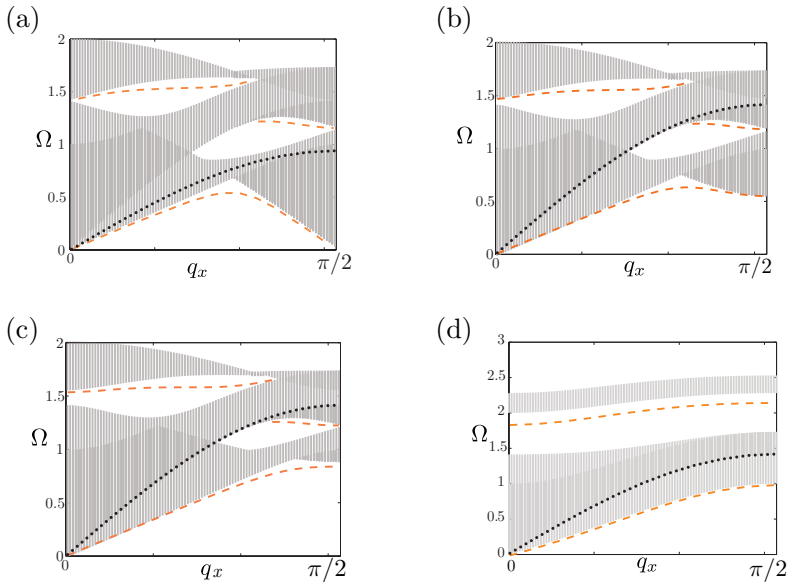

Figure 4.6 – (Color online) Dispersion curves along the q_x direction of the crystal for $\eta = 2$, $p = 2$ and (a) $p_B = 0$, (b) $p_B = 0.02$, (c) $p_B = 0.05$ and (d) $p_B = 0.4$. The shaded areas represent the projected bulk bands along [100], i.e., x direction. The dashed orange curves represent the surface modes and the dotted black curve represents the longitudinal bulk mode propagating along the surface.

One surface mode propagates below the first propagating band, while, one surface or two surface modes can exist between the upper propagating bands of bulk modes depending on the parameters values. In absence of bending rigidity, Fig. 4.6(a), the mode at low frequencies has a nonmonotonous behavior. It presents a ZGVP and vanishes at $q_x = \pi/2$. At the ZGVP the energy that could be pumped into this mode does not propagate away from the region of excitation on the surface. Since at a ZGVP the phase velocity and so the wavelength remain finite, while the group velocity is zero, the energy can be locally trapped in the source area without any transfer to the adjacent medium. The ZGVP was investigated earlier in the case of Lamb waves [21], i.e., in finite thickness structures. Here, this type of singularity is theoretically predicted for semi-infinite medium, i.e., in the case of Rayleigh-type surface waves. When increasing the bending rigidity parameter p_B, the frequency value of this mode increases at $q_x = \pi/2$, Fig. 4.6(b)(c), and then, for sufficiently large value of p_B, the ZGVP disappears, Fig. 4.6(d). The physical origin of the predicted zero-group-velocity surface acoustic wave is in the existence of bulk modes where coupling/hybridization of rotational and transverse motion of the beads produces non-monotonous TR/RT modes with ZGVP, Fig. 4.2. In classical surface Rayleigh waves in the isotropic solids the bulk longitudinal and transverse waves, constituting the SAWs, are coupled by the mechanically free surface. On the mechanically free surface of the granular crystal the

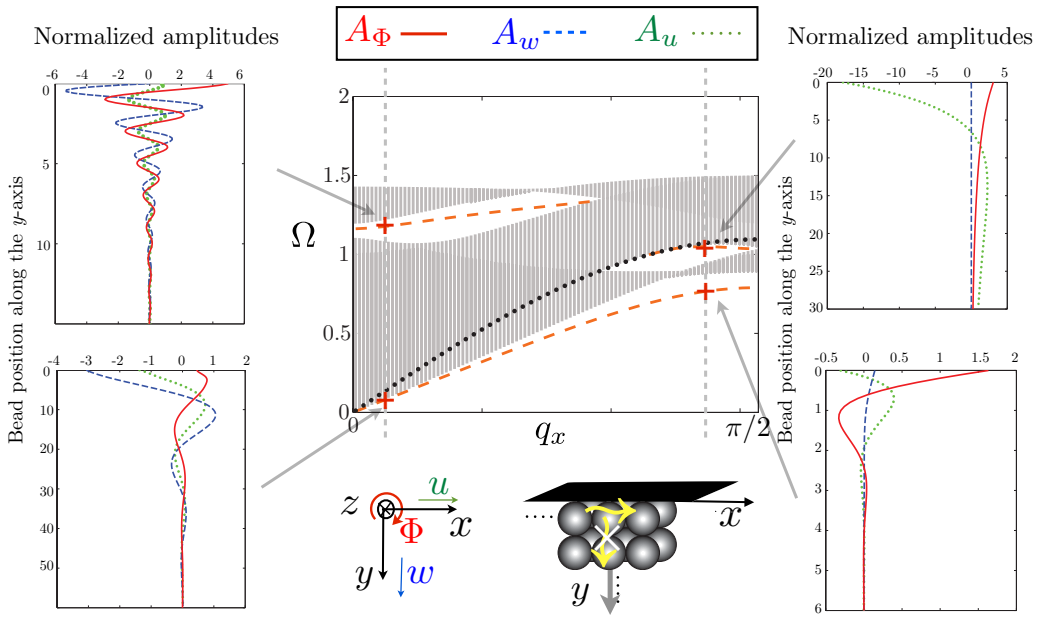

Figure 4.7 – (Color online) Discrete displacement and rotation profiles along the y-axis, i.e., perpendicular to the surface, for two distinct surface modes correponding to each of the two different wave numbers q_x.

longitudinal wave is coupled to TR/RT mode and the non-monotonous character of the latter can be transformed in the non-monotonous dispersion relation for the Rayleigh-type SAW and the existence of the ZGV SAWs. It could be expected that ZGVPs for SAWs, similarly to the ZGVPs in Lamb modes, could find application in nondestructive testing of the materials [22].

4.2.5 Rayleigh-type SAWs propagating at the (110) surface along [1$\bar{1}$0] direction

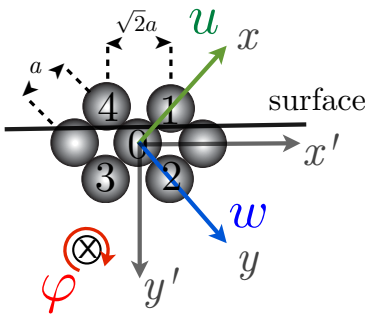

Figure 4.8 – (Color online) Schematic representation of the surface.

Rayleigh-type SAWs propagating at the (110) surface along [1$\bar{1}$0] direction are analyzed in this part. Figure 4.8 illustrates the position of the surface, which is parallel to the diagonal of the cubic crystal, and introduces new axes $x^{'}$ and $y^{'}$. The complete derivation of the bulk dispersion is not given in details here, but the reasoning is the same as in Sect. 4.2.2. In this case, the eigenvalue problem arising from the substitution of the plane wave solutions into the equations of motion is

$$\mathbf{S}_{\text{diag}}\mathbf{v} = 0 \ , \tag{4.14}$$

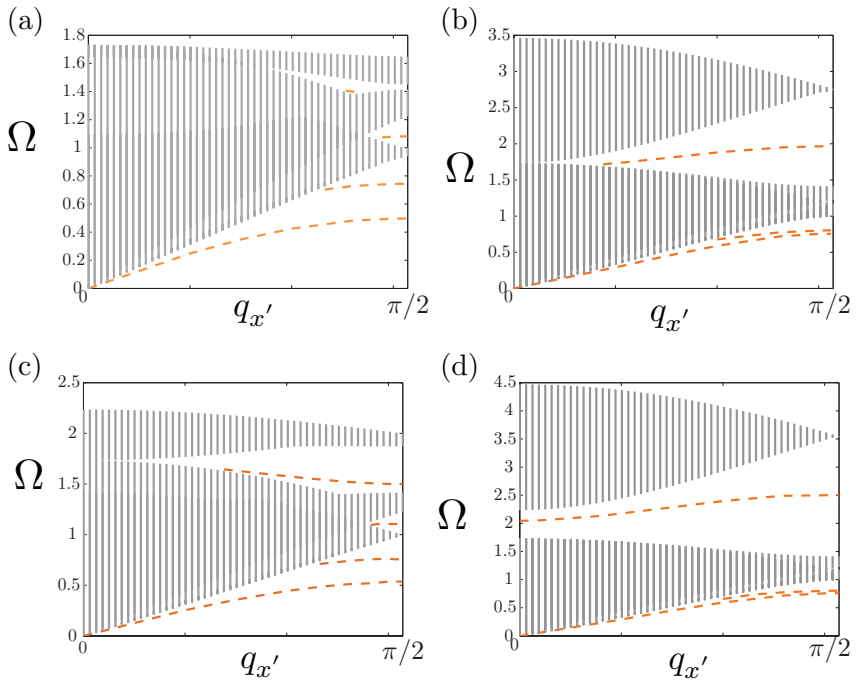

Figure 4.9 – (Color online) Dispersion curves along the diagonal direction of the crystal for $\eta = 2$ in the case of empty and filled spheres, (a) $p = 1.5$ and $p_B = 0.1$, (b) $p = 1.5$ and $p_B = 1$, (c) $p = 2.5$ and $p_B = 0.1$ and (d) $p = 2.5$ and $p_B = 1$. The shaded areas represent the projected bulk bands along $[1\bar{1}0]$ and the dashed orange curves represent the surface modes.

with $\mathbf{v} = \begin{pmatrix} A_u \\ A_w \\ A_\Phi \end{pmatrix}$ and

$$\mathbf{S}_{\text{diag}} = \begin{pmatrix} -\frac{1}{2}(\eta+1)(1-\cos q_x^{'}\cos q_y^{'})+\Omega^2 & -\frac{1}{2}(\eta-1)\sin q_x^{'}\sin q_y^{'} & \frac{1}{\sqrt{2}}\mathrm{j}\cos q_x^{'}\sin q_y^{'} \\ -\frac{1}{2}(\eta-1)\sin q_x^{'}\sin q_y^{'} & -\frac{1}{2}(\eta+1)(1-\cos q_x^{'}\cos q_y^{'})+\Omega^2 & -\frac{1}{\sqrt{2}}\mathrm{j}\sin q_x^{'}\cos q_y^{'} \\ -\frac{p}{\sqrt{2}}\mathrm{j}\cos q_x^{'}\sin q_y^{'} & \frac{p}{\sqrt{2}}\mathrm{j}\sin q_x^{'}\cos q_y^{'} & -(p+4p_Bp)-(p-4p_Bp)\cos q_x^{'}\cos q_y^{'}+\Omega^2 \end{pmatrix}, \tag{4.15}$$

with $q_x^{'}$ and $q_y^{'}$ the normalized wave numbers along $x^{'}$ and $y^{'}$ axes, respectively.

Mechanically free boundary conditions are applied at the surface, i.e., the total forces of beads 1 and 4 acting on bead 0 are zero. The amplitudes A_{u_i}, A_{w_i} and A_{Φ_i} corresponding to one $q_{y_i}^{'}$ can be determined by

$$\frac{A_{u_i}}{\chi_i} = \frac{A_{w_i}}{\epsilon_i} = \frac{A_{\Phi_i}}{\zeta_i} = \Lambda_i, \tag{4.16}$$

where χ_i, ϵ_i and ζ_i are the cofactors of any row of the determinant of the dynamical matrix (4.15) associated with $q_{y_i}^{'}$ $(i = 1, 2, 3)$ and where the Λ_i are determined from the boundary conditions. Hence, the general solution is

$$\begin{pmatrix} u \\ w \\ \Phi \end{pmatrix} = \sum_{i=1}^{3} (\chi_i, \epsilon_i, \zeta_i)\, \Lambda_i\, e^{\mathrm{j}\omega t - \mathrm{j}q_x^{'}x^{'} - \mathrm{j}q_y^{'}y^{'}}. \tag{4.17}$$

Substituting Eq. (4.17) into the boundary condition system leads to

$$\sum_{i=1}^{3} S_{2\mathrm{diag}_{j,i}}\,\Lambda_i = 0 \quad (i,j=1,2,3), \tag{4.18}$$

where

$$\begin{aligned}
S_{2\mathrm{diag}_{1,i}} &= \chi_i \frac{\eta+1}{\sqrt{2}}(1-\cos q_x^{'} e^{\mathrm{j}q_{y_i}^{'}}) - \mathrm{j}\epsilon_i \frac{\eta-1}{\sqrt{2}} \sin q_x^{'} e^{\mathrm{j}q_{y_i}^{'}} - \zeta_i(1+\cos q_x^{'} e^{\mathrm{j}q_{y_i}^{'}}),\\
S_{2\mathrm{diag}_{2,i}} &= -\mathrm{j}\chi_i \frac{\eta-1}{\sqrt{2}} \sin q_x^{'} e^{\mathrm{j}q_{y_i}^{'}} + \epsilon_i \frac{\eta+1}{\sqrt{2}}(1-\cos q_x^{'} e^{\mathrm{j}q_{y_i}^{'}}) + \mathrm{j}\zeta_i \sin q_x^{'} e^{\mathrm{j}q_{y_i}^{'}},\\
S_{2\mathrm{diag}_{3,i}} &= \chi_i \frac{1}{\sqrt{2}}(-1+\cos q_x^{'} e^{\mathrm{j}q_{y_i}^{'}}) + \mathrm{j}\epsilon_i \frac{1}{\sqrt{2}} \sin q_x^{'} e^{\mathrm{j}q_{y_i}^{'}} + \zeta_i \left[(-4p_B+1)\cos q_x^{'} e^{\mathrm{j}q_{y_i}^{'}} + 1 + 4p_B\right].
\end{aligned} \tag{4.19}$$

Surface waves can then be obtained by simultaneous fulfilment of Eqs. (4.14) and (4.18). Figure 4.9 presents the obtained dispersion curves for η=2 and by increasing bending rigidity in the case of a crystal made of empty ($p = 1.5$) and filled ($p = 2.5$) spheres. The shaded areas represent the projected bulk bands along $[1\bar{1}0]$ and the dashed orange curves represent the surface modes. For all parameter values, two surface modes are found below the first propagative band and several branches lie in the gap between the upper propagative bands. Along this direction, the SAWs present a monotonous behavior.

4.3 Shear-Horizontal (SH) type surface waves

4.3.1 Dispersion curves of the propagating modes

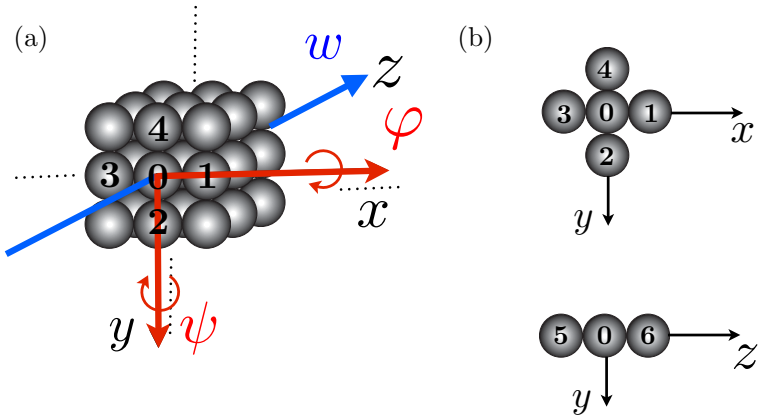

Figure 4.10 – (Color online) (a) Schematic representation of the granular crystal. w denotes the translational displacement motion along the z-axis and φ (respectively ψ) the rotational motion around the x-axis (respectively y-axis). (b) Definition of the bead numbers along the different axes.

The studied granular phononic crystal is composed of spheres distributed periodically on a cubic lattice and possessing two rotational and one translational *dofs*, Fig. 4.10. The shear force at the contact between two adjacent particles is described by a spring of constant rigidity ξ^s. The elongation of the springs introduces forces and momenta that induce the motion of the particles: the rotation φ around the x-axis, the rotation ψ around the y-axis and the displacement w along the z-axis. The equations of motion of the central particle obtained by applying the Lagrange principle are given by

$$m\ddot{w}_0 = -\xi^s\left[\delta s_1 + \delta s_2 + \delta s_3 + \delta s_4\right] , \tag{4.20a}$$

$$I\ddot{\varphi}_0 = -\xi^s R_c\left[-\delta s_4 + \delta s_2 + \delta v_5 - \delta v_6\right] + M_4 + M_2 , \tag{4.20b}$$

$$I\ddot{\psi}_0 = -\xi^s R_c\left[-\delta s_1 + \delta s_3 - \delta h_5 + \delta h_6\right] + M_1 + M_3 , \tag{4.20c}$$

where m is the mass of the particle and I is its momentum of inertia. The spring elongation in the transversal direction between the central and the i-th particle, i.e., the relative displacement between the 0-th and the i-th particle at the contact point, is denoted by δs_{i} and the momenta due to bending rigidity are denoted by M_{i}. The relative displacements are explicitly given by,

$$\begin{aligned}
\delta s_1 &= w_0 - w_1 - R_c(\psi_0 + \psi_1) \ , \\
\delta s_2 &= w_0 - w_2 + R_c(\varphi_0 + \varphi_2) \ , \\
\delta s_3 &= w_0 - w_3 + R_c(\psi_0 + \psi_3) \ , \\
\delta s_4 &= w_0 - w_4 - R_c(\varphi_0 + \varphi_4) \ .
\end{aligned} \tag{4.21}$$

The springs oriented along the x-axis and y-axis for the contact between the 0-th and 5-th beads, and the 0-th and 6-th beads are active in shearing, Fig. 4.10. The beads 5 and 6, oriented along the z-axis, rotate in the same direction and same angle as the central particle, i.e., the bending rigidity is not initiated because $\varphi_0 = \varphi_5 = \varphi_6$ and $\psi_0 = \psi_5 = \psi_6$. Because of the study of SH surface waves, which are a particular 2D motions of the crystal, there is no dependance on the z coordinate, i.e., $w_0 = w_5 = w_6$. Then, the vertical δv_{i} (along y-axis) and horizontal δh_{i} (along x-axis) spring elongations between the central and the 5-th and 6-th beads are

$$\begin{aligned}
\delta v_5 &= 2R_c\varphi_0 \ , \\
\delta v_6 &= -2R_c\varphi_0 \ , \\
\delta h_5 &= -2R_c\psi_0 \ , \\
\delta h_6 &= 2R_c\psi_0 \ .
\end{aligned} \tag{4.22}$$

The equations of motion are solved in the form of plane waves,

$$\mathbf{V}_{\mathrm{i}}^{SH} = \begin{pmatrix} \Phi_{\mathrm{i}}(x,y,t) \\ \Psi_{\mathrm{i}}(x,y,t) \\ w_{\mathrm{i}}(x,y,t) \end{pmatrix} = \mathbf{v}^{SH} e^{\mathrm{j}\omega t - 2\mathrm{j}q_x x_{\mathrm{i}} - 2\mathrm{j}q_y y_{\mathrm{i}}} \ , \tag{4.23}$$

with the new variable $\Phi = R_c\varphi$ and $\Psi = R_c\psi$ and $\mathbf{v}^{SH} = \begin{pmatrix} A_\Phi \\ A_\Psi \\ A_w \end{pmatrix}$ the amplitude vector.

Equation (4.23) is then developed around the equilibrium position (x_0,y_0) of the central particle, $\mathbf{V}_{\mathrm{i}}^{SH} = \mathbf{v}^{SH} e^{\mathrm{j}\omega t - 2\mathrm{j}q_x x_0 - 2\mathrm{j}q_y y_0} e^{-2\mathrm{j}q_x \Delta x_{\mathrm{i}} - 2\mathrm{j}q_y \Delta y_{\mathrm{i}}}$, where $\Delta x_{\mathrm{i}} = x_{\mathrm{i}} - x_0$ and $\Delta y_{\mathrm{i}} = y_{\mathrm{i}} - y_0$ are the relative coordinates between the central particle and the i-th particle, and ω is the angular frequency.

Finally, the substitution of Eq. (4.23) into the set of Eqs. (4.20), (4.21) and (4.22), leads to the eigenvalue problem,

$$\mathbf{S}^{SH}\mathbf{v}^{SH} = 0 \ , \tag{4.24}$$

where $\mathbf{S}^{SH}$ is the dynamical matrix defined by

$$\mathbf{S}^{SH} = \begin{pmatrix} -p(\cos^2 q_y + 1 + p_B \sin^2 q_y) + \Omega^2 & 0 & -\mathrm{j}p \sin q_y \cos q_y \\ 0 & -p(\cos^2 q_x + 1 + p_B \sin^2 q_x) + \Omega^2 & \mathrm{j}p \sin q_x \cos q_x \\ \mathrm{j} \sin q_y \cos q_y & -\mathrm{j} \sin q_x \cos q_x & -\sin^2 q_x - \sin^2 q_y + \Omega^2 \end{pmatrix} \ . \tag{4.25}$$

Nontrivial solutions of Eq. (4.24) require that

$$|S_{j,i}^{SH}| = 0 \ . \tag{4.26}$$

For a given set of parameters p, η and p_B and wave number q_x, Eq. (4.26) relates the frequency Ω and the wave number q_y. Eq. (4.26) can be written in the form of a quadratic equation for $Y = \sin^2 q_y$ or of a cubic equation for Ω^2, see appendix (B.3). Note that for this particular structure, three modes exist, but only two distinct wave numbers q_y with negative imaginary part correspond to a given frequency. This particularity results from the absence of q_y in the second line of the dynamical matrix $\mathbf{S}^{SH}$, Eq. (4.25). From this second line, the following relation between the rotational amplitude A_Ψ and the translational amplitude A_w is derived

$$A_\Psi = \frac{\mathrm{j}p \sin q_x \cos q_x}{p(\cos^2 q_x + 1 + p_B \sin^2 q_x - \Omega^2)} A_w \ . \tag{4.27}$$

Equation (4.27) does not depend on q_y, then, the rotational amplitude A_Ψ has the same distribution along the y-axis as the translational amplitude A_w. From the physics point of view, the similar distribution of modes Ψ and w in depth results from the fact that interaction between them, described by Eq. (4.20c), includes only the beads of the same horizontal plane at a particular depth y and not the beads of different horizontal layers. At all point x and y in the crystal, the transversal and rotational components of the modes are assumed to be of the following form

$$\begin{pmatrix} \Phi \\ \Psi \\ w \end{pmatrix}_{l,n} = \begin{pmatrix} A_\Phi \\ A_\Psi \\ A_w \end{pmatrix} e^{\mathrm{j}\omega t - 2\mathrm{j}q_x l - 2\mathrm{j}q_y n} = A_w \begin{pmatrix} \alpha \\ \beta \\ 1 \end{pmatrix} e^{\mathrm{j}\omega t - 2\mathrm{j}q_x l - 2\mathrm{j}q_y n} \ , \tag{4.28}$$

with $\alpha = \dfrac{-\mathrm{j}p \sin q_y \cos q_y}{p(\cos^2 q_y + 1 + p_B \sin^2 q_y) - \Omega^2}$ and $\beta = \dfrac{\mathrm{j}p \sin q_x \cos q_x}{p(\cos^2 q_x + 1 + p_B \sin^2 q_x) - \Omega^2}$.

Figure 4.11 presents the dispersion curves along the Brillouin zone $M\Gamma XM$ for a filled sphere ($p = 2.5$). Three modes propagate in the structure. The eigenmodes of the granular phononic crystal consist of three components, the translational motion T, the rotational motion R_Φ around the x-axis and the rotational motion R_Ψ around the y-axis. The blue dashed curves correspond to coupled transverse/rotational modes with a predominance of translation, orange dotted curves correspond to coupled transverse/rotational modes with a predominance of rotation. In the case of a propagative wave in the ΓX (respectively XM) direction, a mode called R_Φ-mode (respectively R_Ψ-mode) and shown in red line appears uncoupled from the mixed modes ($T + R_\Psi$) (respectively ($T + R_\Phi$)). Along the ΓM direction, a coupled transverse/rotational ($R_\Phi + R_\Psi + T$) mode, plotted in red line, is propagating with the same predominance for all $q_{x,y}$.

Figures 4.12 and 4.13 present the evolution of the dispersion curves as a function of the bending rigidity parameter for empty ($p = 1.5$) and filled ($p = 2.5$) spheres, respectively. By increasing the bending rigidity parameter p_B, the modes with a predominance of rotation are shifted to high frequencies. A complete band gap, i.e., a band gap in all the directions of the Brillouin zone, exists when $p_B > 2/p - 1$.

4.3.2 Boundary conditions for SH-type SAWs propagating at the (010) surface along [100] direction

We study here the SH-type SAWs on the mechanically free surface of the granular crystal, which is normal to the y-axis, i.e., on (010) surface. As developed in section 4.2.2 for Rayleigh-type SAWs, the boundary conditions are formed by removing all the particles on one side of the boundary layer. For

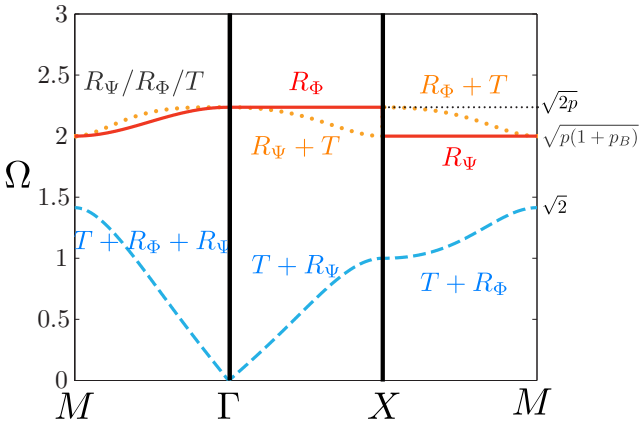

Figure 4.11 – (Color online) Dispersion curves for a crystal made of filled spheres ($p = 2.5$) and $p_B = 0.6$. T represents the translational motion along the z-axis, R_Φ (respectively R_Ψ) represents the rotational motion around the x-axis (respectively y-axis).

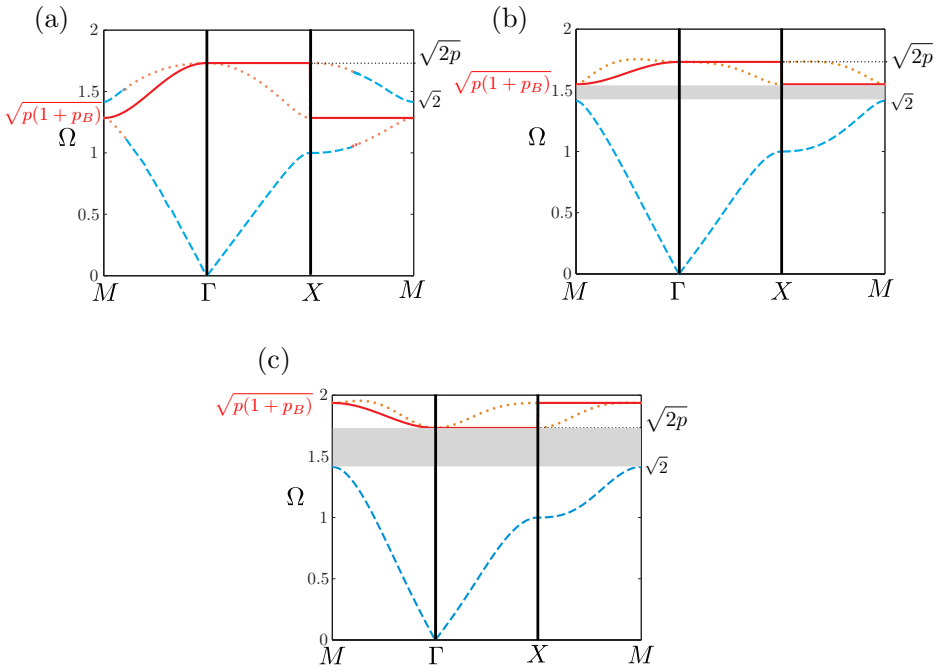

Figure 4.12 – (Color online) Description of the dispersion curves for $p < 2$ ($p = 1.5$) and (a) $0 \leq p_B < 2/p - 1$ ($p_B = 0.1$), (b) $2/p - 1 < p_B < 1$ ($p_B = 0.6$), (c) $p_B > 1$ ($p_B = 1.5$). The complete band gap is shown by the gray shaded area.

this crystal, the mechanically free boundary conditions lead to the following equations

- No shear spring elongation,

$$w_0 - w_4 - (\Phi_0 + \Phi_4) = 0 \ . \tag{4.29}$$

- No rotation, able to activate bending rigidity,

$$\Phi_4 - \Phi_0 = 0 \ . \tag{4.30}$$

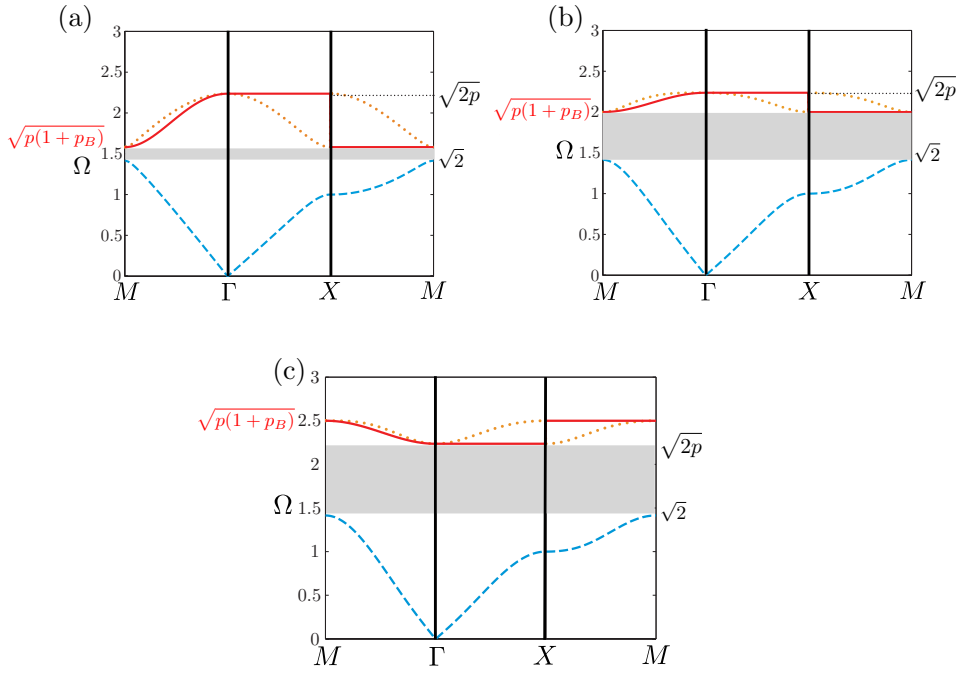

Figure 4.13 – (Color online) Description of the dispersion curves for $p > 2$ ($p = 2.5$) and (a) $0 \leq p_B < 2/p - 1$ ($p_B = 0$), (b) $2/p - 1 < p_B < 1$ ($p_B = 0.6$), (c) $p_B > 1$ ($p_B = 1.5$). The complete band gap is shown by the gray shaded area.

As demonstrated in the previous section, only two wave numbers exist for one frequency, noted q_{y_1} and q_{y_2}, because the amplitude of the rotational component A_Ψ has the same distribution as the amplitude of the transverse component A_w along the y-axis. The boundary conditions are then solved accounting for these two modes. If A_{w_i}, with $i = 1, 2$, are the amplitude of the transversal component of these two modes, the amplitudes of the displacement and rotations can be written in the form

$$\Phi_{l,n} = \sum_{i=1}^{2} A_{w_i}\, \alpha_i\, e^{\mathrm{j}\omega t} e^{-2\mathrm{j}lq_x} e^{-2\mathrm{j}nq_{y_i}} \ , \tag{4.31a}$$

$$\Psi_{l,n} = \sum_{i=1}^{2} A_{w_i}\, \beta\, e^{\mathrm{j}\omega t} e^{-2\mathrm{j}lq_x} e^{-2\mathrm{j}nq_{y_i}} \ , \tag{4.31b}$$

$$w_{l,n} = \sum_{i=1}^{2} A_{w_i}\, e^{\mathrm{j}\omega t} e^{-2\mathrm{j}lq_x} e^{-2\mathrm{j}nq_{y_i}} \ . \tag{4.31c}$$

The substitution of the amplitudes given in Eqs. (4.31) into the boundary conditions (4.29) and (4.30) leads to

$$\sum_{i=1}^{2} A_{w_i} \left(1 - e^{2\mathrm{j}q_{y_i}}\right) - A_{w_i}\alpha_i \left(1 + e^{2\mathrm{j}q_{y_i}}\right) = 0 \ , \tag{4.32a}$$

$$\sum_{i=1}^{2} A_{w_i}\, \alpha_i \left(e^{2\mathrm{j}q_{y_i}} - 1\right) = 0 \ , \tag{4.32b}$$

which can be written in the following form

$$\mathbf{S_2}^{SH} \mathbf{v_2}^{SH} = 0 \ , \tag{4.33}$$

with $\mathbf{v_2}^{SH} = \begin{pmatrix} A_{w_1} \\ A_{w_2} \end{pmatrix}$ and

$$\mathbf{S_2}^{SH} = \begin{pmatrix} (1-e^{2\mathrm{j}q_{y_1}}) - \alpha_1(1+e^{2\mathrm{j}q_{y_1}}) & (1-e^{2\mathrm{j}q_{y_2}}) - \alpha_2(1+e^{2\mathrm{j}q_{y_2}}) \\ \alpha_1(e^{2\mathrm{j}q_{y_1}}-1) & \alpha_2(e^{2\mathrm{j}q_{y_2}}-1) \end{pmatrix} , \tag{4.34}$$

with $\alpha_i = \dfrac{-\mathrm{j}p \sin q_{y_i} \cos q_{y_i}}{p(\cos^2 q_{y_i} + 1 + p_B \sin^2 q_x) - \Omega^2}$ with $i = 1, 2$.

The following equation must be satisfied in order to have nontrivial solutions of Eq. (4.33)

$$|S^{SH}_{2_{j,i}}| = 0 \ . \tag{4.35}$$

4.3.3 Surface mode description

Surface waves are calculated for fixed sets of parameters q_x, p and p_B by simultaneous fulfilment of Eqs. (4.26) and Eqs. (4.35). In absence of bending rigidity ($p_B = 0$), no SH-type surface waves exist in the crystal, see developement in appendix B.4. When $p_B \geq 0$, one surface mode exists in this granular phononic crystal. After some reduction of Eq. (4.35), the analytical form of the surface mode frequency is found

$$\Omega_S^2 = p + \frac{p_B p}{2} - \frac{1}{2} p_B p \frac{\cos(q_{y_1} - q_{y_2})}{\cos(q_{y_1} + q_{y_2})} \ , \tag{4.36}$$

with q_{y_1} and q_{y_2} solutions of Eq. (B.6) (annexe B.3). This mode is plotted in orange dashed line in Fig. 4.14(a) in the case of filled sphere ($p = 2.5$) and with a bending rigidity parameter $p_B = 0.3$. This surface mode is slightly dispersive, Fig. 4.14(c). For various values of the parameters, it is localized around one frequency. The possible reason for this strong localization in the frequency domain is the weak coupling of rotational motion R_Φ with the other motions. According to Eqs. (4.31), the amplitudes of the discrete displacement and rotations of the transversal $w_{l,n}$, rotational $\Phi_{l,n}$ and $\Psi_{l,n}$ components of the surface modes as a function of the particle position (l, n) in the crystal can be determined by combining the two evanescent modes

$$\begin{pmatrix} w_{l,n} \\ \Phi_{l,n} \\ \Psi_{l,n} \end{pmatrix} = A_{w_1} \left[\begin{pmatrix} 1 \\ \alpha_1 \\ \beta \end{pmatrix} e^{\mathrm{j}\omega t} e^{-2\mathrm{j}lq_x} e^{-2\mathrm{j}nq_{y_1}} + Z \begin{pmatrix} 1 \\ \alpha_2 \\ \beta \end{pmatrix} e^{\mathrm{j}\omega t} e^{-2\mathrm{j}lq_x} e^{-2\mathrm{j}nq_{y_2}} \right] , \tag{4.37}$$

with $Z = \dfrac{A_{w_2}}{A_{w_1}} = -\dfrac{\alpha_1(1-e^{-2\mathrm{j}q_{y_1}})}{\alpha_2(1-e^{-2\mathrm{j}q_{y_2}})}$. As illustrated in Fig. 4.14(b), due to the symmetry and configuration of the crystal, this particular mode has mainly a rotational A_Φ component. The decays of the amplitudes are a combination of a monotonously decaying function and a decaying function with few oscillations.

4.3.4 SH-type SAWs propagating at the (110) surface along [1$\bar{1}$0] direction

SH-type SAWs propagating at the (110) surface along [1$\bar{1}$0] direction are investigated in this part. The surface position is the same as the one presented in Fig. 4.8. The eigenvalue problem resulting from the substitution of the plane wave solutions into the equation of motions is

$$\mathbf{S^{SH}_{diag}} \mathbf{v^{SH}} = 0 \ , \tag{4.38}$$

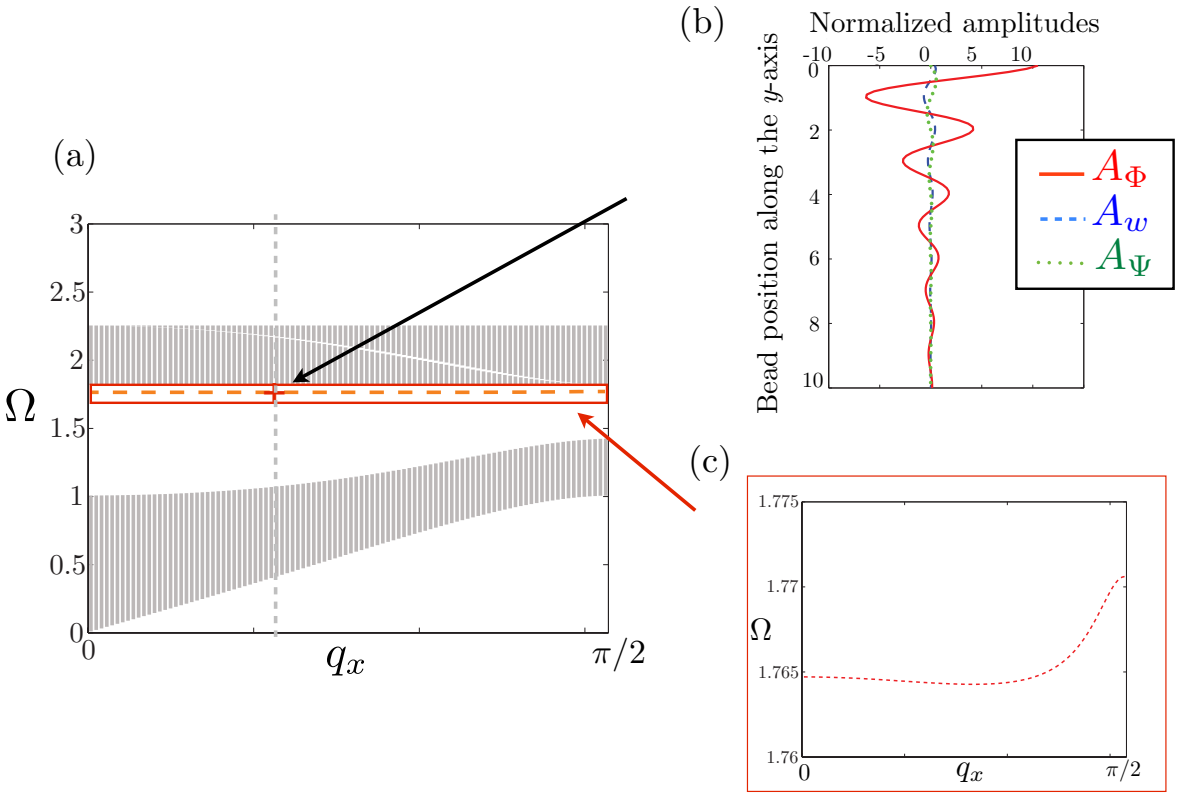

Figure 4.14 – (Color online) (a) Dispersion curves along the q_x direction of the crystal for $p = 2.5$ and (a) $p_B = 0.3$. The shaded areas represent the projected bulk bands along [100], i.e., x direction. The dashed orange curves represent the surface mode. (b) Discrete displacement profiles of the surface modes. (c) Zoom on the surface mode.

with $\mathbf{v}^{\mathbf{SH}} = \begin{pmatrix} A_\Phi \\ A_\Psi \\ A_w \end{pmatrix}$ and

$$\mathbf{S}^{\mathbf{SH}}_{\text{diag}} = \begin{pmatrix} -\frac{p}{2}\cos q_x^{'}\cos q_y^{'}(1-p_B) - \frac{p_B p}{2} - \frac{3p}{2} + \Omega^2 & -\frac{\mathrm{j}}{2}p\sin q_x^{'}\sin q_y^{'} & -\frac{1}{\sqrt{2}}p\cos q_x^{'}\sin q_y^{'} \\ -\frac{1}{2}p\sin q_x^{'}\sin q_y^{'} & -\frac{p}{2}\cos q_x^{'}\cos q_y^{'}(1-p_B) - \frac{p_B p}{2} - \frac{3p}{2} + \Omega^2 & \frac{\mathrm{j}}{\sqrt{2}}p\sin q_x^{'}\cos q_y^{'} \\ \frac{\mathrm{j}}{\sqrt{2}}\cos q_x^{'}\sin q_y^{'} & -\frac{\mathrm{j}}{\sqrt{2}}\sin q_x^{'}\cos q_y^{'} & -1+\cos q_x^{'}\cos q_y^{'}+\Omega^2 \end{pmatrix}. \tag{4.39}$$

Mechanically free boundary conditions are applied at the surface, i.e., the total forces of beads 1 and 4 acting on bead 0 vanish. The amplitudes A_{Φ_i}, A_{Ψ_i} and A_{w_i} corresponding to a particular $q_{y_i}^{'}$ can be determined by

$$\frac{A_{\Phi_i}}{\chi_i} = \frac{A_{\Psi_i}}{\epsilon_i} = \frac{A_{w_i}}{\zeta_i} = \Lambda_i, \tag{4.40}$$

where χ_i, ϵ_i and ζ_i are the cofactors of all row of the dynamical matrix (4.39) associated with $q_{y_i}^{'}$ $(i = 1, 2, 3)$ and where the Λ_i are to be determined from the boundary conditions.
Hence, the general solution is

$$\begin{pmatrix} \Phi \\ \Psi \\ w \end{pmatrix} = \sum_{i=1}^{3} (\chi_i, \epsilon_i, \zeta_i)\, \Lambda_i\, e^{\mathrm{j}\omega t - \mathrm{j}q_x^{'} x^{'} - \mathrm{j}q_y^{'} y^{'}}. \tag{4.41}$$

Substituting Eq. (4.41) into the boundary condition system leads to

$$\sum_{i=1}^{3} S^{SH}_{2\mathrm{diag}_{j,i}} \Lambda_i = 0 \quad (i,j=1,2,3), \tag{4.42}$$

where

$$\begin{aligned}
S^{SH}_{2\mathrm{diag}_{1,i}} &= \chi_i(1-\cos q_x^{'} e^{\mathrm{j}q_{y_i}^{'}}) - \epsilon_i \frac{1}{\sqrt{2}}(1+\cos q_x^{'} e^{\mathrm{j}q_{y_i}^{'}}) + \frac{\mathrm{j}}{\sqrt{2}}\zeta_i \sin q_x^{'} e^{\mathrm{j}q_{y_i}^{'}}, \\
S^{SH}_{2\mathrm{diag}_{2,i}} &= \chi_i(1-\cos q_x^{'} e^{\mathrm{j}q_{y_i}^{'}}) - \epsilon_i \left(\frac{1}{\sqrt{2}}(1+\cos q_x^{'} e^{\mathrm{j}q_{y_i}^{'}}) + \sqrt{2}p_B(1-\cos q_x^{'} e^{\mathrm{j}q_{y_i}^{'}}) \right) + \frac{\mathrm{j}}{\sqrt{2}}\zeta_i \sin q_x^{'} e^{\mathrm{j}q_{y_i}^{'}}, \\
S^{SH}_{2\mathrm{diag}_{3,i}} &= \mathrm{j}\chi_i \sin q_x^{'} e^{\mathrm{j}q_{y_i}^{'}} + \frac{\mathrm{j}}{\sqrt{2}}\epsilon_i \sin q_x^{'} e^{\mathrm{j}q_{y_i}^{'}} - \zeta_i \left(\frac{1}{\sqrt{2}}(1+\cos q_x^{'} e^{\mathrm{j}q_{y_i}^{'}}) + \sqrt{2}p_B(1-\cos q_x^{'} e^{\mathrm{j}q_{y_i}^{'}}) \right).
\end{aligned} \tag{4.43}$$

Surface waves can then be obtained by simultaneous fulfilment of Eqs (4.38) and (4.42).

The required condition for the existence of surface waves is the presence of bending rigidity ($p_B > 0$). Figures 4.15(a) and (b) illustrate the obtained surface modes in the case of $p_B = 0.5$ and empty sphere ($p = 1.5$) and filled sphere ($p = 2.5$), respectively. Two branches are found in the gap between the two first propagation bands.

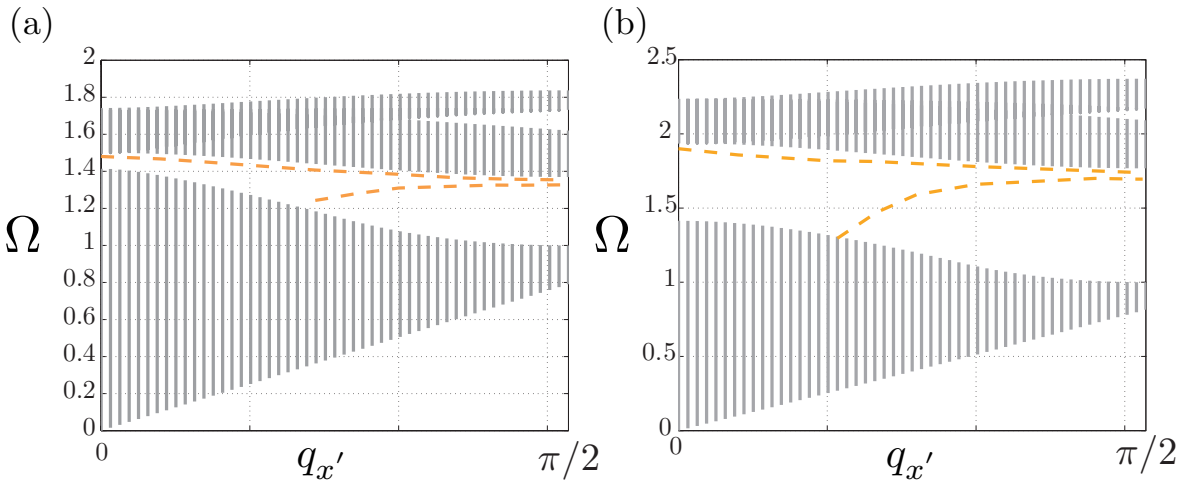

Figure 4.15 – (Color online) Dispersion curves along the diagonal direction of the crystal for $p_B = 0.5$ and (a) empty sphere ($p = 1.5$) and (b) filled sphere ($p = 2.5$). The shaded areas represent the projected bulk bands along $[1\bar{1}0]$ and the dashed orange curves represent the surface modes.

Another important feature of the predicted surface acoustic wave, which is described by Eq. (4.36), is its existence only in the presence of bending rigidity of the contacts. If the direct bending-type interactions between the rotations of the beads are neglected this surface mode transforms into the purely vibrational mode with frequency equal to $\sqrt{p}$ and zero group velocity. This is a non-negligible bending rigidity of the contact which induces propagation of this surface acoustic wave. It is worth noticing here that in chapters **??** it was demonstrated that some zero-energy, i.e., $w = 0$, modes of granular phononic crystals become propagative due the the bending-type interactions between the beads.

4.4 Comparison with the Cosserat theory

4.4.1 Brief introduction to the Cosserat theory

One hundred years ago, the Cosserat brothers developed a continuum elasticity theory accounting for the rotational *dofs* of point bodies (infinitesimal particles) constituting deformable solids [23]. Currently, this theory is known as the Cosserat theory, and the related and advanced theories are known as theories of Cosserat continuum or as theories of micropolar continuum [7]. In the Cosserat theory, each material point has six *dofs*, three of which correspond to the translations as in the classical theory of elasticity, and the three others correspond to rotations. The stress tensor is asymmetric and an additional couple-stress tensor is introduced, which plays the analogous role for torques than the stress tensor plays for forces. The theory predicts a contribution of rotations to the dispersion of the shear elastic wave velocity as well as the existence of additional rotational bulk modes. More information on the Cosserat theory can be found in the appendix B.5.

The additional effects predicted by this theory have never been observed experimentally and have been subjected to criticism [7, 24]. More recently, the rotational modes have been revealed experimentally in a 3D granular phononic crystal [15]. A theoretical comparison of the bulk waves in homogenized three-dimensional granular phononic crystals with those in the Cosserat continuum has demonstrated that the Cosserat theory does not account for all the influences of the material inhomogeneity on its elastic behavior. To go further in these previous conclusions, a theoretical comparison of surface waves in the granular crystals with those in the reduced Cosserat theory is performed below.

4.4.2 Comparison of SAWs in granular crystals and in reduced Cosserat medium

In continuum elasticity, the Cosserat theory [23] and its various extensions [7, 25–28] introduce the rotational *dofs* of an elementary volume for modeling wave phenomena in micro-inhomogeneous materials. In these theories the motion of an elementary "point" is characterized, in addition to the mechanical displacement vector $\vec{u}$, by the vector of mechanical rotation (angle) $\vec{\theta}$. In the simplest case of the so-called reduced Cosserat continuum, in addition to Lamé moduli λ and μ, just a single modulus α, coupling the displacements and rotations, is introduced. For the harmonic waves of cyclic frequency ω with wave vector $\vec{k}$ the coupled equations of the reduced Cosserat continuum are [29]

$$\rho\,\omega^2\vec{u} = (\lambda+2\mu)\vec{k}(\vec{k}\vec{u}) - (\mu+\alpha)\left[\vec{k}[\vec{k}\vec{u}]\right] + \mathrm{j}2\alpha[\vec{k}\vec{\theta}], \tag{4.44}$$

$$J\omega^2\vec{\theta} = 4\alpha\vec{\theta} + 2\mathrm{j}\alpha[\vec{k}\vec{u}], \tag{4.45}$$

where ρ is the density and J denotes the density of the moment of inertia.

From Eq. (4.45) it follows that the modulus α together with J control the rotational resonance frequency ω_0 of elementary volumes

$$\vec{\theta} = \mathrm{j}\frac{\omega_0^2}{2(\omega^2-\omega_0^2)}[\vec{k}\vec{u}] \quad \text{with} \quad \omega_0 = 2\sqrt{\frac{\alpha}{J}}. \tag{4.46}$$

Subsitution of Eq. (4.46) into Eq. (4.44) gives

$$\rho\,\omega^2\vec{u} = (\lambda+2\mu)\vec{k}(\vec{k}\vec{u}) - \left(\mu+\alpha\frac{\omega^2}{\omega^2-\omega_0^2}\right)\left[\vec{k}[\vec{k}\vec{u}]\right]. \tag{4.47}$$

Eq. (4.47) demonstrates that the acoustic waves with the longitudinal polarization of displacement, $[\vec{k}\vec{u}] = 0$, are not modified in comparison with classical elasticity theory, while the modification of the waves with transverse polarization of the displacement, $(\vec{k}\vec{u}) = 0$, takes place as in a metamaterial with resonant inclusions [30, 31]. Moreover, because local resonances of the reduced Cosserat metamaterial are rotational, they modify the effective modulus of the "metamaterial" and not its density (see [31, 32] and references therein). In accordance with Eq. (4.47), the dispersion relation of the coupled transverse/rotational modes, $(\vec{k}\vec{u}) = 0$, can be presented in the form

$$k^2 = \frac{\omega^2}{C_T^2} \frac{1}{1 + \frac{\alpha}{\mu} \frac{\omega^2}{\omega^2 - \omega_0^2}}. \tag{4.48}$$

It describes two branches, the RT branch at frequencies above ω_0 and TR branch at frequencies below $\omega_1 = \frac{\mu}{\mu + \alpha}\omega_0 = \left(\frac{C_{TR}}{C_{RT}}\right)^2 \omega_0$, separated by the band gap, $\omega_1 \leq \omega \leq \omega_0$, where there is no propagative mode because of the negative effective modulus of reduced Cosserat medium. In the above formula C_{TR} denotes the velocity of the lower mode when $\omega \to 0$ ($k \to 0$), while C_{RT} denotes the velocity of the upper mode when the mode extends at $\omega \to \infty$ ($k \to \infty$).

The SAWs in reduced Cosserat continuum have been studied in details quite recently [29]. The theory predicted that coupling of the TR and RT bulk modes with longitudinal bulk acoustic waves at the mechanically free surface leads to the existence of two branches of Rayleigh type SAWs. The lower branch of SAWs is below the TR bulk branch. The upper branch of Rayleigh-type SAWs is below the dispersion curves of RT and L bulk branches and above the low edge, $\omega = \omega_1$, of the bulk band gap. Note that surface waves can be propagative at frequencies forbidden for bulk TR and RT wave propagation. Because of the above formulated requirements, the minimum possible wave number, k, for the upper branch of Rayleigh-type SAW cannot be smaller than $k_{min} = \omega_1/C_L$, where $C_L = \sqrt{\frac{\lambda + 2\mu}{\rho}}$ is the velocity of dispersionless bulk longitudinal waves. The theory of SAWs in granular phononic crystals, which was presented above, confirms the predictions of the reduced Cosserat theory on the possible existence of multiple Rayleigh-type surface acoustic modes (see Figs. 4.6 and 4.9). In comparison with the Cosserat theory some of the upper branches of Rayleigh-type SAW can start at finite ω from $k = 0$ (see Fig. 4.6), which is forbidden in the Cosserat theory. This is related to the opening, in phononic crystal, of band gaps for the propagation of bulk longitudinal modes, which can be located near $k = 0$ for finite ω. Thus the limiting condition $k_{min} = \omega_1/C_L$ is lifted. However, the most important difference with the reduced Cosserat theory, from the physics point of view, is related to physical origins of wave dispersion. As it was pointed out earlier in the comparison of bulk waves in granular phononic crystal and in the Cosserat media [15], in the former the dispersion comes both from the repulsion/hybridization of transverse and rotational motions and from multiple scattering of the waves (induced by natural spatial inhomogeneity/periodicity of phononic crystals), while in the latter the wave dispersion is caused by hybridization phenomena only. The situation with surface acoustic waves is similar. For example, in the dispersion of the lower branch of Rayleigh-type SAW at $\omega \to 0$ there are contributions due to both the interaction between different modes and also to the explicit existence in phononic crystals of a characteristic scale of spatial inhomogeneity, which is absent in the reduced Cosserat medium. Thus our comparison indicates that for the correct modeling of the wave phenomena in micro-inhomogeneous media the Cosserat theories should be at least combined with

higher order gradient theories of elasticity, which explicitly contain the characteristic spatial length of micro-inhomogeneity and, thus, account for wave scattering by spatial inhomogeneities.

Our theoretical analysis of the SH-type SAWs in granular crystals can be also compared with the theoretical predictions of the reduced Cosserat continuum [29]. In fact the theory [29] has predicted the absence of energy transporting SH-type SAWs in the reduced Cosserat continuum. It has just predicted the existence of k-independent vibrations, $\omega(k) = \omega_1$ =constant, at frequency ω_1 where the effective modulus of the reduced Cosserat medium is equal to zero. These zero-group-velocity vibrational modes can be arbitrary distributed in depth [29]. The theory developed above for the granular phononic crystal demonstrates that these types of vibrational modes also exist and, moreover, they transform into true localized and energy carrying SAWs when bending rigidity of the contacts between the beads is taken into account (see Figs. 4.14 and 4.15). Thus our theory highlights the crucial role of bending-type interactions for some surface acoustic wave phenomena. In chapters **??** it was demonstrated that these types of interaction between beads induce true propagative modes in granular phononic chains and in bulk granular phononic crystals, which are otherwise zero-energy, i.e., $\omega = 0$, modes. The theory developed above confirms that neglecting in the reduced Cosserat theory, relative to the general Cosserat theory, the direct interaction between the rotations of elementary volumes, which mathematically manifests itself in the absence of any terms containing spatial derivatives of $\vec{\theta}$ in Eq. (4.45), can have profound consequences in terms of wave phenomena predicted by this theory.

For the case of the SH-type surface acoustic waves the predictions of the reduced Cosserat theory of localized vibrations only, at a particular single frequency [29], is drastically different from the prediction by the general Cosserat theory of a true surface acoustic wave, existing in the complete domain of frequencies and wave numbers [11]. The SH-type SAW dispersion curve predicted by the general Cosserat theory starts at $\omega = 0$ ($k = 0$) and up to $\omega = \infty$ ($k = \infty$) and is located below all the dispersion curves of bulk modes. In classical terminology it is an acoustical-type surface phonon mode. Our theory predicts possible existence of optical-type SH surface acoustic mode, which dispersion curve starts at $k = 0$ from $\omega \neq 0$ (Fig. 4.14). This slow mode is much closer to the surface vibrational mode predicted by the reduced Cosserat model than to the acoustical-type SH-type SAW predicted by the general Cosserat theory. Thus our theory indicates that the reduced Cosserat model can be a fruitful tool for the prediction of wave phenomena in some particular granular crystals and micro-inhomogeneous materials. The reduced Cosserat theory clearly reveals some wave phenomena which existence is so deeply hidden in the general Cosserat theory that it could be easily missed.

4.5 Conclusions

In summary, the propagation of surface waves has been analyzed at the mechanically free surface of two different granular phononic crystals. A first case with the surface along the (010) plane of a cubic crystal and surface waves propagating in the [100] direction is investigated. In the first studied granular phononic crystal, where the particles possess two translational and one rotational *dofs*, generalized type Rayleigh surface waves and one pure longitudinal mode skimming along the surface direction, i.e., in [100] direction, are found. The analysis shows a nonmonotonous behavior with a zero-group velocity point for the lower frequency Rayleigh surface mode, which can be interesting for non-destructive

characterization applications. The surface waves amplitude decay in depth is a combination of an exponentially decaying function with few oscillations. In the second granular phononic crystal studied, with particles possessing two rotational and one translational *dofs*, one shear-horizontal type surface wave is found. This mode has the particularity to be localized around one particular frequency. We have demonstrated that the existence of this mode is due to the bending-type interaction between the rotating grains in contact and that the dispersion of this mode can be tuned by modifying the ratio of the bending and shear rigidities acting between the particles. In addition, the existence of Rayleigh-type and SH-type SAWs propagating at the (110) surface along $[1\bar{1}0]$ direction is theoretically revealed. Our findings are of interest in non-destructive testing of materials and in the design of devices devoted to frequency filtering or waveguiding.

A comparison of the results obtained in the granular phononic crystals with the predictions of surface waves in the Cosserat continuum is made. When the wavelength is shortened and becomes comparable to the particle size, the Cosserat theories are unable to describe the dispersive phononic properties. However these theories also fail to correctly account for all consequences of the material inhomogeneity in the long-wavelength limit. The obtained results confirm that the Cosserat theories do not account correctly for all effects of the material inhomogeneity on its elastic behavior, and should be combined with higher order gradient theories. The generalized elasticity theory should explicitly incorporate the spatial scale of the inhomogeneity in order to account for the multiple scattering of the waves. Our theoretical results also indicate the usefullness of some simplified Cosserat theories, such as the reduced Cosserat theory, in revealing some surface wave phenomena which could be easily hidden in the frame of the general Cosserat theory. In perspectives, an experimental validation of the surface modes in the granular phononic crystals would be interesting; in particular in order to evaluate the physical constants appearing in the Cosserat theory. These results would allow to compare analytically discrete lattice theory and Cosserat theory and thus to identify more precisely the limits of the Cosserat theory.

Bibliography

[1] Y. Tanaka and S.I. Tamura. Surface acoustic waves in two-dimensional periodic elastic structures. *Phys. Rev. B.*, 58:7958, 1998.

[2] R. Stoneley. The propagation of surface elastic waves in a cubic crystal. *Proc. Roy. Soc.*, A232:447, 1955.

[3] D.C. Gazis, R. Herman, and R.F. Wallis. Surface elastic waves in cubic crystals. *Phys. Rev.*, 119:533, 1960.

[4] I.M. Lifshitz and S.I. Pekar. *Usp. Fiz. Nauk*, 56:531, 1955.

[5] H. Kaplan. Effect of an imprity lattice on surface waves. *Phys. Rev.*, 125:1271, 1962.

[6] W. Nowacki. *Theory of Asymmetric Elasticity.* Pergamon, Oxford, 1986.

[7] A. Eringen. *Microcontinuum Field Theories. I.Foundations and Solids.* Springer, New York, 1999.

[8] E.F. Grekova, M.A. Kulesh, and G.C. Herman. Waves in linear elastic media with microrotations, part 2: Isotropic reduced Cosserat model. *Bulletin of the seismological society of America*, 99:1423–1428, 2009.

[9] M.A. Kulesh, V. P. Matveenko, and I.N. Shardakov. Propagation of surface elastic waves in the Cosserat medium. *Acoustical Physics*, 52:186, 2006.

[10] M.A. Kulesh, E.F. Grekova, and I.N. Shardakov. Rayleigh wave in the isotropic and linear, reduced Cosserat continuum. *Advanced Problems in Mechanics*, 53:290, 2006.

[11] *Surfaces waves propagation in Cosserat continuum: construction of solution and analysis using wavelet transform*, 2007.

[12] A. Merkel, V. Tournat, and V.E. Gusev. Elastic waves in noncohesive frictionless granular crystals. *Ultrasonics*, 50(2):133 – 138, 2009.

[13] A. Merkel, V. Tournat, and V.E. Gusev. Dispersion of elastic waves in three-dimensional noncohesive granular phononic crystals: Properties of rotational modes. *Phys. Rev. E.*, 82(3):031305, 2010.

[14] V. Tournat, I. Pèrez-Arjona, A. Merkel, V. Sanchez-Morcillo, and V.E Gusev. Elastic waves in phononic monolayer granular membranes. *New Journal of Physics*, 13(7):073042, 2011.

[15] A. Merkel, V. Tournat, and V.E. Gusev. Experimental evidence of rotational elastic waves in granular phononic crystals. *Phys. Rev. Lett.*, 107(22):225502, 2011.

[16] H. Pichard, A. Duclos, J-P. Groby, V. Tournat, and V.E. Gusev. Two-dimensional discrete granular phononic crystal for shear wave control. *Phys. Rev. B.*, 86:134307, 2012.

[17] H. Pichard, A. Duclos, J-P. Groby, V. Tournat, and V.E. Gusev. Localized transversal-rotational modes in linear chains of equal masses. *Phys. Rev. E.*, 89:013201, January 2014.

[18] I.A. Kunin. *Elastic Media with Microstructure Three-Dimensional Models vol 2.* Springer, Berlin, 1983.

[19] H.-B. Muhlhaus. *Continuum models for materials with micro-structure.* J. Wiley, New York, 1995.

[20] J.D. Joannopoulos, R.D. Meade, and J.N. Winn. *Photonic crystals : Modeling the Flow of Light.* Princeton University Press, Princeton, 1995.

[21] C. Prada, O. Balogun, and T. W. Murray. Laser-based ultrasonic generation and detection of zero-group velocity lamb waves in thin plates. *Appl. Phys. Lett.*, 87:194109, 2005.

[22] J. Blitz and G. Simpson. *Ultrasonic methods of non-destructive testing.* Champman et Hall, London, 1996.

[23] E. Cosserat and F. Cosserat. *Théorie des corps déformables.* Herman et Fils, Paris, 1909.

[24] E. Pasternak and H.-B. Muhlhaus. *Cosserat and non-local continuum models for problems of wave propagation in fractured materials.* Pergamon, Amsterdam, 2000.

[25] R.D. Mindlin. Micro-structure in linear elasticity. *Arch. Ration. Mech. Anal.*, 16:51–78, 1964.

[26] R.A. Toupin. Theory of elasticity with couple-stress. *Arch. Ration. Mech. Anal.*, 17(85-112), 1984.

[27] A.C. Eringen. *Theory of micro-polar elasticity.* Academic press, New York, 1968.

[28] A. Askar. *Lattice dynamical foundations of continuum theories.* World Scientific, Singapore, 1986.

[29] M.A. Kulesh, E.F. Grekova, and I.N. Shardakov. The problem of surface wave propagation in a reduced Cosserat medium. *Acoustical Physics*, 55(2):218–226, 2009.

[30] Z. Liu, X. Zhang, Y. Mao, M. Zhu, S. Yang, and P. Sheng. Locally resonant sonic materials. *Science*, 289:1734–1736, 2000.

[31] Liu X.N., G.K. Hu, G.L. Huang, and C.T. Sun. An elastic metamaterial with simulaneously negative mass density and bulk modulus. *Appl. Phys. Lett.*, 98(251907), 2011.

[32] V. E. Gusev and O.B. Wright. Double-negative flexural acoustic metamaterial. *New Journal of Physics*, 16:123063, 2014.

Conclusion générale

L'objectif de ce travail de thèse était d'étudier théoriquement la propagation d'ondes de volume, localisées et de surface dans différents cristaux phononiques granulaires. Cette étude s'inscrit dans la continuité de plusieurs travaux réalisés au Laboratoire d'Acoustique de l'Université du Maine. Parmi eux, la description de la propagation d'ondes de volume dans un cristal phononique granulaire hexagonal tridimensionnel avait été réalisée théoriquement [1, 2]. L'importance de la prise en compte des degrés de liberté de rotation des particules dès lors que la friction au niveau des contacts n'est plus négligeable avait été démontrée. Des modes de rotation avait été mis en évidence expérimentalement [3], ouvrant à nouveau la question de la validité de la théorie de Cosserat dans les milieux granulaires. Cette théorie, généralisation de la théorie classique de l'élasticité, prend en compte la rotation des éléments infinitésimaux du matériau. Une étude théorique et numérique des mouvements hors plan intégrant les rotations des particules sphériques d'une membrane granulaire avait également été effectuée [4]. Cette dernière avait en particulier montré l'importance des valeurs des différentes forces agissant entre les particules. Pour une valeur critique du ratio entre les rigidités de cisaillement et de flexion des ressorts modélisant le contact entre les sphères, la structure présentait une bande interdite totale. Aussi, l'existence d'une bande interdite totale en basses-fréquences avait été démontrée lorsque la rigidité normale au contact entre la membrane et un substrat ainsi que la rigidité de flexion au contact entre les particules avaient toutes deux des valeurs importantes.

Les différents phénomènes rencontrés dans ces travaux ont donc largement ouvert des perspectives d'études sur les cristaux phononiques granulaires. Dans ce travail de thèse, l'intérêt s'est porté sur l'influence de la prise en compte des degrés de liberté de rotation des particules sur la propagation des ondes dans différents cristaux phononiques granulaires. Les cristaux étudiés diffèrent dans leur structure, dans la forme et l'arrangement des particules les constituant, ainsi que dans les mécanismes d'interaction entre les particules. Aussi, l'effet de la nature des conditions aux limites appliquées aux cristaux, conduisant à l'existence de modes localisés et de modes de surface, a été analysé.

Une chaîne monoatomique constituée de particules cylindriques identiques a d'abord été étudiée. Les particules cylindriques possèdent deux degrés de liberté, un en translation et un en rotation. Le contact entre les particules est modélisé par des ressorts en cisaillement et en flexion. Les modes de propagation dans la chaîne infinie ont été décrits puis les conditions nécessaires à l'existence d'un mode localisé à l'extrémité d'une chaîne semi-infinie ont été établies. L'interaction entre ondes de translation et ondes de rotation conduit à l'existence de deux modes propagatifs, séparés par une bande de fréquences interdites. Un mode "mou" (*soft mode*) a été décrit lorsque la rigidité de flexion est nulle.

L'existence de ce mode est liée à une compensation entre mouvements de rotation et de translation. Selon le type de conditions aux limites (libre, intermédiaire ou rigide), la fréquence du mode localisé peut se situer dans la bande interdite ou au-dessus du mode propagatif de plus hautes fréquences. Les profils discrets des amplitudes des déplacements et rotations des particules du mode localisé ont été décrits en fonction de la position des particules ainsi que selon le type de conditions aux limites appliquées. Ce mode localisé est composé de deux modes évanescents, spécifiques à cette chaîne de cylindres, possédant deux degrés de liberté chacun. Ceci est une importante différence par rapport à de précédentes études portant sur des modes localisés de type longitudinal dans des chaînes de billes et dans des structures multicouches. En effet, dans ces structures, pour chaque fréquence, seul un mode évanescent peut exister.

La propagation des ondes dans un cristal phononique granulaire bidimensionnel a ensuite été décrite. Le cristal est composé de particules cylindriques disposées selon une maille cubique. Les particules possèdent deux degrés de liberté en translation et un en rotation. Le contact entre les particules est modélisé par des rigidités normale, de cisaillement et de flexion. Ce travail montre que des bandes interdites complètes peuvent être rencontrées dans ce cristal phononique granulaire. L'existence d'un cône de Dirac, situé dans une bande propagative avec une composante rotationnelle, est possible lorsque le cristal phononique granulaire est composé de cylindres creux. Le modèle théorique montre une forte interaction entre les mouvements rotationnels et de translation aux basses fréquences le long d'une direction du cristal. Deux régions de vitesse de groupe positive et négative, séparées par un point où la vitesse de groupe est nulle, existent. Cela résulte en la propagation de modes non-monotones. Ces derniers sont trouvés pour une large gamme de valeur des rapports relatifs entre les rigidités normale, de cisaillement et de flexion. Cette particularité du cristal résulte en un phénomène de biréfraction aux basses fréquences. Si les conditions permettant l'observation du phénomène de biréfraction sont réunies, des dispositifs anti-sismiques pourraient être envisagés. Lorsque le paramètre de rigidité de flexion augmente, les modes à prédominance rotationnelle sont décalés vers les hautes fréquences et les modes non-monotones disparaissent. Une explication physique à l'origine de ces modes est donnée : leur existence provient de l'hybridisation entre les mouvements de rotation et de translation ainsi que de la présence d'un mouvement d'énergie nulle. Ce modèle discret de la propagation des ondes dans un cristal phononique granulaire peut être utile dans la description de matériaux granulaires innovants ainsi que dans la compréhension de phénomènes, tels que la propagation de modes non-monotones dans des structures périodiques composites.

Une description de modes propagatifs et de surface, existant dans deux cristaux phononiques granulaires tridimensionnels, a enfin été présentée. Ces deux cristaux sont constitués de particules sphériques et disposées selon une maille cubique. Des ondes de Rayleigh sont étudiées dans le premier cristal dont les particules possèdent deux degrés de liberté en translation et un en rotation. Des ondes de surface de type cisaillement horizontal sont analysées dans le second cristal dont les particules possèdent un degré de liberté en translation et deux en rotation. Le contact entre les particules est toujours modélisé avec des rigidités normale, de cisaillement et de flexion. L'existence d'ondes à une surface mécaniquement libre de ces deux cristaux phononiques granulaires est possible lorsque cette surface est le long de la face du cristal cubique (famille de plan <100>). Dans le premier cristal, deux ondes de surface de type Rayleigh, séparées par une bande interdite, sont mises en évidence. Un mode plan purement

longidudinal se propageant le long de la surface est aussi trouvé dans cette structure. Dans le second cristal, l'existence d'une onde de surface de cisaillement horizontal est révélée. Cette onde possède la particularité d'être localisée autour d'une seule et unique fréquence. Une comparaison de ces modes de surface avec les modes de surface prédits par la théorie de Cosserat est effectuée. Les résultats indiquent que la théorie de Cosserat ne reflète pas correctement tous les effets dus aux inhomogénéités du matériau. L'échelle spatiale des inhomogénéités doit être prise en compte afin de décrire correctement la diffusion multiple des ondes. La théorie de Cosserat devrait être combinée avec des modèles d'élasticité d'ordres supérieurs. Ces conclusions, issues de cette étude théorique du comportement de structures ordonnées, sont aussi valides pour des systèmes désordonnés. En effet, la localisation des ondes due à la diffusion multiple peut avoir lieu dans des structures périodiques (effets phononiques) mais aussi dans des structures désordonnées via la localisation d'Anderson.

L'évaluation théorique des différents modes se propageant dans les cristaux phononiques granulaires étudiés dans ce travail, a permis de mettre en lumière l'avantage de ces structures discrètes. En comparaison avec des cristaux phononiques composites par exemple, elles permettent de décrire analytiquement les courbes de dispersion en tout point de la zone de Brillouin. En plus de la périodicité, les cristaux granulaires présentent un caractère discret qui leur est spécifique. Il en résulte des phénomènes particuliers liés à la propagation des ondes qui ont été mis en évidence. L'enjeu principal de ce travail a été d'analyser ces différents phénomènes afin de permettre le design de cristaux pour des applications spécifiques tels que des dispositifs de filtrage, ou bien le contrôle non-destructif de structures. Actuellement, un fort intérêt se porte sur les matériaux présentant un assemblage périodique de nanoparticules, tel que le graphène qui possèdent des propriétés physiques étonnantes. Dans cet esprit, ce travail pourrait être utile à la compréhension et au design de structures nanogranulaires. Si l'échelle est bien choisie, ces stuctures peuvent présenter simultanément des propriétés photoniques et phononiques (cristaux phoxoniques), ouvrant alors la voie à une nouvelle optoacoustique dans laquelle l'interaction de la lumière et du son pourrait être magnifiée par l'ingénierie des nanostructures.

Différentes perspectives de ce travail peuvent être envisagées. D'un point de vue théorique, il serait intéressant d'étudier l'existence d'ondes de surface dans ces mêmes cristaux phononiques granulaires 3D dans le cas où la surface est orientée selon la diagonale du cristal cubique (famille de plan <110>). Cette nouvelle condition aux limites devrait engendrer des modes de surface ayant des propriétés différentes. En particulier, nous pourrions supposer que cette nouvelle surface modifierait la propagation du mode plan purement longitudinal, mode qui pourrait être évanescent dans ce cas. Comme exposé précédemment, les phénomènes notés dans les structures de bandes des cristaux phononiques granulaires dépendent fortement des rigidités des ressorts modélisant le contact entre les particules. Afin de mettre en évidence des phénomènes supplémentaires, différentes rigidités, telles que la rigidité de torsion, pourraient être considérées. Il serait aussi intéressant d'étudier ces structures dans le régime non linéaire et selon différents arrangements des particules (cristaux hexagonaux par exemple). Que ce soit dans des chaînes granulaires ou des cristaux de plus grandes dimensionalités, différents phénomènes non linéaires ont été révélés, telles que la génération d'harmoniques, la propagation d'ondes solitaires, ou bien l'existence de modes localisés. La prise en compte de non linéarités, associée aux effets dus aux degrés de liberté de rotation des particules, pourrait mener à de nouveaux effets sur la propagation des ondes dans ces structures.

La validation expérimentale des différents phénomènes théoriques prédits et discutés dans ce travail serait aussi nécessaire. Les cristaux phononiques granulaires pourraient être réalisés en utilisant des billes magnétiques, ce qui permettrait de maintenir le contact entre les particules. Dans cette idée, des mesures préliminaires ont été effectuées sur une chaîne de sphères magnétiques. La chaîne a été excitée de manière transversale à l'aide d'un pot vibrant dans le but de se rapprocher de la configuration étudiée dans le deuxième chapitre, où les particules possèdent un degré de liberté en translation et un en rotation. Des premiers résultats encourageants ont permis de mettre en évidence les deux modes se propageant dans la chaîne. L'idée serait par la suite de générer et mesurer des modes localisés en appliquant diverses conditions aux limites à une extrémité de la chaîne. Afin de comparer les résultats expérimentaux aux résultats théoriques de manière précise, il serait nécessaire d'estimer les paramètres utilisés dans le modèle dans un premier temps. Pour ce faire, les rigidités des ressorts modélisant le contact entre les particules pourraient être estimées en mesurant les fréquences de résonance de cisaillement et de flexion au contact entre deux particules. À partir d'un modèle théorique, la valeur de ces fréquences de résonance permettrait de calculer les rigidités. En modifiant la force magnétique agissant entre les particules, ces rigidités pourraient être contrôlées afin de reproduire les différentes courbes de dispersion décrites dans la présente étude théorique. De la même manière, les cristaux phononiques granulaires bi et tridimensionnels étudiés dans ce travail pourraient être fabriqués. Il serait en particulier intéressant de mesurer expérimentalement les modes de surface existant dans les cristaux phononiques granulaires 3D, afin d'évaluer les constantes physiques apparaissant dans la théorie de Cosserat. Cela permettrait de comparer analytiquement la théorie discrète et la théorie de Cosserat afin d'identifier plus précisément les limites de cette théorie. Enfin, si les effets dus à la diffusion multiple sont mis en évidence expérimentalement dans ces structures granulaires périodiques, cela apporterait des perspectives encourageantes concernant, par exemple, la mise en évidence expérimentale de la localisation d'Anderson dans des structures désordonnées.

Bibliographie

[1] A. Merkel, V. Tournat, and V.E. Gusev. Elastic waves in noncohesive frictionless granular crystals. *Ultrasonics*, 50(2) :133 – 138, 2009.

[2] A. Merkel, V. Tournat, and V.E. Gusev. Dispersion of elastic waves in three-dimensional noncohesive granular phononic crystals : Properties of rotational modes. *Phys. Rev. E.*, 82(3) :031305, 2010.

[3] A. Merkel, V. Tournat, and V.E. Gusev. Experimental evidence of rotational elastic waves in granular phononic crystals. *Phys. Rev. Lett.*, 107(22) :225502, 2011.

[4] V. Tournat, I. Pèrez-Arjona, A. Merkel, V. Sanchez-Morcillo, and V.E Gusev. Elastic waves in phononic monolayer granular membranes. *New Journal of Physics*, 13(7) :073042, 2011.

Appendix A

Description of the band structure of the chain of cylinders

A.1 General description of the dispersion curves

In order to study the possible localization of the waves in this system, a complete description of the band structure is needed. To have a localized mode, two evanescent waves with a decreasing amplitude must be combined. So, it is important to know in what situation the wave numbers q_+ and q_- are both complex with a negative imaginary part at one particular frequency.
To determine this, the range of values of

$$S_\pm^2 = \sin^2 q_\pm = \Omega^2 \frac{1 + p(p_B - 1)}{2 p_B p} \left(1 \pm \sqrt{1 - \frac{4 p_B p (\Omega^2 - p)}{\Omega^2 (1 + p(p_B - 1))^2}} \right) \tag{A.1}$$

is analyzed as function of p and p_B. This description provides informations on the wave numbers. On one hand, if

$$0 \leq \sin^2 q \leq 1, \tag{A.2}$$

a real solution for the wave number q exists and the corresponding mode is propagative. On the other hand, if

$$\sin^2 q < 0 \qquad \text{or} \qquad \sin^2 q > 1, \qquad \text{or} \qquad \sin^2 q = \beta^{'} + \mathrm{i}\beta^{''}, \tag{A.3}$$

no purely real solution for q exists and the corresponding mode is evanescent.
When at least one of $S_\pm^2$ satisfies Eq. (A.2) the corresponding frequency Ω lies in a propagative band. In the case where both S_+^2 and S_-^2 satisfy one of the inequalities of Eq. (A.3), the corresponding frequency lies in a band gap.

A.1.1 Analysis of $\sin^2 q_\pm$ as a function of the parameters

In the next figures illustrating the following analysis, the meaningful frequencies in the description of the curves are indicated and marked by horizontal lines. These characteristic values are $\sqrt{p}$, $\sqrt{p_B p}$, 1 and $\Omega_{\,\mathrm{ZGVP}}$. They correspond to the limits where the description of S_+^2 and/or S_-^2 changes. The band structure is analyzed by increasing p_B. The zero-group velocity point (ZGVP) of the high frequency mode Ω_+ is found by solving

$$\frac{\partial \Omega_+^2}{\partial \sin^2 q} = 0. \tag{A.4}$$

The resolution of Eq. (A.4) leads to

$$\sin^2(q_{\text{ZGVP}}) = \frac{2p(1+p_Bp-p)}{4p_Bp-(1+p_Bp-p)^2}, \tag{A.5}$$

with $4p_Bp-(1+p_Bp-p)^2>0$ because by definition $p \geq 1$. The value of Ω_+ at this ZGVP is

$$\Omega_{\text{ZGVP}} = \left[\frac{4p_Bp^2}{4p_Bp-(1+p_Bp-p))^2}\right]^{1/2}. \tag{A.6}$$

Note that when Ω_{ZGVP} is real positive, then Ω_{ZGVP} is larger than the maximum of $[\sqrt{p}, \sqrt{p_Bp}]$. When $\Omega > \Omega_{\text{ZGVP}}$, $S_\pm^2$ are complex with $\text{Re}(S_+^2) = \text{Re}(S_-^2)$ and $\text{Im}(S_+^2) = -\text{Im}(S_-^2)$.

A.1.1.1 Monotonous second propagative band with negative group velocity

Fig. A.1 presents the different real and imaginary parts of $S_\pm^2$ and the corresponding dispersion curves when $p_B < 1-1/p$. In this case Ω_+ is monotonous with a negative group velocity and $\text{Max}(\Omega_+) = \sqrt{p}$.
In the first band gap $S_+^2 < 0$ and $S_-^2 > 1$ and when Ω lies in the second propagating band, at least one of $S_\pm^2$ satisfies Eq. (A.2).
At small $p_B < (1-\frac{1}{\sqrt{p}})^2$, Fig. A.1(a) and Fig. A.1(b), Ω_{ZGVP} is purely imaginary. The first band gap is between $\sqrt{p_Bp}$ and 1 and, with increasing p_B, the low-frequency mode starts to close the gap. The upper propagating band is not influenced by the bending rigidity and its width is proportional to $(\sqrt{p}-1)$. In the upper band gap, both $S_\pm^2 < 0$.

When $(1-\frac{1}{\sqrt{p}})^2 < p_B < 1-1/p$, Ω_{ZGVP} is real positive. As illustrated in Fig. A.1(c) and Fig. A.1(d), in the upper band gap, when $\Omega \in [\sqrt{p}, \Omega_{\text{ZGVP}}]$, both $S_\pm^2 < 0$, and when $\Omega > \Omega_{\text{ZGVP}}$, $S_\pm^2$ are complex.

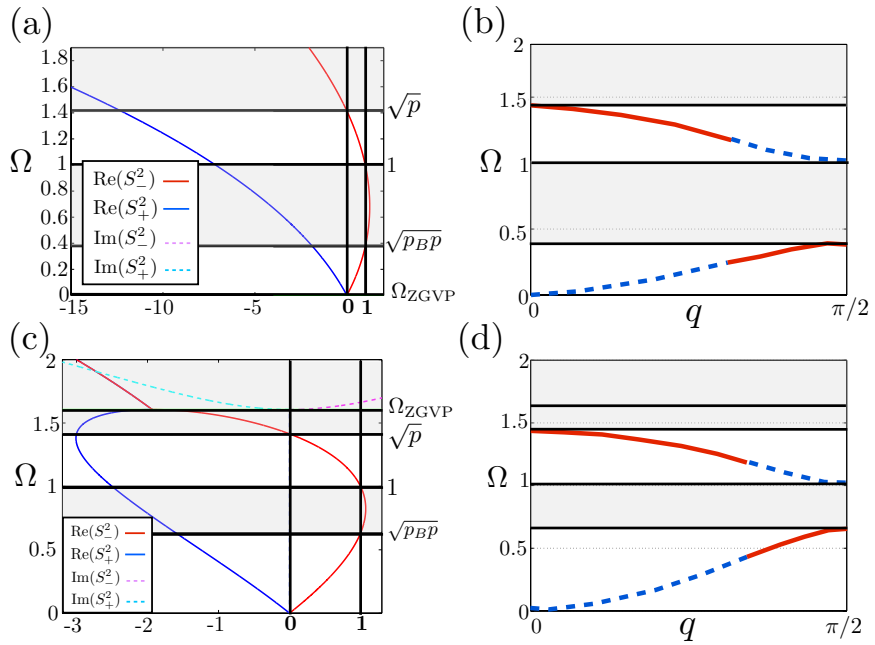

Figure A.1 – Real and imaginary parts of S_+^2 and S_-^2 as a function of the frequency Ω for homogeneous cylinders ($p = 2$) (a) small $p_B < (1 - \frac{1}{\sqrt{p}})^2$ ($p_B = 0.07$ and Ω_{ZGVP} is purely imaginary), (c) $(1 - \frac{1}{\sqrt{p}})^2 < p_B < 1 - 1/p$ ($p_B = 0.2$ and Ω_{ZGVP} is real positive); (b) and (d) represent the corresponding dispersion curves $\Omega = \Omega(q)$, Ω_+ is monotonous with negative group velocity.

A.1.1.2 Nonmonotonous second propagative band with zero-group velocity point.

Fig. A.2 presents the situation when $1 - 1/p < p_B < 1 + 1/p$. In this case, Ω_+ is nonmonotonous with a zero-group velocity point and $\text{Max}(\Omega_+) = \Omega_{\text{ZGVP}}$. In the first band gap $S_+^2 > 1$ and $S_-^2 < 0$. When Ω lies in the second propagating band at least one of $S_\pm^2$ satisfies Eq. (A.2) and above Ω_{ZGVP}, $S_\pm^2$ are complex.

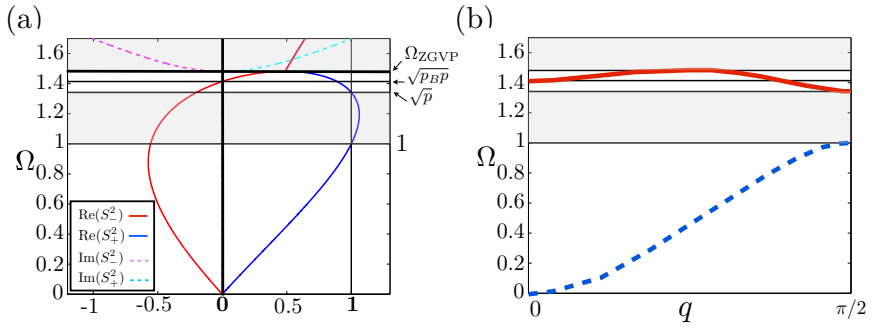

Figure A.2 – (a) Real and imaginary parts of S_+^2 and S_-^2 as a function of the frequency Ω for homogeneous cylinder ($p = 2$) when $1 - 1/p < p_B < 1 + 1/p$ ($p_B = 0.9$); (b) corresponding dispersion curves $\Omega = \Omega(q)$, Ω_+ is nonmonotonous with a zero-group velocity point.

A.1.1.3 Monotonous second propagative band with positive group velocity

Fig. A.3 illustrates the description when $p_B > 1 + 1/p$. In this case, Ω_+ is monotonous with a positive group velocity and $\text{Max}(\Omega_+) = \sqrt{p_B p}$. The dispersion relations are characterized by the

stabilized first band gap and by an increase of the width of the second propagating band proportional to $(\sqrt{p_B}-1)\sqrt{p}$. In the first band gap $S_+^2 > 1$ and $S_-^2 < 0$. When Ω lies in the second propagating band, at least one of $S_\pm^2$ satisfies Eq. (A.2).

When $1 + 1/p < p_B < (1 + \frac{1}{\sqrt{p}})^2$ (Fig. A.3(a) and Fig. A.3(b)) Ω_{ZGVP} is real positive. So, in the upper band gap, when $\Omega \in [\sqrt{p_B p}, \Omega_{\text{ZGVP}}]$, both $S_\pm^2 > 1$ and above Ω_{ZGVP}, $S_\pm^2$ are complex.

At large $p_B > (1 + \frac{1}{\sqrt{p}})^2$, Fig. A.3(c) and Fig. A.3(d), Ω_{ZGVP} is purely imaginary. Then, when $\Omega > \sqrt{p_B p}$ both $S_\pm^2 > 1$.

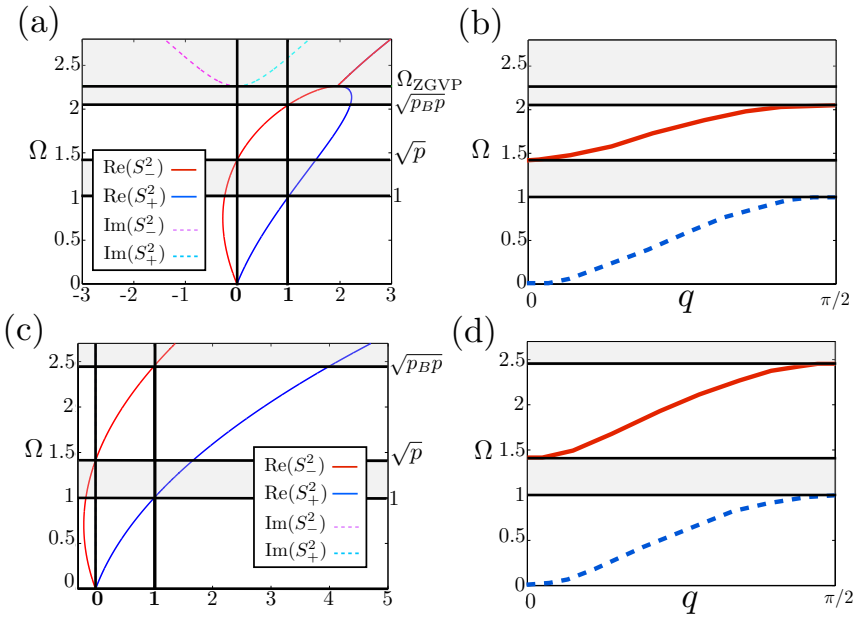

Figure A.3 – Real and imaginary parts of S_+^2 and S_-^2 as a function of the frequency Ω for homogenous cylinders ($p = 2$) when (a) $1 + 1/p < p_B < (1 + \frac{1}{\sqrt{p}})^2$ ($p_B = 2.1$ and Ω_{ZGVP} is real positive), (c) for large $p_B > (1 + \frac{1}{\sqrt{p}})^2$ ($p_B = 3$ and Ω_{ZGVP} is purely imaginary); (b) and (d) represent the corresponding dispersion curves $\Omega = \Omega(q)$, Ω_+ is monotonous with positive group velocity.

A.1.2 Summary of the description when the two evanescent waves lies in a band gap

To summarize, the situations where two waves are evanescent at the same frequency can be described. They correspond to values of p and p_B where both S_+^2 and S_-^2 lie in a band gap and thus satisfy one of the inequalities of Eq. (A.3). These cases are the following :

- When Ω lies in the first band gap
  - $S_+^2 < 0$ and $S_-^2 > 1$: this is the case when $p_B < 1 - 1/p$.
  - $S_-^2 < 0$ and $S_+^2 > 1$: this is the case when $p_B > 1 - 1/p$.
- When Ω lies in the second band gap
  - $S_+^2 < 0$ and $S_-^2 < 0$: this is the case where Ω_+ is monotonous with a negative group velocity and either $p_B < (1 - \frac{1}{\sqrt{p}})^2$ and $\Omega > \sqrt{p}$, Fig. A.1(a), or $(1 - \frac{1}{\sqrt{p}})^2 < p_B < 1 - 1/p$ and $\Omega \in [\sqrt{p}, \Omega_{\text{ZGVP}}]$, Fig. A.1(c).

- $S_+^2 > 1$ and $S_-^2 > 1$: this is the case where Ω_+ is monotonous with a positive group velocity and either $1 + 1/p < p_B < (1 + \frac{1}{\sqrt{p}})^2$ and $\Omega \in [\sqrt{p_B p}, \Omega_{\text{ZGVP}}]$, Fig. A.3(a), or $p_B > (1 + \frac{1}{\sqrt{p}})^2$ and $\Omega > \sqrt{p_B p}$, Fig. A.3(c).
- When $S_\pm^2$ are complex: this is the case where $(1 - \frac{1}{\sqrt{p}})^2 < p_B < (1 + \frac{1}{\sqrt{p}})^2$ and $\Omega > \Omega_{\text{ZGVP}}$.

A.2 Form of the wave number

In a general case, the wave number is given by

$$q = \text{arcsinh}(\pm H), \tag{A.7}$$

with H is the square root of the right-hand side of Eq. (A.1), whose value depends on either q_+ or q_- is searched. When the wave number is complex, the choice of the sign $\pm$ before H in Eq. (A.7) is made in such a way that its imaginary part be negative. If H has a negative/positive imaginary part, the sign $+/-$ will be chosen, respectively. Note that this choice is possible because the both cases, i.e., either $+$ or $-$ chosen, provide the same value of Ω.
The following analysis shows that, when $S_\pm^2$ are purely real, the expression of the wave numbers q_+ and q_- can be given in more details. When the wave is evanescent, the wave number can be split into a real and an imaginary parts

$$q = \text{Re}(q) \pm \text{i}\,\text{Im}(q). \tag{A.8}$$

Then, the following relation is deduced

$$\begin{aligned} \sin^2 q = {} & \sin^2(\text{Re}(q)) \cosh^2(\text{Im}(q)) - \sinh^2(\text{Im}(q)) \cos^2(\text{Re}(q)) \\ & \pm 2\text{i} \sin(\text{Re}(q)) \cos(\text{Re}(q)) \cosh(\text{Im}(q)) \sinh(\text{Im}(q)). \end{aligned} \tag{A.9}$$

If $S_\pm^2$ is real and according to Eq. (A.9), the following relations are found

$$\sin^2(\text{Re}(q)) \cosh^2(\text{Im}(q)) - \sinh^2(\text{Im}(q)) \cos^2(\text{Re}(q)) = H^2, \tag{A.10}$$

$$\sin(\text{Re}(q)) \cos(\text{Re}(q)) \cosh(\text{Im}(q)) \sinh(\text{Im}(q)) = 0. \tag{A.11}$$

In Eq. (A.11), the term $\cosh(\text{Im}(q))$ is always strictly positive and the term $\sinh(\text{Im}(q))$ is equal to zero only when $\text{Im}(q) = 0$, which is not the case of localization ($\text{Im}(q) \neq 0$). So the relation $\sin(\text{Re}(q)) \cos(\text{Re}(q)) = 0$ is deduced, i.e., $\text{Re}(q) = m'\pi/2$, with $m' = 0, \pm 1, ...$ an integer.

If m'=0, Re(q)=0 and Eq. (A.10) becomes $-\sinh^2(\text{Im}(q)) = H^2$. In this case, due to $-\sinh^2(\text{Im}(q)) < 0$, the solution exists when $H^2 < 0$. From Eq. (A.8), the wave number corresponding to evanescent waves attenuated in the positive direction takes the form

$$q_1 = -\text{i}\,\text{arcsinh}(|H|), \tag{A.12}$$

which corresponds to a simple exponential decay.

If m'=1, Re(q)=$\pi/2$ and Eq. (A.10) becomes $\cosh^2(\text{Im}(q)) = H^2$. Due to $\cosh^2(\text{Im}(q)) > 1$, the

solution exists for $H^2 > 1$. From Eq. (A.8), the wave number corresponding to evanescent waves attenuated in the positive direction takes the form

$$q_2 = -\frac{\pi}{2} - \mathrm{i}\,\mathrm{arccosh}(|H|), \tag{A.13}$$

which corresponds to a decay with additional oscillations.

So, for example, for small $p_B < 1 - 1/p$, in the first band gap : $S_+^2 < 0$ and $S_-^2 > 1$. For $S_+^2 < 0$ ($H^2 < 0$), q_+ takes the form of Eq. (A.12): $q_+ = -\mathrm{i}\,\mathrm{arcsinh}(|S_+|)$, and for $S_-^2 > 1$ ($H^2 > 1$), q_- takes the form of Eq. (A.13): $q_- = -\frac{\pi}{2} - \mathrm{i}\,\mathrm{arccosh}(|S_-|)$. While, for $p_B > 1 - 1/p$, in the first band gap $S_-^2 < 0$, so $q_- = -\mathrm{i}\,\mathrm{arcsinh}(|S_-|)$ and $S_+^2 > 1$, so $q_+ = -\frac{\pi}{2} - \mathrm{i}\,\mathrm{arccosh}(|S_+|)$.

If $S_\pm^2$ is complex, the wave numbers attenuated in the positive direction are given by

$$q_3 = q_3^{'} - \mathrm{i}\,q_3^{''}, \tag{A.14}$$

with $q_3^{'} = \mathrm{Re}(\mathrm{arcsinh}(|H|))$ and $q_3^{''} = \mathrm{Im}(\mathrm{arcsinh}(|H|))$, which corresponds to an exponential decay with additional oscillations. Contrary to the oscillations corresponding to q_2, these oscillations depend on the parameters p and p_B.

Appendix B

Supplementary material on chapter 4

B.1 Dispersion relation in the granular phononic crystal with particles possessing two translational and one rotational *dofs*

The determinant of the eigenvalue problem (4.1) leads to

$$\begin{aligned}
&\left[-\eta \sin^2 q_x - \sin^2 q_y + \Omega^2\right] \\
&\times \left[\left(-\eta \sin^2 q_y - \sin^2 q_x + \Omega^2\right)\left(-p(1-\sin^2 q_x + 1 - \sin^2 q_y) - 4p_B p(\sin^2 q_x + \sin^2 q_y) + \Omega^2\right) - p \sin^2 q_x (1 - \sin^2 q_x)\right] \\
&- p \sin^2 q_y (1 - \sin^2 q_y)\left(-\eta \sin^2 q_y - \sin^2 q_x + \Omega^2\right) = 0 \ , \qquad \text{(B.1)}
\end{aligned}$$

which can be written as a cubic equation for $Y = \sin^2 q_y$

$$\begin{aligned}
&Y^3 \left[-4p_B p \eta\right] \\
&+ Y^2 \left[p\left(\eta(-1 + \sin^2 q_x + \sin^2 q_x \eta) - 4p_B \sin^2 q_x (1 + \eta + \eta^2)\right) + \Omega^2 \left(\eta - p\eta + 4p_B p(1+\eta)\right)\right] \\
&+ Y \left[\Omega^4 \left(-1 + p - 4p_B p - \eta\right) + \Omega^2 \left(\sin^2 q_x (1+\eta^2) + p(1 + 2\eta + 2(-1 + 4p_B)\sin^2 q_x (1+\eta))\right)\right] \\
&+ Y \left[p \sin^2 q_x \left(\eta(\sin^2 q_x - 2\eta + \eta \sin^2 q_x) - 4p_B \sin^2 q_x (1 + \eta + \eta^2)\right)\right] \\
&- p \sin^4 q_x (1 + 4p_B \sin^2 q_x)\eta + \sin^2 q_x \Omega^2 \left[\sin^2 q_x \eta + p(1 + 2\eta - \sin^2 q_x \eta + 4p_B \sin^2 q_x (1+\eta))\right] \\
&+ \Omega^4 \left[-\sin q_x (1+\eta) + p(-2 + \sin^2 q_x - 4p_B \sin^2 q_x)\right] + \Omega^6 = 0 \ , \qquad \text{(B.2)}
\end{aligned}$$

and as a cubic equation for Ω^2

$$\begin{aligned}
&(\Omega^2)^3 \\
&+ (\Omega^2)^2 \left[p(-2 + \sin^2 q_x (1 - 4p_B) + \sin^2 q_y (1 - 4p_B)) - (\sin^2 q_x + \sin^2 q_y)(1+\eta)\right] \\
&+ \Omega^2 \left(\sin^4 q_x \eta + \sin^4 q_y \eta + \sin^2 q_x \sin^2 q_y (1+\eta^2) + p(\sin^4 q_x (-\eta + 4p_B(1+\eta))\right. \\
&\left. + \sin^2 q_y (1 + 2\eta - \eta \sin^2 q_y + 4p_B \sin^2 q_y (1+\eta)) + \sin^2 q_x (1 + 2\eta + 2(-1+4p_B)\sin^2 q_y (1+\eta))\right) \\
&- p(\eta(\sin^4 q_y - \sin^4 q_x (-1 + \sin^2 q_y + \sin^2 q_y \eta) - \sin^2 q_x \sin^2 q_y (\sin^2 q_y - 2\eta + \sin^2 q_y \eta)) \\
&+ 4p_B (\sin^2 q_x + \sin^2 q_y)(\sin^4 q_x \eta + \sin^4 q_y \eta + \sin^2 q_x \sin^2 q_y (1+\eta^2))) = 0 \ . \qquad \text{(B.3)}
\end{aligned}$$

Since it is a cubic equation in $\sin^2 q_y$ and in Ω^2, for a given frequency Ω, there are six corresponding wave numbers q_y. The analysis is restricted to displacement and rotational components of the surface waves whose amplitudes decrease as n increases. Therefore, the attenuation of surface waves is provided by complex wave numbers with a negative imaginary part, i.e., by three of the six wave numbers given by Eq. (B.2).

B.2 Pure longitudinal mode

From the development of the boundary condition, the determinant Eq. (4.12) exhibit a pure longitudinal mode $\Omega^2 = \eta \sin^2 q_x$. As developed below the term $\Omega^2 - \eta \sin^2 q_x$ can be factorized in the determinant.

$$
\begin{aligned}
|S_{2_{j,i}}| = 0 \Leftrightarrow & \begin{vmatrix} -\beta_1 & -\beta_2 & -\beta_3 \\ \alpha_1 + \dfrac{\cos q_{y_1}}{\mathrm{j} \sin q_{y_1}} & \alpha_2 + \dfrac{\cos q_{y_2}}{\mathrm{j} \sin q_{y_2}} & \alpha_3 + \dfrac{\cos q_{y_3}}{\mathrm{j} \sin q_{y_3}} = 0 \\ 1 & 1 & 1 \end{vmatrix} = 0 \\
\Leftrightarrow & \begin{vmatrix} \dfrac{1}{\eta \sin^2 q_{y_1} + \sin^2 q_x - \Omega^2} & \dfrac{1}{\eta \sin^2 q_{y_2} + \sin^2 q_x - \Omega^2} & \dfrac{1}{\eta \sin^2 q_{y_3} + \sin^2 q_x - \Omega^2} \\ \alpha_1 + \dfrac{\cos q_{y_1}}{\mathrm{j} \sin q_{y_1}} & \alpha_2 + \dfrac{\cos q_{y_2}}{\mathrm{j} \sin q_{y_2}} & \alpha_3 + \dfrac{\cos q_{y_3}}{\mathrm{j} \sin q_{y_3}} \\ 1 & 1 & 1 \end{vmatrix} = 0 \\
\Leftrightarrow \mathrm{j}(\Omega^2 - \eta \sin^2 q_x) & \begin{vmatrix} \dfrac{1}{\eta \sin^2 q_{y_1} + \sin^2 q_x - \Omega^2} & \dfrac{1}{\eta \sin^2 q_{y_2} + \sin^2 q_x - \Omega^2} & \dfrac{1}{\eta \sin^2 q_{y_3} + \sin^2 q_x - \Omega^2} \\ \dfrac{\cos q_{y_1}}{\sin q_{y_1} (\eta \sin^2 q_x + \sin^2 q_{y_1} - \Omega^2)} & \dfrac{\cos q_{y_2}}{\sin q_{y_2} (\eta \sin^2 q_x + \sin^2 q_{y_2} - \Omega^2)} & \dfrac{\cos q_{y_3}}{\sin q_{y_3} (\eta \sin^2 q_x + \sin^2 q_{y_3} - \Omega^2)} \\ 1 & 1 & 1 \end{vmatrix} = 0 \ .
\end{aligned}
\tag{B.4}
$$

B.3 Dispersion relation in the granular phononic crystal with particles possessing one translational and two rotational *dofs*

The determinant of the eigenvalue problem (4.24) leads to

$$
\begin{aligned}
& - p \cos^2 q_x \sin^2 q_x \left(p - \Omega^2 + p \cos^2 q_y + p_B p \sin^2 q_y \right) \\
& + \left[p - \Omega^2 + p \cos^2 q_x + p_B p \sin^2 q_x \right] \\
& \times \left[-p \cos^2 q_y \sin^2 q_y + \left(-\Omega^2 + \sin^2 q_x + \sin^2 q_y \right) \left(p - \Omega^2 + p \cos^2 q_y + p_B p \sin^2 q_y \right) \right] = 0 \ ,
\end{aligned}
\tag{B.5}
$$

which can be written in a characteristic equation for $Y = \sin^2 q_y$

$$
\begin{aligned}
& Y^2 \left[p_B p \left(p - \Omega^2 + p \cos^2 q_x + p_B p \sin^2 q_x \right) \right] \\
& + Y \left[-(p - \Omega^2)(-p + \Omega^2 + p_B p \Omega^2) - p(\Omega^2 + p(-1 + p_B \Omega^2)) \cos^2 q_x - p_B p(-2p + 2\Omega^2 + p_B p \Omega^2) \sin^2 q_x + p^2 p_B^2 \sin^4 q_x \right] \\
& - (p - \Omega^2 + p \cos^2 q_y)(p\,\Omega^2 \cos^2 q_x + (\Omega^2 - \sin^2 q_x)(p - \Omega^2 + p_B p \sin^2 q_x)) = 0 \ ,
\end{aligned}
\tag{B.6}
$$

and in a cubic equation for Ω^2

$$
\begin{aligned}
& - (\Omega^2)^3 \\
& + (\Omega^2)^2 \left[p_B p \sin^2 q_x + p_B p \sin^2 q_y + p \cos^2 q_x + p \cos^2 q_y + 2p + \sin^2 q_x + \sin^2 q_y \right] \\
& - \Omega^2 p (p_B^2 p \sin^2 q_x \sin^2 q_y + \cos^2 q_y \left((p_B p + 1) \sin^2 q_x + p \right) + \cos^2 q_x \left((p p_B + 1) \sin^2 q_y + p \cos^2 q_y + p \right) \\
& + p_B p \sin^2 q_x + p p_B \sin^2 q_y + p + 2 p_B \sin^2 q_x \sin^2 q_y + p_B \sin^4 q_x + p_B \sin^4 q_y + 2 \sin^2 q_x + 2 \sin^2 q_y) \\
& + p^2 \left(\sin^2 q_x \left(\left(p_B \sin^2 q_y + 1 \right)^2 + \cos^2 q_y \right) + \left(\cos^2 q_x + 1 \right) \sin^2 q_y \left(p_B \sin^2 q_y + 1 \right) + p_B \sin^4 q_x \left(p_B \sin^2 q_y + \cos^2 q_y + 1 \right) \right) \\
& = 0 \ .
\end{aligned}
\tag{B.7}
$$

B.4 Inexistence of SH surface waves in the absence of bending rigidity

When the bending rigidity parameter p_B is zero, Eq. (B.6) reduces to

$$\begin{aligned} &Y\left[\left(p-\Omega^2\right)\left(-p\sin^2 q_x+p\Omega^2+p-\Omega^2\right)+p\left(p\Omega^2+p-\Omega^2\right)\cos^2 q_x\right] \\ &+\left(\Omega^2-2p\right)\left(\left(p-\Omega^2\right)\left(\Omega^2-\sin^2 q_x\right)+p\Omega^2\cos^2 q_x\right)=0\ , \end{aligned} \tag{B.8}$$

which leads to the wave number q_{y_1}

$$q_{y_1}=\arcsin\sqrt{\frac{2\left(2p-\Omega^2\right)\left(\left(p-\Omega^2\right)\left(\Omega^2-\sin^2 q_x\right)+p\Omega^2\cos^2 q_x\right)}{p^2\left(3\Omega^2+2\right)+p\left(p\left(\Omega^2+2\right)-2\Omega^2\right)\cos(2q_x)-2p\left(\Omega^2+2\right)\Omega^2+2\Omega^4}}\ . \tag{B.9}$$

To each frequency corresponds one wave number q_{y_1}. In absence of bending rigidity, only the boundary condition Eq. (4.29) is applied, which leads to the equation

$$\begin{aligned} &(1-e^{2\mathrm{j}q_{y_1}})-\alpha_1(1+e^{2\mathrm{j}q_{y_1}})=0\ , \\ &\Leftrightarrow \alpha_1=\frac{2\mathrm{j}\sin q_{y_1}}{2\cos q_{y_1}}\ , \\ &\Leftrightarrow \frac{-\mathrm{j}p\sin q_{y_1}\cos q_{y_1}}{p(\cos^2 q_{y_1}+1)-\Omega^2}=\frac{\mathrm{j}\sin q_{y_1}}{\cos q_{y_1}}\ , \\ &\Leftrightarrow \Omega^2=p\ . \end{aligned} \tag{B.10}$$

This result is in accordance with the surface mode frequency Eq. (4.36) with $p_B=0$. Nevertheless, in this case, no surface mode exists because the frequency $\Omega=\sqrt{p}$ lies in a propagation band. In fact, according to Eq. (B.9), the corresponding wave number is purely real, and equal to $q_{y_1}=\pi/2$.

B.5 Cosserat and reduced Cosserat models

Solid materials can be seen as conglomerate of microstructural elements that are adhesively interacting as a result of micro-structural forces. Two different ways are generally used to describe the mechanical behavior of such solid materials: discrete models and continuum models. A considerable advantage of discrete models in comparison to continuum models is that the inhomogeneity effects at the micro-level can be accounted for more accurately. However, the number of representative microstructural elements in a macro-structural configuration is normally very large, which increases the number of equations that has to be solved for a discrete system. For this reason, researchers have incorporated the inhomogeneous material behavior in continuum formulations with a "characteristic material length". This internal length scale is a macroscopic representation of the micro-structural parameters, such as the size of the micro-elements, the distribution of the micro-element contact forces and the geometry of the micro-structure. A well-known enhanced continuum formulation is the Cosserat continuum, also called micro-polar continuum, where the rotational degrees of freedom (*dofs*) of the micro-elements are accounted for. The development of the Cosserat continuum formulation started with the pioneering work of the Cosserat brothers [1]. The idea was then developed by a numerous of investigators [2–6] and has gained a large popularity for analyzing wave propagation phenomena [7–15].

The Cosserat model of the medium whose deformation is described not only by the displacement vector $\mathbf{u}$ but also by a kinematically independent rotation vector $\boldsymbol{\theta}$ has attracted attention of researches

for a long time. These two vectors are function of the spatial coordinates and time. They characterize the displacements and rotations of infinitely small particles. To account for structural effects, which are not captured through classical continuum model, the framework of the fields theories requires the development of generalized continuum models. For instance, current effective medium theories, based on classical elasticity, do not properly describe strong dispersive behavior of wave propagation observed sometimes [16]. When the rotational *dofs* cannot be neglected, the continuum description of deformation is based on the Cosserat theory. In this theory the rotational *dofs* of structural element are taken into consideration in addition to displacements, while higher derivatives of the fields are accounted by higher-order gradient models [17, 18]. This theory (with various modifications) found its applications in the modeling of geomaterials, especially layered [19] and granular matter [20]. In modeling granular materials with elastic Cosserat continuum, the physical constants describing the microstructure would vary considerably depending on the packing density and grain type. Even in the simplest isotropic elastic Cosserat medium, the constitutive equations involve six independent elastic constants contrary to only two in the classical isotropic elasticity. While in some cases the Cosserat physical constants can be derived from the particularities of the material microstructure [19, 21], the determination of these parameters generally requires special experimental measurements. Thus, the application of the Cosserat theory is often limited to a numerical stabilizer for otherwise mesh-dependent numerical models [9]. For example, micro-structural phenomena such as micro-cracking and void cause discontinuous deformation processes which cannot be described with classical continuum model. Therefore, various kinds of modifications and generalizations of the standard continuum plasticity have been proposed to avoid a spurious solution for the localization zone and an excessive mesh dependence [8, 22].

The deformation behavior of elastic bodies in this theory has some specific features. The elastic body can acquire a stress-strain state significantly different from that predicted by the classical (symmetric) theory of elasticity. The stress σ and moment stress M tensors are asymmetric. The temperature effect being ignored, the dynamic behavior of an isotropic elastic medium is characterized by eight constants: two Lame constants μ and λ, the material density ρ, the parameter describing the rotational inertia of the medium I (the inertia moment density) and four elastic constants γ, β, ε and α, which characterize the microstructure.

Each material point in asymmetric theory of elasticity within the framework of the Cosserat medium is an oriented infinitesimal solid. The particle kinematic is described by the displacement vector $\mathbf{u} = \{u_x, u_y, u_z\}$ of the center of mass and by the rotation vector $\boldsymbol{\theta} = \{\theta_x, \theta_y, \theta_z\}$. In the case of the Cosserat medium both vectors are continuous functions of spatial coordinates and time. Thus, the elastic Cosserat continuum is described by the following equations [5, 23]

$$\rho \frac{\partial^2 u_i}{\partial t^2} = \frac{\partial \sigma_{ij}}{\partial x_j}, \quad I \frac{\partial^2 \theta_i}{\partial t^2} = \frac{\partial M_{ij}}{\partial x_j} + E_{ijk}\sigma_{jk} \ , \tag{B.11}$$

with E_{ijk} is the Levi-Civita tensor of third rank. In the case of isotropic and centrosymmetric material the stress tensor σ_{ij} and moment stress tensor M_{ij} are given by

$$\begin{aligned} \sigma_{ij} &= 2\mu\, \epsilon_{(ij)} + 2\alpha\, \epsilon_{<ij>} + \lambda\, \epsilon_{kk}\delta_{ij} \ , \\ M_{ij} &= 2\gamma\, \Theta_{(ij)} + 2\varepsilon\, \Theta_{<ij>} + \beta\, \Theta_{kk}\delta_{ij} \ , \end{aligned} \tag{B.12}$$

where $\epsilon_{ij} = \partial u_i/\partial x_j + \epsilon_{ijk}\theta_k$, and $\Theta_{ij} = \partial \theta_i/\partial x_j$. () and <> denote the symmetric and antisymmetric parts of tensor.

The equations of motions for an isotropic material are then given by

$$\rho\ddot{\boldsymbol{u}} = (2\mu+\lambda)\text{grad div}\,\boldsymbol{u} - (\mu+\alpha)\text{rot rot}\boldsymbol{u} + 2\alpha\,\text{rot}\,\boldsymbol{\theta}\ , \tag{B.13}$$

$$I\ddot{\boldsymbol{\theta}} = (\beta+2\gamma)\text{grad div}\,\boldsymbol{\theta} - (\gamma+\varepsilon)\text{rot rot}\boldsymbol{\theta} + 2\alpha\,\text{rot}\,\boldsymbol{u} - 4\alpha\boldsymbol{\theta}\ . \tag{B.14}$$

Pasternak et al. [24, 25] proposed a method to estimate the Cosserat physical constants μ, λ, γ, β, ε and α through the measurements of the longitudinal, shear and twist wave velocities in a particular material consisting of spherical particles. The spherical particles are connected by elastic links that can be decomposed into springs of four types: normal, shear, torsion and bending springs, with stiffnesses ξ^n, ξ^s, ξ^T and ξ^B, respectively. In particular, it was shown that for the Cosserat continuum that in such a material, the physical constants can be linked to the stiffnesses through the following relations

$$\begin{aligned} \mu &= \frac{1}{5}f\left(\xi^n + \frac{3}{2}\xi^s\right)\ , \qquad \lambda = \frac{1}{5}f\left(\xi^n - \xi^s\right)\ , \qquad \alpha = \frac{1}{2}f\xi^s\ , \\ \gamma &= \frac{1}{5}f\left(\xi^T + \frac{3}{2}\xi^B\right)\ , \qquad \beta = \frac{1}{5}f\left(\xi^T - \xi^B\right)\ , \qquad \varepsilon = \frac{1}{2}f\xi^B\ , \end{aligned} \tag{B.15}$$

with $f = k_*\nu_s/(\pi D)$, D is the diameter of the particles, k_* is the coordination number, ν_s is the volume fraction of the particles. Then α is the modulus relating rotations and non-symmetric shear stress, γ, β and ε are moduli relating the components of curvature-twist tensor and moment stress.

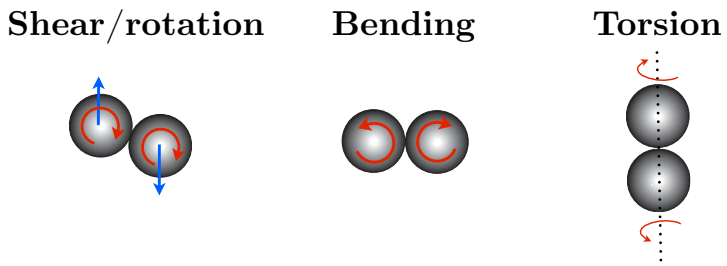

Figure B.1 – Models of the different rotational motions between two particles taken into account in [25].

Other cases of the Cosserat medium model are known, including the reduced Cosserat medium [26]. In this reduced theory, the microstructure only depends on the physical constant α making the stress tensor asymmetric. Bending and torsional rigidities, Fig. B.1, are negligible. Then, the constants γ, β and ε are zero and hence the tensor of momentum does not exist [26]. The elastic constant α describes the resistance to rotation of the point body with respect to the background. If $\alpha = 0$, the theory reduces to classical elasticity. The stress depends on the rotation of a particle relative to the continuum mass centers. Because the constants γ, β and ε are zero, there are no term with some spatial differential operators acting on $\boldsymbol{\theta}$ in Eq. (B.14). Therefore, there is no interaction between neighbor infinitesimal particles caused by difference in their rotations in this theory.

A serie of publications [26–30] has been devoted to the study of surface elastic waves propagation in both Cosserat and reduced Cosserat medium. In keeping with the comparison of the bulk waves in homogenized granular phononic crystal with those in the Cosserat continuum [31], it is then interesting to compare the results of the propagation of Rayleigh and SH surface waves obtained in the granular

phononic crystals with these studies. In the granular phononic crystals studied here, only bending and shear/rotational motions are considered ($\xi^T = 0$). In the reduced Cosserat theory, only the constant α is non zero, i.e., there is no bending and torsional rigidities, Eqs. (B.15), which corresponds to $p_B = 0$ in our discrete models.

Bibliography

[1] E. Cosserat and F. Cosserat. *Théorie des corps déformables*. Herman et Fils, Paris, 1909.

[2] R.D. Mindlin. Micro-structure in linear elasticity. *Arch. Ration. Mech. Anal.*, 16:51–78, 1964.

[3] R.A. Toupin. Theory of elasticity with couple-stress. *Arch. Ration. Mech. Anal.*, 17(85-112), 1984.

[4] A.C. Eringen. *Theory of micro-polar elasticity*. Academic press, New York, 1968.

[5] A. Eringen. *Microcontinuum Field Theories. I.Foundations and Solids*. Springer, New York, 1999.

[6] A. Askar. *Lattice dynamical foundations of continuum theories*. World Scientific, Singapore, 1986.

[7] H.B. Mühlaus and F. Oka. Dispersion and wave propagation in discrete and continous models for granular materials. *International Journal of Solids and Structures*, 33:2841, 1996.

[8] R. Borst and H.-B. Muhlhaus. *Computational strategies for gradient continuum models with a view to localisation of deformation*, volume 239-260. Proc. Int. Conf. on Nonlinear Engng Comp., Pineridge Press, Swansea, 1991.

[9] L.J. Sluys, R. Borst, and H.-B. Muhlhaus. Wave propagation, localization and dispersion in a gradient-dependent medium. *International Journal of Solids and Structures*, 30(9):1153–1171, 1993.

[10] L.J. Sluys. *Wave propagation localisation and dispersion in softening solids*. PhD thesis, Delft University of technology, The Netherlands, 1992.

[11] A.S.J. Suiker, R. de Borst, and C. S. Chang. Micro-mechanical modelling of granular material. part 1: Derivation of a second-gradient micro-polar constitutive theory. *Acta Mechanica*, 149:161–180, 2001.

[12] A.S.J. Suiker, R. de Borst, and C. S. Chang. Micro-mechanical modelling of granular material. part 2: Plane wave propagation in infinite media. *Acta Mechanica*, 149(Part2):181–200, 2001.

[13] A.S.J. Suiker, R. de Borst, and C. S. Chang. Comparison of wave propagation characteristics of the Cosserat continuum model and corresponding discrete lattice models. *International Journal of Solids and Structures*, 38(9):1563 – 1583, 2001.

[14] I.S. Pavlov, A.I. Potapov, and G.A. Maugin. A 2D granular medium with rotating particles. *International Journal of Solids and Structures*, 43(20):6194 – 6207, 2005.

[15] A.I. Potapov, I.S. Pavlov, and S.A. Lisina. Acoustic identification of nanocrystalline media. *Journal of sound and vibration*, 322:564–580, 2008.

[16] J.A. Hudson and L. Knopoff. Predicting the overall properties of composite materials with small-scale inclusions or cracks. *Pure Appl. Geophys.*, 131(4):551–576, 1989.

[17] N. Triantafyllidis and S. Bardenhagen. On higher order gradient continuum theories in 1D nonlinear elasticity. Derivation from and comparison to the corresponding discrete models. *J. Elasticity*, 33:259–293, 1993.

[18] N.A. Fleck and J.W. Hutchinson. Strain gradient plasticity. *Adv. Appl. Mech.*, 33:295–361, 1997.

[19] N.V. Zvolinskii and K.N. Shkhinek. Continual model of laminar elastic medium. *Mech.Solids*, 1:1–9, 1984.

[20] L. Limat. Percolation and Cosserat elasticity : exact results on a deterministic fractal. *Phys. Rev. B.*, 37(1):672–675, 1988.

[21] D.P. Adhikary and V.A. Dyskin. A Cosserat continuum model for layered materials. *Comput. Geotech.*, 20(1)(15-45), 1997.

[22] E.C. Aifantis. On the microstructural original of certain inelastic models. *J. Engng Mater. Technol.*, 106:326–334, 1984.

[23] W. Nowacki. *Theory of Asymmetric Elasticity.* Pergamon, Oxford, 1986.

[24] E. Pasternak, H.-B. Muhlhaus, and V.A. Dyskin. On the possibility of elastic strain localisation in a fault. *Pure Appl. Geophys.*, 161:2309–2326, 2004.

[25] E. Pasternak and V.A. Dyskin. On a possibility of reconstruction of Cosserat moduli in particulate materials using long waves. *Acta Mechanica*, 225:2409–2422, 2014.

[26] M.A. Kulesh, E.F. Grekova, and I.N. Shardakov. The problem of surface wave propagation in a reduced Cosserat medium. *Acoustics of structurally inhomogeneous solid media*, 55(2):218–226, 2009.

[27] M.A. Kulesh, V. P. Matveenko, and I.N. Shardakov. Propagation of surface elastic waves in the Cosserat medium. *Acoustical Physics*, 52:186, 2006.

[28] M.A. Kulesh, E.F. Grekova, and I.N. Shardakov. Rayleigh wave in the isotropic and linear, reduced Cosserat continuum. *Advanced Problems in Mechanics*, pages 53–54, 2006.

[29] M.A. Kulesh, V. P. Matveenko, and I.N. Shardakov. Constructing an analytical solution for Lamb waves using the Cosserat continuum approach. *Journal of Applied Mechanics and Technical Physics*, 48(1):119–125, 2007.

[30] M.A. Kulesh, M. Holschneider, and I.N. Shardakov. Surfaces waves propagation in Cosserat continuum: construction of solution and analysis using wavelet transform. *APM Processings*, pages 281–289, 2007.

[31] A. Merkel, V. Tournat, and V.E. Gusev. Experimental evidence of rotational elastic waves in granular phononic crystals. *Phys. Rev. Lett.*, 107(22):225502, 2011.

l'université nantes angers le mans
PÔLE DE RECHERCHE ET D'ENSEIGNEMENT SUPÉRIEUR

Université du Maine

Thèse de Doctorat

Hélène PICHARD

Étude théorique d'ondes de volume, localisées et de surface dans les cristaux phononiques granulaires

Propagative, localized and surface waves in granular phononic crystals

Résumé

Ce travail de thèse porte sur l'étude de la propagation d'ondes de volume et d'ondes de surface dans des cristaux phononiques granulaires en régime linéaire. Différents aspects sont développés dans ce manuscrit. L'effet de la prise en compte des degrés de liberté en rotation des particules sur la structure de bande de différents cristaux phononiques granulaires est étudié. En effet, l'introduction de ces degrés de liberté additionnels rend possible l'existence de modes de rotation qui interagissent fortement avec les modes transverses. Ce travail s'intéresse aussi à l'existence d'ondes localisées et d'ondes de surface dans des cristaux phononiques granulaires et en particulier à la comparaison des théories développées avec les prédictions de la théorie de Cosserat. Dans un premier temps, l'étude d'une chaîne phononique granulaire monoatomique est présentée. En considérant la chaîne semi-infinie avec une condition aux limites appliquée à son extrémité, le modèle analytique démontre l'existence de modes localisés, chaque mode étant composé de deux modes évanescents. Ensuite, une description théorique des modes se propageant dans un cristal phononique granulaire en deux dimensions est présentée. Les particules possèdent trois degrés de liberté, deux en translation et un en rotation. L'analyse des interactions entre ondes de translation et ondes de rotation permet de mettre en évidence une grande richesse de structure de bandes ainsi que des phénomènes particuliers (bandes interdites complètes, cône de Dirac, modes non-monotones, phénomène de double réfraction). Dans un dernier temps, une analyse de l'existence d'ondes de Rayleigh et de cisaillement horizontal dans un cristal phononique granulaire en trois dimensions est effectuée. Les limites de la théorie de Cosserat dans la description d'ondes acoustiques de surface dans les milieux micro- et nano-inhomogènes sont établies.

Mots clés

Cristal phononique granulaire, modes de surface, bandes interdites, cône de Dirac, hybridisation, Cosserat

Abstract

This work is devoted to the analysis of propagating and surface acoustic waves in granular phononic crystals in the linear regime. First, the propagation and localization of transversal-rotational waves in a two-dimensional granular chain of equal masses are analyzed. By considering the semi-infinite chain with a boundary condition applied at its beginning, the analytical study demonstrates the existence of localized modes, each mode composed of two evanescent modes. Secondly, the phononic properties of a two-dimensional discrete phononic crystal, made of circular cross-section, infinitely long contacting elastic cylinders arranged on a simple cubic lattice, are described analytically. The theoretical analysis provides a clear physical explanation for the existence of a zero-group velocity point of the lowest-energy acoustic mode in particular directions of the phononic crystal and demonstrates the birefraction phenomenon. Finally, the existence of surfaces elastic waves at mechanically free surface of granular phononic crystals is presented. Depending on the degrees of freedom of the particles, different types of surface waves exist in the structure. First, Rayleigh type surface waves are demonstrated in a granular phononic crystal with particles possessing two translational and one rotational degrees of freedom ; and secondly, shear-horizontal surface waves are studied in a granular phononic crystal with particles possessing two rotational and one translational degrees of freedom. A comparison with surface waves predicted by the Cosserat theories is made in order to establish the limitations of the Cosserat theories.

Key Words

Granular phononic crystal, surface modes, band gaps, Dirac cone, hybridization, Cosserat